NBS

Technical Note No. 339

OBSERVED PHASE-FRONT DISTORTION IN SIMULATED EARTH-TO-SPACE MICROWAVE TRANSMISSIONS

H. B. JANES AND M. C. THOMPSON, JR.

U. S. DEPARTMENT OF COMMERCE
NATIONAL BUREAU OF STANDARDS

THE NATIONAL BUREAU OF STANDARDS

The National Bureau of Standards is a principal focal point in the Federal Government for assuring maximum application of the physical and engineering sciences to the advancement of technology in industry and commerce. Its responsibilities include development and maintenance of the national standards of measurement, and the provisions of means for making measurements consistent with those standards; determination of physical constants and properties of materials; development of methods for testing materials, mechanisms, and structures, and making such tests as may be necessary, particularly for government agencies; cooperation in the establishment of standard practices for incorporation in codes and specifications; advisory service to government agencies on scientific and technical problems; invention and development of devices to serve special needs of the Government; assistance to industry, business, and consumers in the development and acceptance of commercial standards and simplified trade practice recommendations; administration of programs in cooperation with United States business groups and standards organizations for the development of international standards of practice; and maintenance of a clearinghouse for the collection and dissemination of scientific, technical, and engineering information. The scope of the Bureau's activities is suggested in the following listing of its four Institutes and their organizational units.

Institute for Basic Standards. Applied Mathematics. Electricity. Metrology. Mechanics. Heat. Atomic Physics. Physical Chemistry. Laboratory Astrophysics.* Radiation Physics. Radio Standards Laboratory:* Radio Standards Physics; Radio Standards Engineering. Office of Standard Reference Data.

Institute for Materials Research. Analytical Chemistry. Polymers. Metallurgy. Inorganic Materials. Reactor Radiations. Cryogenics.* Materials Evaluation Laboratory. Office of Standard Reference Materials.

Institute for Applied Technology. Building Research. Information Technology. Performance Test Development. Electronic Instrumentation. Textile and Apparel Technology Center. Technical Analysis. Office of Weights and Measures. Office of Engineering Standards. Office of Invention and Innovation. Office of Technical Resources. Clearinghouse for Federal Scientific and Technical Information.**

Central Radio Propagation Laboratory.* Ionospheric Telecommunications. Tropospheric Telecommunications. Space Environment Forecasting. Aeronomy.

---

* Located at Boulder, Colorado 80301.

** Located at 5285 Port Royal Road, Springfield, Virginia 22171.

NATIONAL BUREAU OF STANDARDS

Technical Note 339

ISSUED May 12, 1966

OBSERVED PHASE-FRONT DISTORTION IN SIMULATED EARTH-TO-SPACE MICROWAVE TRANSMISSIONS

H. B. Janes and M. C. Thompson, Jr.
Institute for Telecommunication Sciences and Aeronomy*
Environmental Science Services Administration
Boulder, Colorado

NBS Technical Notes are designed to supplement the Bureau's regular publications program. They provide a means for making available scientific data that are of transient or limited interest. Technical Notes may be listed or referred to in the open literature.

**Formerly the Central Radio Propagation Laboratories of the National Bureau of standards. CRPL was transferred to ESSA in October, 1965 but will continue to use NBS publications series pending inauguration of their own.*

For sale by the Superintendent of Documents, U. S. Government Printing Office
Washington, D.C. 20402
Price: 50¢

TABLE OF CONTENTS

Observed Phase-Front Distortion in Simulated Earth-to-Space Microwave Transmissions

H. B. Janes and M. C. Thompson, Jr.

An experimental study has been made of the time and space statistics of the phase-front distortion of microwave signals sent from a ground terminal to an elevated terminal. These phase-front characteristics are important in systems involving phase measurements between a ground station and a moving air-borne or space terminal. To isolate atmospheric errors from random motion of the upper terminal, the latter was simulated by a series of mountain-top antenna arrays. Phase-front distortion was analyzed in terms of time variations in radio range on a single path and in first and second range differences from pairs of paths. The cross-correlations of (1) range variations on adjacent paths, and (2) range difference variations on both adjoining and separated pairs of paths are investigated, including the strong dependence of correlation on the portion of the power spectrum included in the data. The effect of the mountain-top terrain on the spatial homogeneity of the phase-front was examined and found to be insignificant. A diurnal pattern in the variance of 15-minute range difference samples was observed, with minimum variance in the early morning hours. This pattern was not observed in the range variances, nor were the range and range difference variances significantly correlated with refractive index, air temperature, pressure or wind speed data at the lower terminal.

1. Introduction

A microwave signal transmitted through the troposphere is subjected to random retardations because of space and time variations in the atmospheric refractive index along the radio path. These retardations result in random variations of the phase-of-arrival of the signal, and are an important source of error in radio measurements of range and/or angular position.

Several experimental studies of range and range difference (angular position) variations caused by the atmosphere have been conducted over the past several years on slant paths to simulate ground-to-space transmissions [Norton, et al., 1961; and Janes and Thompson, 1964]. To minimize contamination of the data from geometric variations in range, these tests were all made on geometrically-stable paths with the upper terminal on a mountain.

Extension of these fixed-path data to the moving beam case in which the lateral movement of the upper terminal imparts a non-zero angular velocity to the propagation path requires a knowledge of the spatial statistics of the phase-of-arrival along the horizontal path of the moving upper terminal. In effect, the phase-front of a signal originating at the lower terminal will be distorted or "crinkled" by the time it arrives at the line of travel of the upper terminal and the time variability of the observed phase will be a function of the spatial wave-front statistics and the velocity of the upper terminal.*

In June and July of 1964, the Central Radio Propagation Laboratory of the National Bureau of Standards** performed an experiment under the sponsorship of the United States Air Force Avionics Laboratory*** to study the time and space statistics of this elevated phase-front. In particular, the objective was to obtain a detailed statistical description of time and space variations in the phase-front to serve as a basis for predicting atmospheric errors in microwave range and/or angular position measurements involving a moving upper terminal.

*In this discussion, we assume for convenience that the signal is originating at the lower terminal and the phase is being observed at the upper terminal, but the transmitting and receiving roles could, of course, be interchanged without changing the results.
**On October 11, 1965, the CRPL was redesignated the Institute for Telecommunication Sciences and Aeronomy of the Environmental Science Services Administration.
*** Project 4108, Task 4108 02, D.O. AF(33-657) 63-391

The purpose of this report is to describe the experiment, the data obtained, and the results of the statistical analysis.

2. General Description of the Experiment

2.1 Propagation paths, antenna arrangements

In principle, the best experimental arrangement would have included a moving terminal (e.g., an aircraft or satellite) sweeping with a perfectly determined trajectory across the sky to measure the phase-front characteristics of a ground-based signal. However, this possibility was ruled out at the outset for compelling technological reasons. It was decided to substitute an array of fixed mountain-top antennas for the moving terminal, and make phase-of-arrival and phase-difference recordings at several points on the array simultaneously. This arrangement, illustrated in figure 1, isolates the purely atmospheric effects from the random motion of any practical airborne terminal and permits the collection of statistically large data samples of phase-front behavior.

The site chosen is on the Island of Maui, Hawaii, with propagation paths extending from a point 25 meters above sea level at the abandoned Puunene airport to an array of four antennas approximately 3000 meters above sea level at the summit of Mt. Haleakala. The paths were from 24.5 to 24.9 km in length and were tilted at an angle of 7 degrees from the horizontal. A map and terrain profile are shown in figures 2 and 3.

All phase measurements were made at a radio frequency of 9.4 GHz. Parabolic antennas 122 cm in diameter were used at both upper and lower sites. At the latter site the antenna was mounted 163 cm above ground and the upper antennas were mounted 91 cm above local terrain. In both cases, the antenna beams were sufficiently narrow to avoid ground reflections.

The phase measurement equipment used was a modification of a basic system described previously [Thompson and Vetter, 1958].

The experiment was divided into 9 "runs" or periods of continuous recording activity, each approximately 24 hours long. Each run was characterized by a particular arrangement of the 4 antennas at the upper site. The several arrangements were chosen to give as wide a variety of path separations as possible. Two basic configurations were used, and these are shown in a sketch in figure 4. Configuration A provided two pairs of adjacent paths, the antenna separation of one pair (A, C and C, D) being twice that of the other (A, B and B, C). In addition, path pair A, D provided a separation twice that of A, C and C, D. Configuration B provided two path pairs with equal antenna separations, the pairs in turn being separated by various distances up to a maximum of 790 meters.

Table I gives the inclusive times and antenna arrangement for each run. The "antenna locations" noted in the table refer to the positions of the four upper-site antennas in use in each run as identified by the circled numbers on the topographic map of the Haleakala site in figure 5.

2. 2. Data Output

The principal data consist of continuous recordings of time variations of 1) the phase-of-arrival of signals sent over one (and in some cases two) of the four paths in use at any one time, 2) the difference in the phase-of-arrival observed on pairs of paths, and 3) the second difference, or the difference of two phase difference variables observed on two pairs of paths.

Although these data were originally calibrated in terms of phase-of-arrival at the radio frequency of 9.4 GHz, the results are discussed here in terms of variations in the apparent or radio path lengths, and their first and second differences, and will be referred to as range (R), range difference (ΔR), and second range difference ($\Delta^2 R$), respectively. This permits description of the phase front in terms of spatial deviations or "crinkling" of an imagined surface of constant phase.

The range and first and second range difference data were recorded as continuous variables on magnetic tape and on paper strip charts. The pass-band of the measuring and tape recording system extended from 0 to about 10 Hz. Some typical paper chart recordings of range and range difference are shown in figures 6, 7, and 8.

Secondary data consisted of magnetic tape and paper chart recordings of atmospheric refractivity at 1.5 meters above ground at the lower site, paper chart recordings of wind speed and direction measured at 3.7 meters above ground at the upper site, and 6.4 meters above ground at the lower sites, and paper chart recordings of refractivity at 1.5 meters above ground at from 2 to 4 points on the upper antenna array. In addition, hourly or half-hourly readings of wet and dry bulb temperature and barometric pressure were taken at both sites. To record cloudiness, 35 mm pictures of the path were taken at both sites at hourly or half-hourly intervals.

3. Analysis of Results

The objective of the data analysis was to describe as completely as possible the time and space variability of the phase-front after being "crinkled" or distorted in its passage from the lower site to the mountain-top antenna array. In the analysis the time behavior of the phase-front observed at several points was first examined. The resulting time (and frequency) statistics were then used to study 1) the degree of spatial homogeneity of the data gathered along the phase-front, and 2) the spatial covariance of the phase (range) variable, R, and of its spatial differential, ΔR. The correlations of these phase-front statistics with time of day and with several meteorological parameters were finally investigated.

The basic input to the analysis consisted of continuous data from 45 fifteen-minute sample periods -- 5 samples from each of the 9 runs. The only criteria used in selecting the samples were that all variables be free of recording defects and that the sample times be distributed as evenly as possible around the clock. Each sample was digitized at the rate of 25 to (in some cases) 30 points per second, giving a total of 22,000 to 27,000 discrete points per sample per variable. The basic output of the analysis consists of variances, power spectra and cross-correlation coefficients arranged to illustrate the statistical characteristics of the phase-front.

3.1 The variance and power spectrum

A few preliminary comments on these statistics may be helpful in interpreting the results.

The power density spectrum (i.e., the Fourier cosine transform of the autocovariance function) is a widely-used statistical tool for analyzing the variability of a given quantity as well as the covariability of two quantities. It indicates the amount of variance (i.e., mean-squared deviation from the sample mean) contributed by the fluctuations lying in a given band of fluctuation frequencies. Its integral over all fluctuation frequencies is the total sample variance. In the case of discrete data, this relationship is given by

$$s^2(X) = \frac{1}{n-1} \sum_{i=1}^{n} (X_i - \overline{X})^2 = \left[\frac{1}{2} W(f_o) + \sum_{j=1}^{m-1} W(f_j) + \frac{1}{2} W(f_m) \right] \Delta f,$$

where $s^2(X)$ = sample variance of X, determined from n values of X,

$W(f_j)$ = power density (in units of variance per unit bandwidth) in a frequency band of width Δf centered on f_j, and

m = number of non-zero frequencies at which W(f) is estimated in a given computation. (In this analysis m = 100, although for graphical clarity, not all values are plotted.)

In the case of two variables, one can obtain the normalized cospectral density, i.e., the coefficient of cross-correlation of fluctuations occurring in the frequency increment Δf centered on f. If $W_1(f)$, $W_2(f)$, and $W_{(1-2)}(f)$ are the spectral densities of the two variables and of their difference, respectively, the normalized cospectral density is given by

$$C(f) = \frac{W_1(f) + W_2(f) - W_{(1-2)}(f)}{2\sqrt{W_1(f)\, W_2(f)}} .$$

If $W_1(f) = W_2(f) = W(f)$, a valid assumption in most cases discussed in this report, this simplifies to

$$C(f) = 1 - \frac{W_{(1-2)}(f)}{2W(f)} .$$

In this report, most of the variance and correlation data are represented by two sets of values for each sample. One set of results, computed from the "raw" data, includes the entire pass-band of the input data from zero to 1.5 Hz or (in some cases) 1.25 Hz. (The two upper frequency limits resulted from a change-over to new digitizing equipment. Since it has no significant effect on the results, the upper limit is given simply as "approximately 1.4 Hz.") The second set of values, labeled "approximately 0.007 to 1.4 Hz," was obtained by integrating the power spectra over the specified frequency range, i.e., it consists of only that part of the total variance contributed by the frequency band covered by the computed power spectrum. This computation is analogous to passing the continuous data through an infinitely sharp band-pass filter. These "filtered" data variances are of interest because longer-term trends which often dominate the "raw" data have been, in effect, removed prior to the computation of variances, correlation coefficients, etc.

3.2 Range variations

Examples of time variations in range as seen at one antenna are shown in figures 6, 7, and 8. (The abrupt shifts in level occurring whenever the trace nears either edge of the chart are the result of an automatic scale-shift device used to insure that the level stays within the range of the recorder while at the same time permitting maximum resolution.) The power spectra of all 15-minute range data samples are plotted in figures 9 to 17, inclusive. They are shown here to illustrate the wide variability in magnitude of spectral density. For example, the spectral density at 0.1 Hz ranges from about 0.2 to 3×10^{-4} cm^2/Hz. On the other hand, the slope of the spectrum varies only slightly from sample to sample, and is approximately -2.5, the same value that has been obtained repeatedly in previous experiments [Thompson, Janes and Kirkpatrick, 1960; Thompson and Janes, 1964; Janes, Kirkpatrick, Waters, and Smith, 1965]. (In this context, a slope of -2.5 means that the spectral density is proportional to $f^{-2.5}$.)

In these graphs, a distinction is made between day and night samples to illustrate any persistent diurnal effect. However, with the exception of run 2, no such effect was clearly seen. (The dependence of variance on time of day will be discussed in a later section.)

The curve in each figure joins median values and will serve as representative range spectra for comparison with other spectra.

Having examined the spectral characteristics of range variations at each of several locations, we find the next question to be investigated is whether these characteristics are influenced by the particular location of the upper terminal. The map in figure 5 illustrates the very rugged terrain over which the antennas were distributed on Mt. Haleakala, and it would not be unreasonable to ask if the phase-front structure was distorted by the local terrain. To illustrate the spatial homogeneity of the phase-front, the range variances observed simultaneously at pairs of points on the array are compared in figure 18. It can be seen that despite the wide range of variance levels, the variances are highly correlated on paths separated by as much as 790 meters. This suggests that if the mechanisms causing the range variations are influenced by the presence of the mountain, they are at least being influenced uniformly over the 800-meter segment of the phase-front.

One of the most important characteristics of the phase-front is the so-called spatial correlation of range at an instant of time as a function of separation. In the absence of a continuous record of range versus position along the phase-front, this spatial correlation function can be estimated by the time cross-correlation of range variations observed at pairs of points as a function of separation.

Some caution must be exercised in making this estimation of spatial correlation from time correlation, however. This is because the coefficient of cross-correlation of time variations in range is a function not only of path separation but also of the spectral frequency pass-band over which the data are being examined. For example, figure 19 shows the correlation coefficients of range versus upper terminal separation, using first "raw" data (nominal pass-band 0 to 1.4 Hz) and then the "filtered" data (using only the pass-band covered by the power spectra, i.e., about 0.007 to 1.4 Hz). The line segments join median values of correlation at each separation. The necessity for specifying the data pass-band is obvious in this figure. It should also be borne in mind that the finite sample length itself acts as a high-pass filter in that it removes variance contributions from frequencies that are low compared to the reciprocal of the sample length. For example, if one-hour sample periods had been used instead of 15 minutes, the "raw" data correlations (0 to 1.4 Hz) would have, in general, been higher than those shown.

The spectral distribution of correlation can be examined by comparing the power spectra of range (R) and range difference (ΔR), as explained in section 3. 1. This is done in figures 20, 21, and 22, using the median spectra from the range spectrum graphs discussed previously, along with the corresponding median spectra of range difference data. (The individual ΔR spectra from which the latter were obtained are shown in figures 38 to 46, inclusive.)

Keeping in mind that the extent to which the ΔR spectrum falls below twice the level of the R spectrum is a measure of the correlation of the two R variables (section 3. 1), two characteristics of phase-front variations are shown clearly in these figures. Firstly, the correlation of the two R variables at a given separation decreases with increasing spectral frequency until a critical frequency is reached beyond which the ΔR spectral density is approximately equal to twice that of R, indicating a complete lack of correlation. (Because of random sampling errors and the use of median spectra, these spectral density relationships are only approximately fulfilled in these graphs.) Secondly, the minimum frequency above which the ranges are uncorrelated and the degree of correlation at any lower frequency are both inverse functions of path separation. Note, for example, that the range variations on paths separated by 1.25 meters (run 3, figure 20) are well correlated over the entire spectrum frequency range, 0.01 to about 1.5 Hz, while those at separations of 790 meters (run 6, figure 21) show no correlation whatever in the same two-decade band. At a separation of 10 meters (runs 1 and 2, figure 20) the critical frequency dividing correlated and uncorrelated regions appears to be about 0.1 Hz.

3.3 Range difference variations

An analysis somewhat analogous to the range analysis can be made of the range difference (ΔR) data, which represent time variations in the space differential of the phase-front. It was seen in connection with the correlation analysis in the previous section that the spectral density of ΔR at low frequencies decreases with decreasing path separation. The corresponding dependence of ΔR variance on path separation is shown in figure 23, where again the "raw" or total variances are compared to the "filtered" variances computed only for the frequency band covered by the spectra. It is not surprising that the latter process, which in effect removes low frequency trends from the data before computing the variance, produces a relatively larger reduction in variance at the large separations, where trends are more evident, than at the small separations. This effect shows up as a reduction in the slope of the points in the right-hand graph in figure 23.

It is interesting to note that if the deviation of the observed phase-front from a non-crinkled (free-space) phase-front could be depicted by a simple wedge-shaped distortion that prevailed over the whole phase-front, the points would fall on a line with slope of + 2. It is clear that the data in both graphs fail to conform to this simple model, and if the data had been filtered further to remove more low-frequency variance (e.g., by using shorter samples) the departure of the data from this model would have been even greater. This again emphasizes the caution that must be exercised in deriving spatial statistics from time data.

Figures 24, 25, and 26 show a comparison of pairs of range difference variances obtained simultaneously at different parts of the phase-front. As in the case of the range data, there appears to be good spatial homogeneity in the phase difference data. In other words, these graphs suggest that the ΔR data were not contaminated in any persistent way by local terrain features along the mountain top.

The question of correlation of range difference variations at different points on the phase-front is complicated by a spectral frequency dependence similar to that already observed in the range data. To illustrate this, a comparison is made in figure 27 of the power spectra of range differences (ΔR) and of the difference of two ΔR variables ($\Delta^2 R$), using medians of the individual spectra in both cases. Here again, correlation is indicated by the amount by which the $\Delta^2 R$ spectrum falls below twice the ΔR spectrum (see section 3.1). In this figure all ΔR data were recorded on adjoining path pairs, i.e., one path was common to both pairs. The 1.25- and 2.5-meter pairs in run 3 show high correlation at the lower frequencies, but none of the other pairs show definite correlation over this spectral frequency region, with the possible exception of the 10-meter pair in run 1. Figure 28 shows a similar comparison for separated path pairs, and it is clear that the correlation is negligible over the entire two decades from 10^{-2} to 1 cycle per second.

The cross-correlation coefficients computed from the 15-minute ΔR samples are plotted in figure 29 for both "raw" and "filtered" data. The abscissa is the separation of the path pairs, measured from their centers. Comparing these spatial correlation functions for ΔR with the corresponding graphs for the range data (figure 19), it can be seen that the ΔR correlations decrease more rapidly with increasing separation. It is also interesting to note that "filtering" the data has less effect on the range difference correlation function than on the range correlation functions. This is because the ΔR variances are not as dominated by low frequency contributions, and hence eliminating the latter before computing the correlation coefficient has relatively less effect on the result.

A significant feature of the range difference correlation functions is that the correlation is negligible for all spacings (between centers of path pairs) greater than about 20 meters, regardless of the antenna separation within each pair. (Note that for all spacings of 20 meters or less, the path pairs adjoin, i.e., one path was common to each pair.) It should be borne in mind that in general, reducing the sample length below the 15 minutes used here would reduce the correlation further. Since any system involving a moving air-borne or space terminal would probably have considerably less than 15 minutes available to make an angle determination from ΔR data, the correlations shown here are almost certainly higher than could be realized in an operational situation.

3.4 Variances of R and ΔR versus time of day and/or meteorological parameters

It has been evident throughout this investigation that the variances of the 15-minute samples of range and range difference vary widely from sample to sample. Although this variability is to be expected in any sampling process, it should be determined how much of this variability in sample variances can be traced to a dependence on time of day or on various meteorological data. Any such dependence would be valuable in predicting periods of increased phase-front distortion.

In figure 30, the range variances of all 15-minute samples are plotted versus time of day. As before, both "raw" and "filtered" data (pass bands: 0 to 1.4 and 0.007 to 1.4 Hz, respectively) are shown. Neither variance shows a clear-cut diurnal pattern, except for a slight reduction in the spread or range of variance values from about 0800 to 1400. In the case of the filtered data, there also appears to be a reduction in the variance level around 0600.

The corresponding range difference variances are plotted versus time of day in figures 31 and 32. Here a slightly more definite diurnal pattern can be seen. In both the raw data of figure 31 and the filtered data in figure 32, there is a tendency for the variances to increase gradually during the daylight hours, reach a maximum in late afternoon, and then subside slowly during the evening. For example, at the smaller separations (1. 25 to 10 meters) the average variance increases by a factor of about 10 from early morning to mid-afternoon.

The search for relationships between range or range difference variance and refractive index or other meteorological variables was considerably less fruitful. Since the radio range is proportional to the average refractive index along the path, the range variance might be expected to be proportional to the refractive index variance observed at a point on the path. To check this possibility, in figure 33, the range variances are compared to the corresponding variances of refractive index (expressed in refractivity (N) units) recorded at the lower site. It is clear from these graphs that no close relationship exists in these sample statistics.

Similarly, in figures 34 to 37, inclusive, the range variances and the difference variances for three representative path separations are compared with air temperature, refractivity and wind speed observed at the upper and lower sites. The temperature and refractivity values were estimated by interpolation of the meteorological data read at half-hour intervals at the upper site and hourly at the lower. The wind speeds were taken from the continuous anemometer recordings by visually estimating the average speed during each of the 15-minute sample periods. (The data pass-bands noted in the figures refer, of course, only to the radio data.)

The purpose of these graphs is to illustrate any obviously strong correlations. The number of data points available, especially in the case of the range differences, is too small to justify a sophisticated search for subtle correlations, especially since weak correlations would be of little value operationally. The strongest correlations appear to be between variance and wind speed at the lower site, and even these are not impressive. The correlation coefficients of the logarithm of variance versus wind speed in each case is listed below:

	Radio data pass-band	
Variable	0 to 1.4 Hz	0.007 to 1.4 Hz
Range	+0.42	+0.60
Range Difference		
5-meter path separation	+0.52	+0.36
40-meter path separation	+0.21	+0.56
750-790-meter path separation	+0.54	+0.07

4. Summary and Conclusions

In this experiment a study has been made of the statistical structure of the elevated phase-front of a ground-based microwave signal that has been distorted by propagation through the lower layers of the troposphere. Time statistics of phase-front variations (in terms of radio slant range and range difference) have been examined with the spacing of the several phase sensors along the phase-front as a parameter.

The principal results can be summarized as follows:

1. Although the antennas for the phase measurements at the upper site were mounted on very uneven terrain on a mountain summit, the results obtained at various points of the array indicated no significant bias as a function of sensor antenna location. Although it is probable that the presence of the mountain did have some effect on the data, it appears that any such effect was uniform over the entire segment of the

phase-front "seen" by the mountain-top array. Although the influence of the mountain is difficult to assess quantitatively, results obtained in a companion experiment at this site sponsored by the U. S. Air Force Electronic Systems Division lend support to a belief that such an influence was small in at least some respects. In the latter experiment a comparison was made of the refractive index profiles measured with an airborne refractometer in vertical ladder flights near the lower terminal as opposed to profiles from slant descent flights directly down the radio path. No systematic difference was found between these two types of profile, indicating that the mountain had no significant effect on long-term (e.g., hour-to-hour) changes in average refractive index along the radio path. Its effect on short-term phase statistics, however, is unknown.

2. The cross-correlation of range variations at separated points on the phase-front was investigated as a function of path separation. Although spatial correlation functions are shown, it is emphasized that the cross-correlation of range variations on two paths is not only a function of their separation but also of the sample length and the fluctuation frequency pass-band of the range data. For this reason, application to a particular system will require careful modification of these results to fit the effective pass-band of the system.

3. Similarly, the cross-correlation of range difference variations on both adjoining and separated pairs of paths was studied. It was found to drop off more rapidly with increasing separation than did the range data, although here again the spectral frequency dependence of the correlation was evident. Using 15-minute samples, the correlation of range difference variables was negligible when the distance between path pairs exceeded about 20 meters regardless of the path separation within each pair. Reducing the sample length further would, in general, have reduced the correlation at a given separation accordingly.

4. An analysis of the range and range difference variances of 15-minute samples revealed little or no significant dependence on several meteorological parameters (i.e., temperature, pressure, refractive index, wind speed at both terminals). The range variance was not found to be correlated with time of day or with the variance of refractive index observed at the lower terminal. On the other hand, the range difference variances (especially for small antenna separations) did show a definite diurnal pattern, with values during the afternoon hours on the order of 10 times larger than night-time values.

5. Appendix

In addition to the material discussed in preceding sections of this report, there were other data recorded and processed in the course of the experiment which are not discussed in detail here but which may prove helpful in further interpretation of the results, and are of interest from the standpoint of basic radio propagation research.

Figures 38 through 46 show the power spectra of all range difference samples, plotted to distinguish between day-time and night-time samples. The medians of these sample spectra, represented by the line through the points in each graph, were used in comparing range and range difference spectra in section 3.2.

Figures 47 through 55 show long-term variations in range observed at one point on the phase-front along with refractivity and relative humidity computed from meteorological data taken at each site. The corresponding air temperature, pressure and wind velocity data are plotted in figures 56 through 64.

To show cloud activity during (or near) each of the day-time sample periods, the appropriate path photographs taken at each path terminal are shown in figures 65 through 73. The locations of upper and lower sites are indicated on figure 69.

Tables II through V list variances of range and first and second range differences computed from all of the 15-minute sample periods. These tables include "raw" variances (pass-band: approximately 0 to 1.4 Hz) computed directly from the digitized data, and "filtered" variances (pass-band: approximately 0.007 to 1.4 Hz) computed by integrating the power spectra over that frequency range.

6. References

Janes, H. B., A. W. Kirkpatrick, D. M. Waters, and D. Smith (Apr. 12, 1965) Phase and amplitude diversity in over-water transmissions at two microwave frequencies, NBS Technical Note 307.

Janes, H B., and M. C. Thompson, Jr. (Nov. 1964) Errors induced by the atmosphere in microwave range measurements, Radio Sci. J. Res. NBS/USNC-URSI, 68D, No. 11, 1229-1235.

Norton, K. A., J. W. Herbstreit, H. B. Janes, K. O. Hornberg, C. F. Peterson, A. F. Barghausen, W. E. Johnson, P. I. Wells, M. C. Thompson, Jr., M. J. Vetter, and A. W. Kirkpatrick (1961), An experimental study of phase variations in line-of-sight microwave transmissions, NBS Monograph 33.

Thompson, M. C., Jr., H. B. Janes, and A. W. Kirkpatrick (Jan. 1960), An analysis of time variations in tropospheric refractive index and apparent radio path length, J. Geophy. Res. 65, No. 1, 193-201.

Thompson, M. C., Jr., and H. B. Janes (Nov. 15, 1964), Radio path length stability of ground-to-ground microwave links, NBS Technical Note 219.

Thompson, M. C., Jr., and M. J. Vetter (Feb. 1958), Single path phase measuring system for three-centimeter radio waves, Rev. Sci. Instru. 29, No. 2, 148-150.

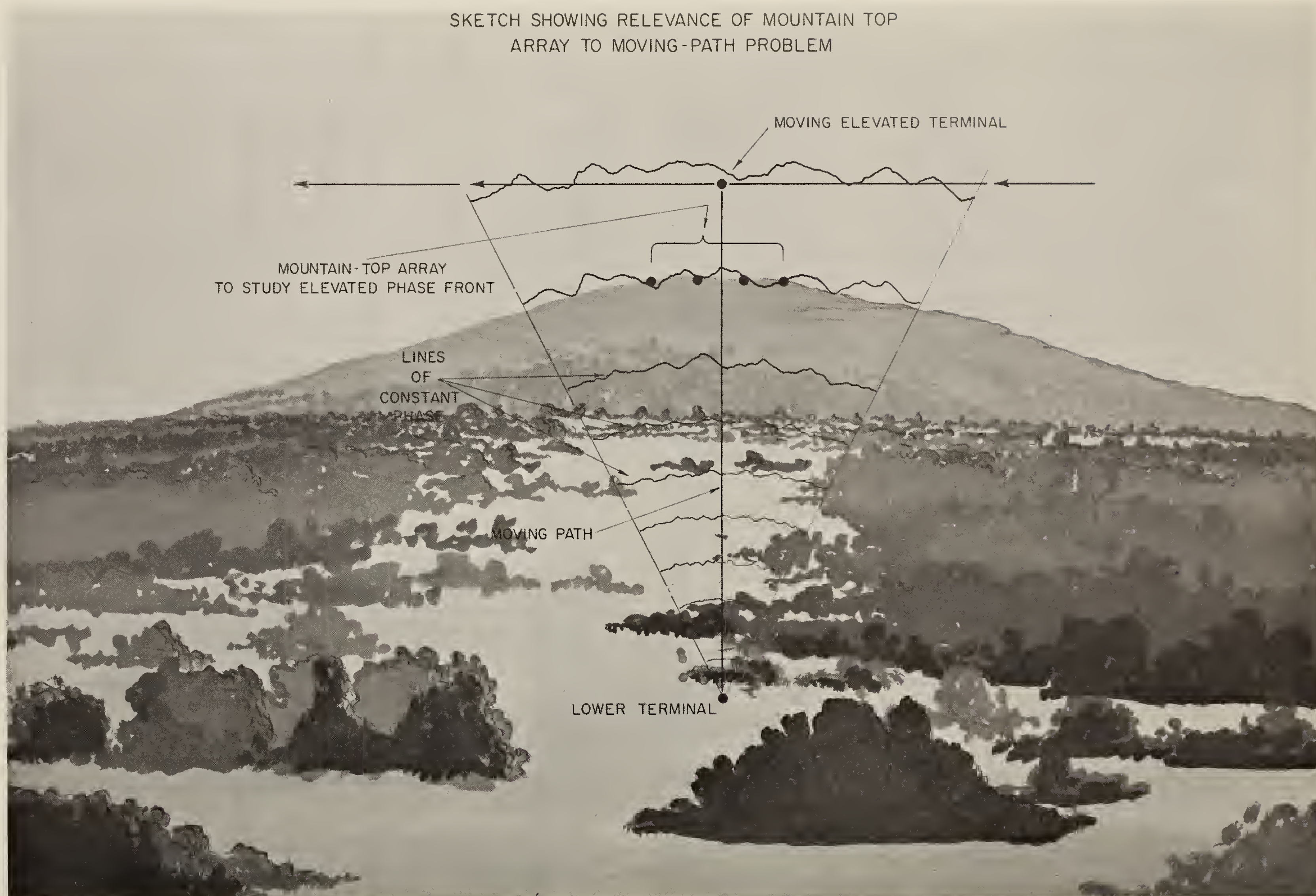
SKETCH SHOWING RELEVANCE OF MOUNTAIN TOP
ARRAY TO MOVING-PATH PROBLEM
MOVING ELEVATED TERMINAL
MOUNTAIN-TOP ARRAY
TO STUDY ELEVATED PHASE FRONT
LINES
OF
CONSTANT
PHASE
MOVING PATH
LOWER TERMINAL

Figure 1

LOCATION OF PROPAGATION PATH USED IN MAUI EXPERIMENT

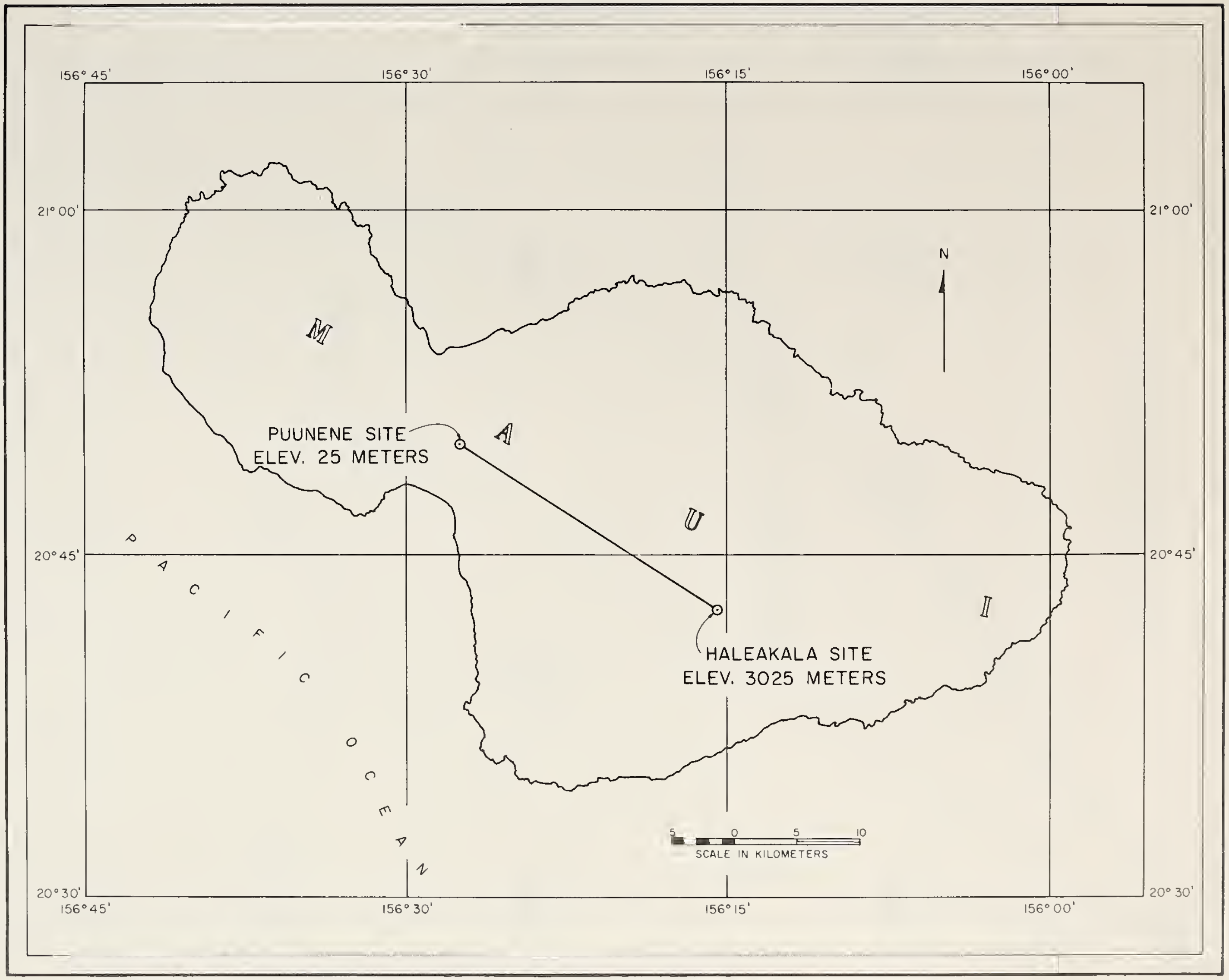

Figure 2

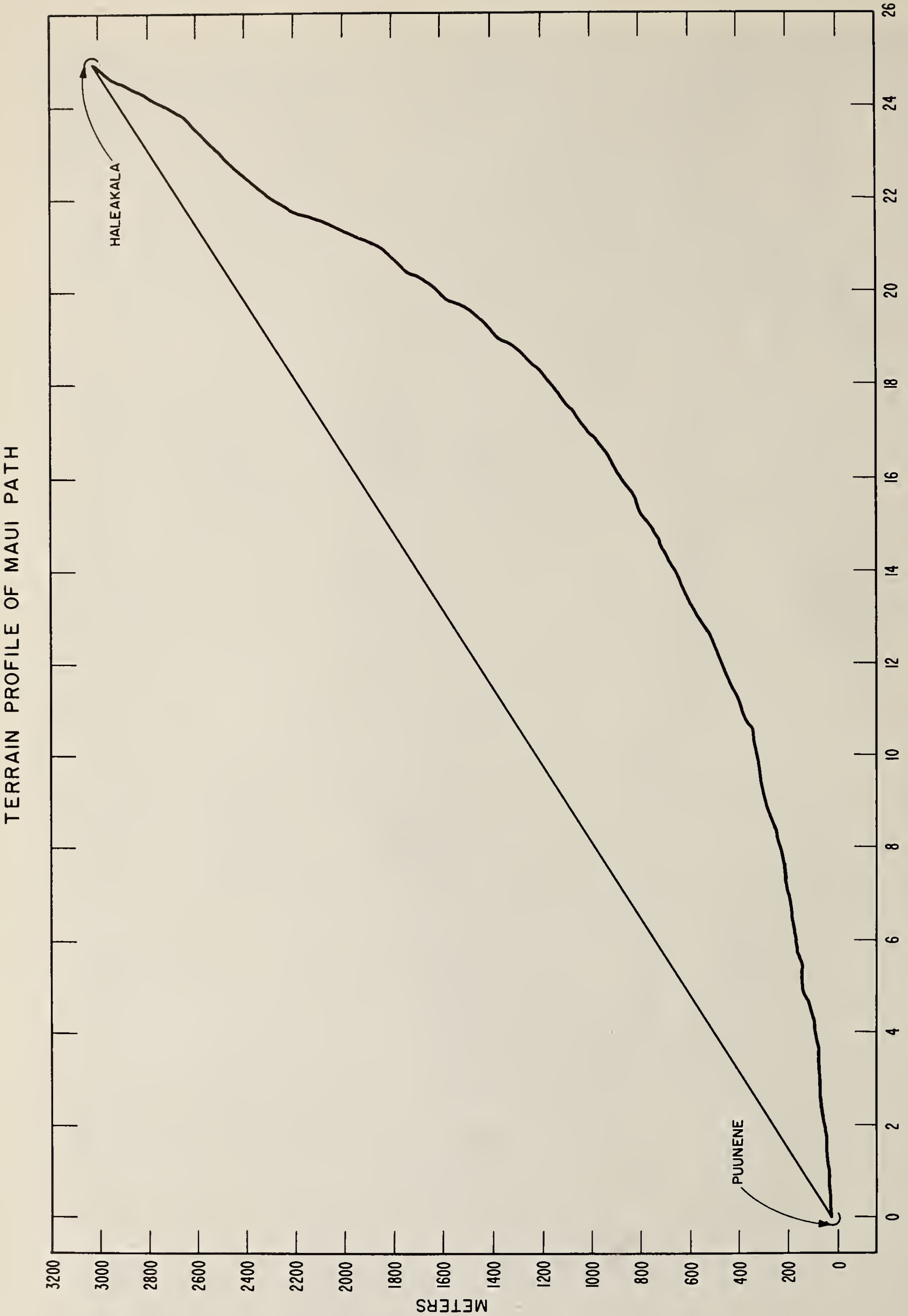
TERRAIN PROFILE OF MAUI PATH
HALEAKALA
PUUNENE
METERS
3200
3000
2800
2600
2400
2200
2000
1800
1600
1400
1200
1000
800
600
400
200
0
km
0
2
4
6
8
10
12
14
16
18
20
22
24
26

Figure 3

ANTENNA AND ANEMOMETER ARRANGEMENTS AT UPPER (HALEAKALA) TERMINAL

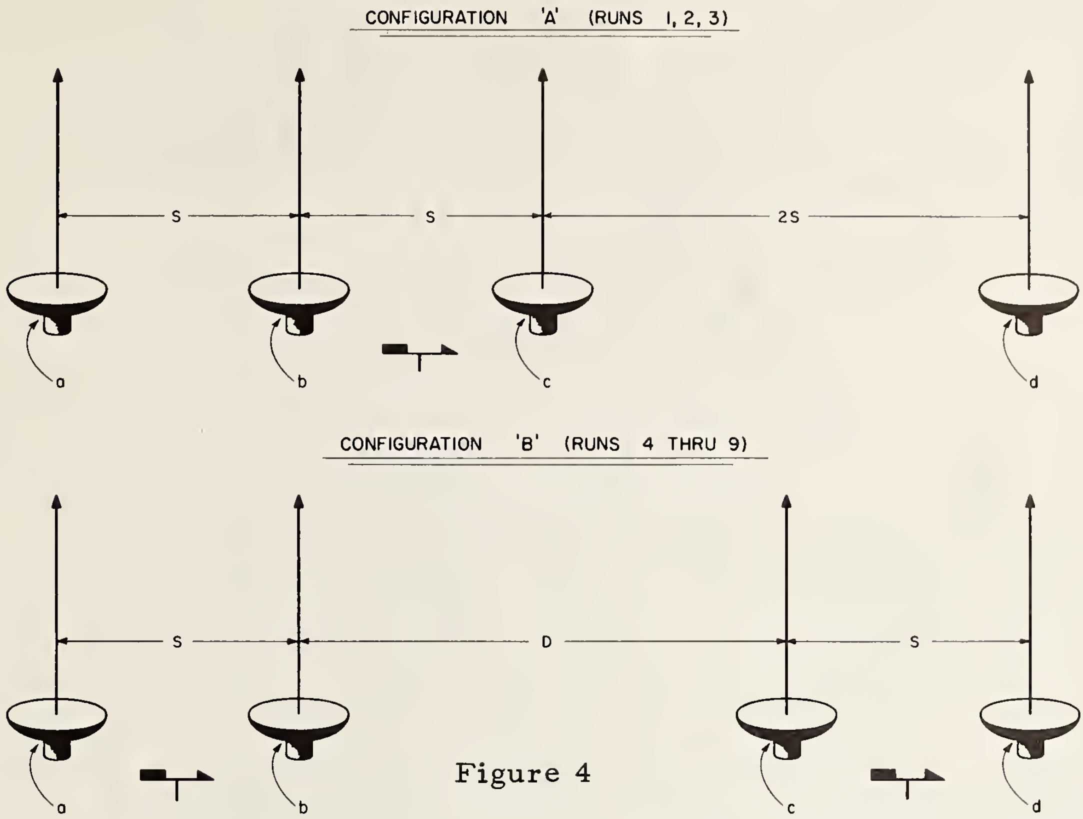

Figure 4

TABLE I

Schedule of Recording Periods

Run	Period (local time)	Configuration	S	D	Antenna Locations
1	1000 June 29 - 1020 June 30	A	10. m	-	7, 9, 13, 14
2	1355 June 30 - 1415 July 1	A	2.5	-	9, 11, 12, 13
3	1749 July 1 - 1645 July 2	A	1.25	-	9, 10, 11, 12
4	0855 July 7 - 0811 July 8	B	40.	105. m	7, 14, 16, 18
5	1302 July 9 - 1300 July 19	B	10.	165.	7, 9, 17, 18
6	0800 July 15 - 0615 July 16	B	185.	605.	1, 5, 7, 18
7	1300 July 16 - 1630 July 17	B	90.	660.	1, 4, 6, 15
8	1528 July 21 - 1400 July 22	B	20.	770.	1, 3, 7, 13
9	1553 July 22 - 1500 July 23	B	5.	785.	1, 2, 7, 8

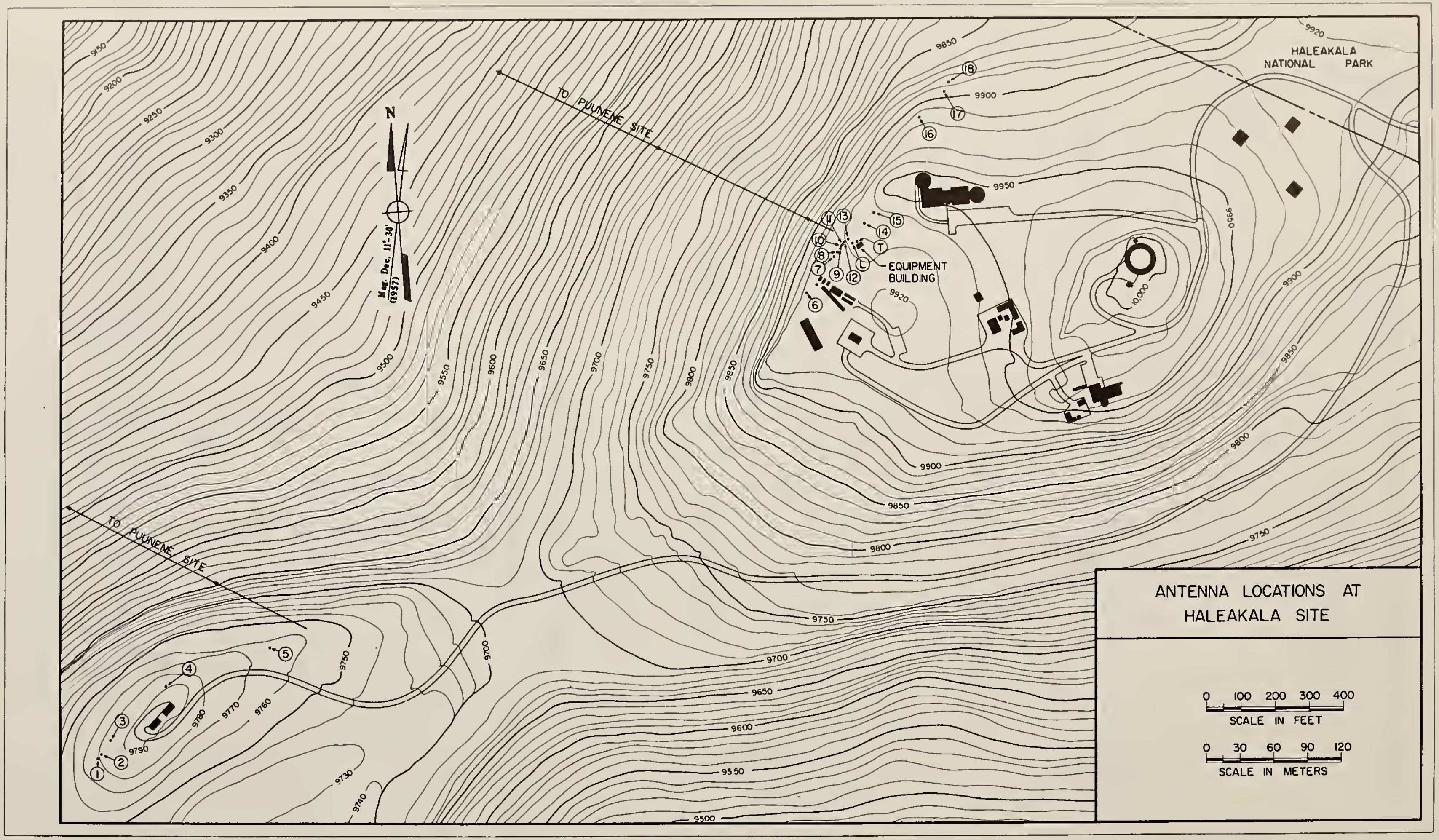
ANTENNA LOCATIONS AT
HALEAKALA SITE
0 100 200 300 400
SCALE IN FEET
0 30 60 90 120
SCALE IN METERS
HALEAKALA
NATIONAL PARK
TO PUUNENE SITE
TO PUUNENE SITE
EQUIPMENT
BUILDING
N
Mag. Dec. 11°-30'
(1957)
10,000
9950
9920
9900
9850
9800
9750
9700
9650
9600
9550
9500
9450
9400
9350
9300
9250
9200
9150
9790
9780
9770
9760
9740
9730

Figure 5

SAMPLE CHART RECORDINGS FROM RUN 1

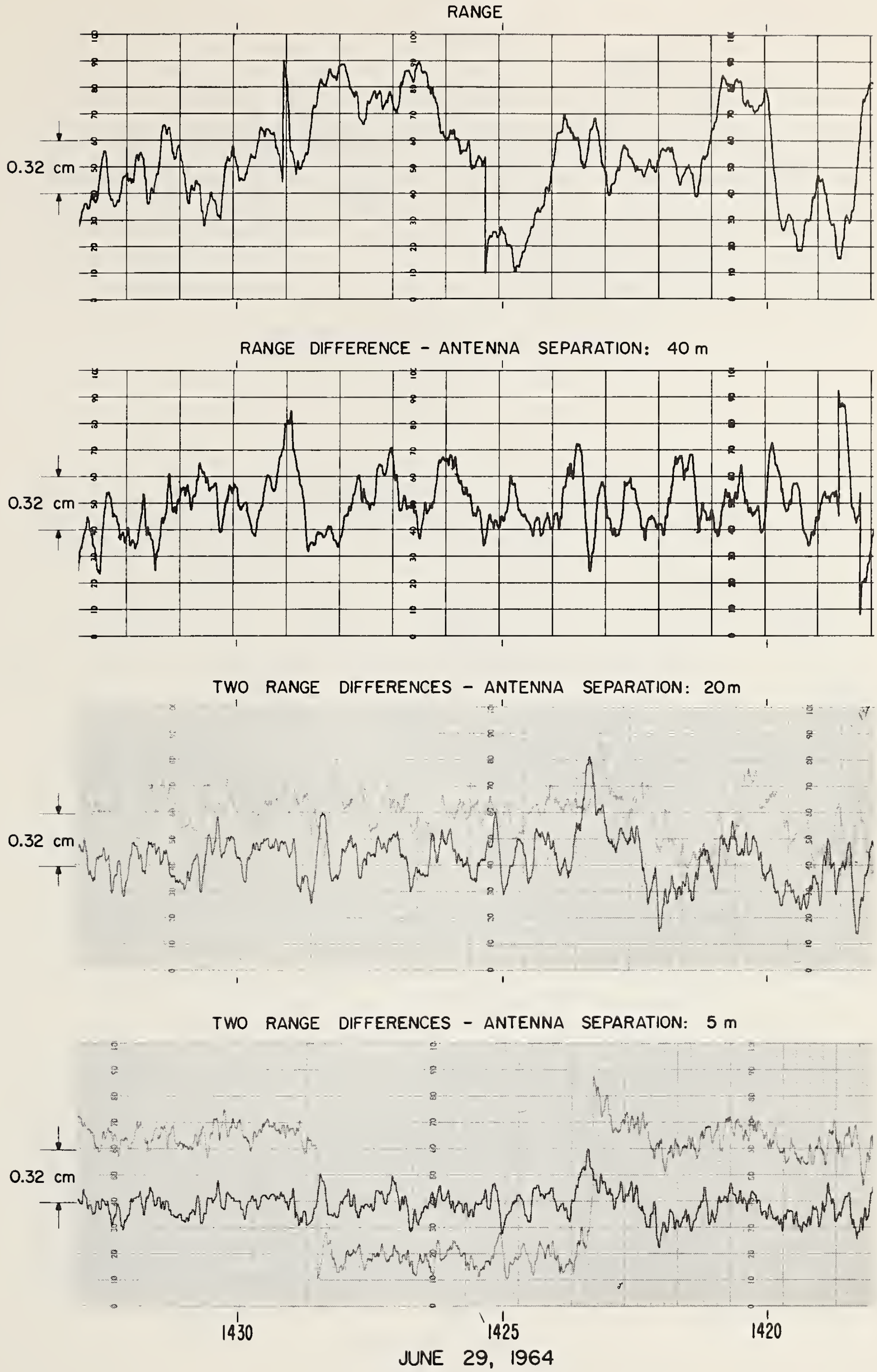

Figure 6

SAMPLE CHART RECORDINGS FROM RUN 2

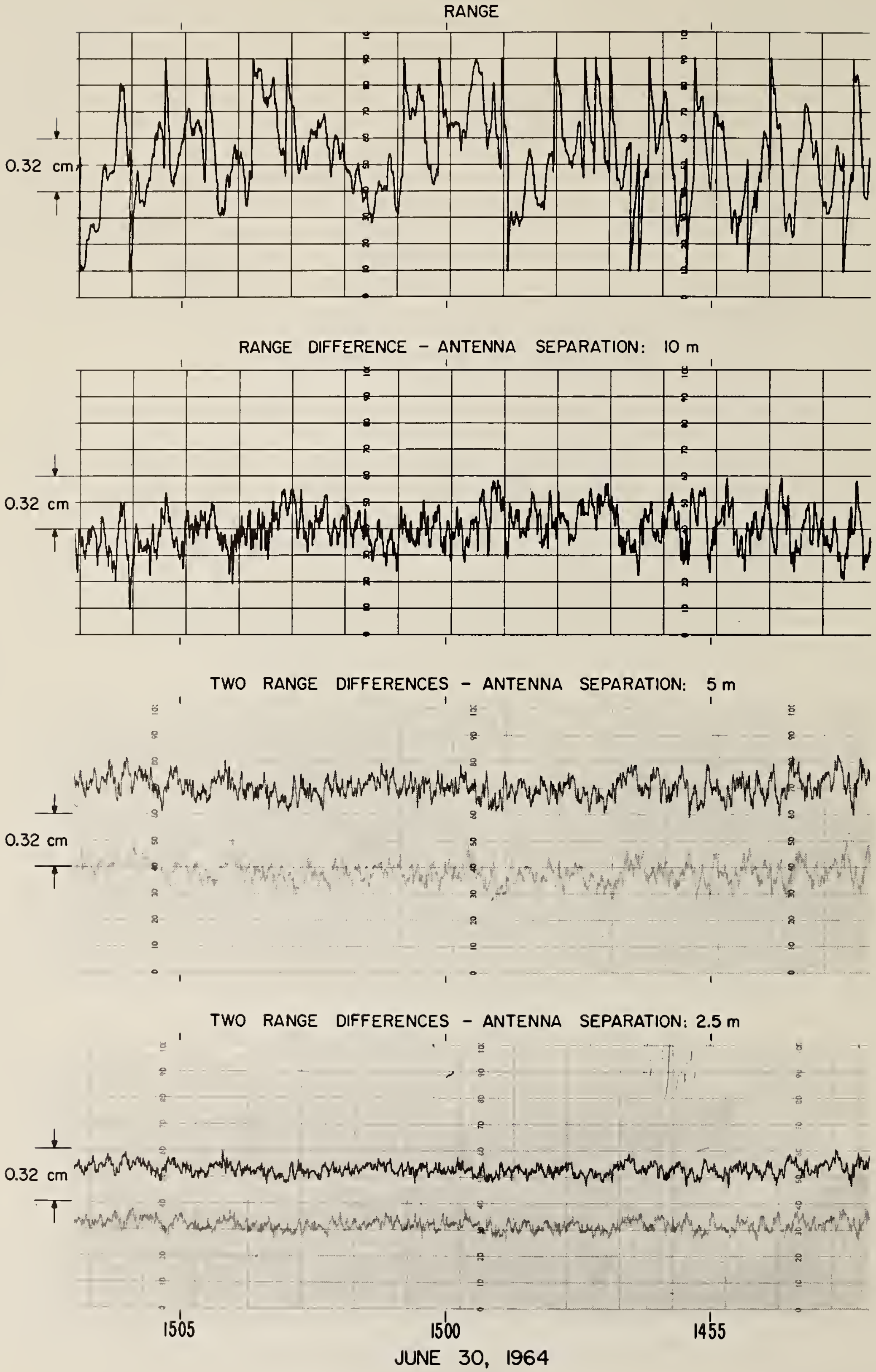

Figure 7

SAMPLE CHART RECORDINGS FROM RUN 6

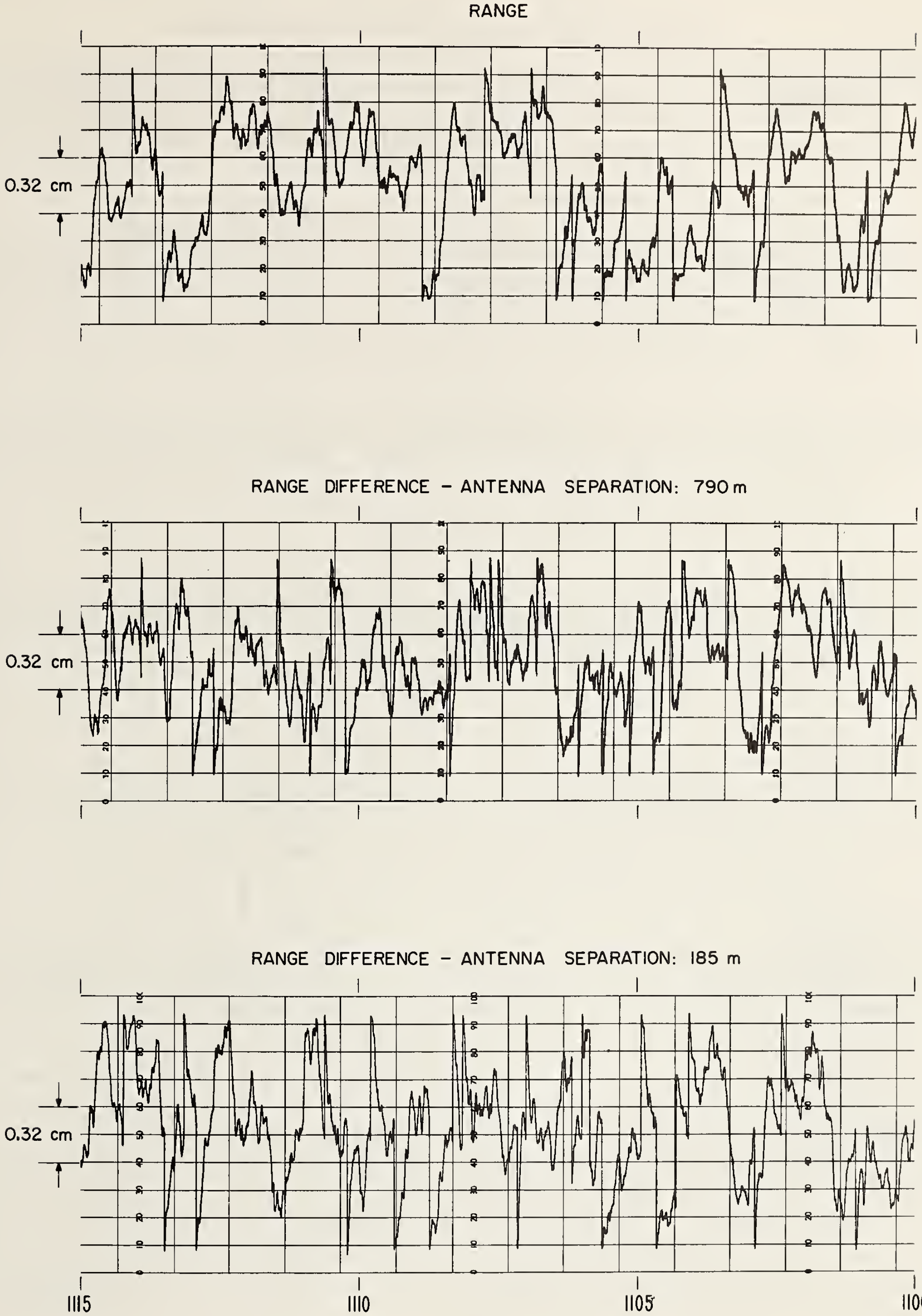

JULY 15, 1964

Figure 8

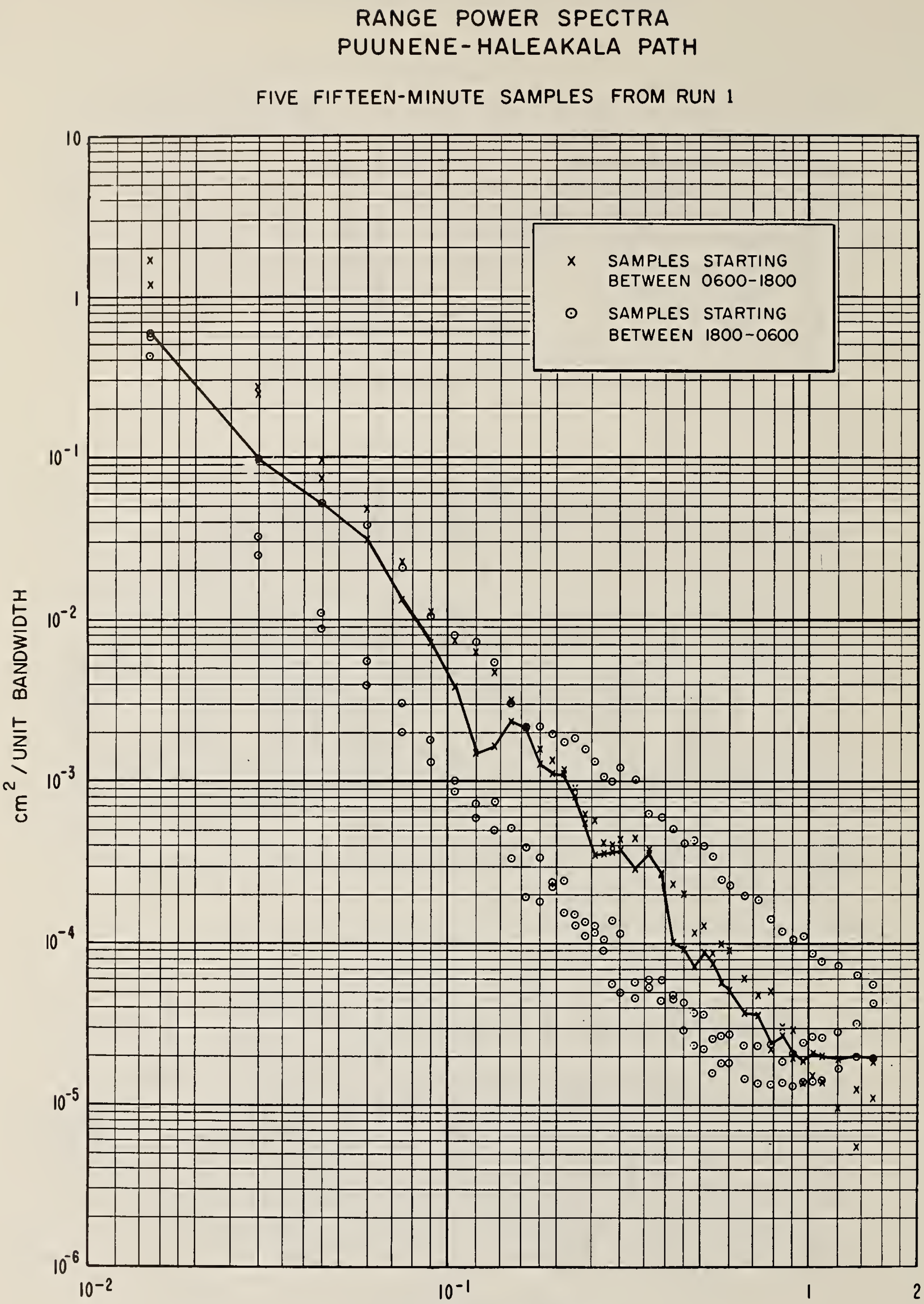
RANGE POWER SPECTRA
PUUNENE-HALEAKALA PATH
FIVE FIFTEEN-MINUTE SAMPLES FROM RUN 1
SAMPLES STARTING BETWEEN 0600-1800
SAMPLES STARTING BETWEEN 1800-0600
cm^2 / UNIT BANDWIDTH
CYCLES PER SECOND
10
1
10^{-1}
10^{-2}
10^{-3}
10^{-4}
10^{-5}
10^{-6}
10^{-2}
10^{-1}
1
2

Figure 9

RANGE POWER SPECTRA
PUUNENE-HALEAKALA PATH

FIVE FIFTEEN-MINUTE SAMPLES FROM RUN 2

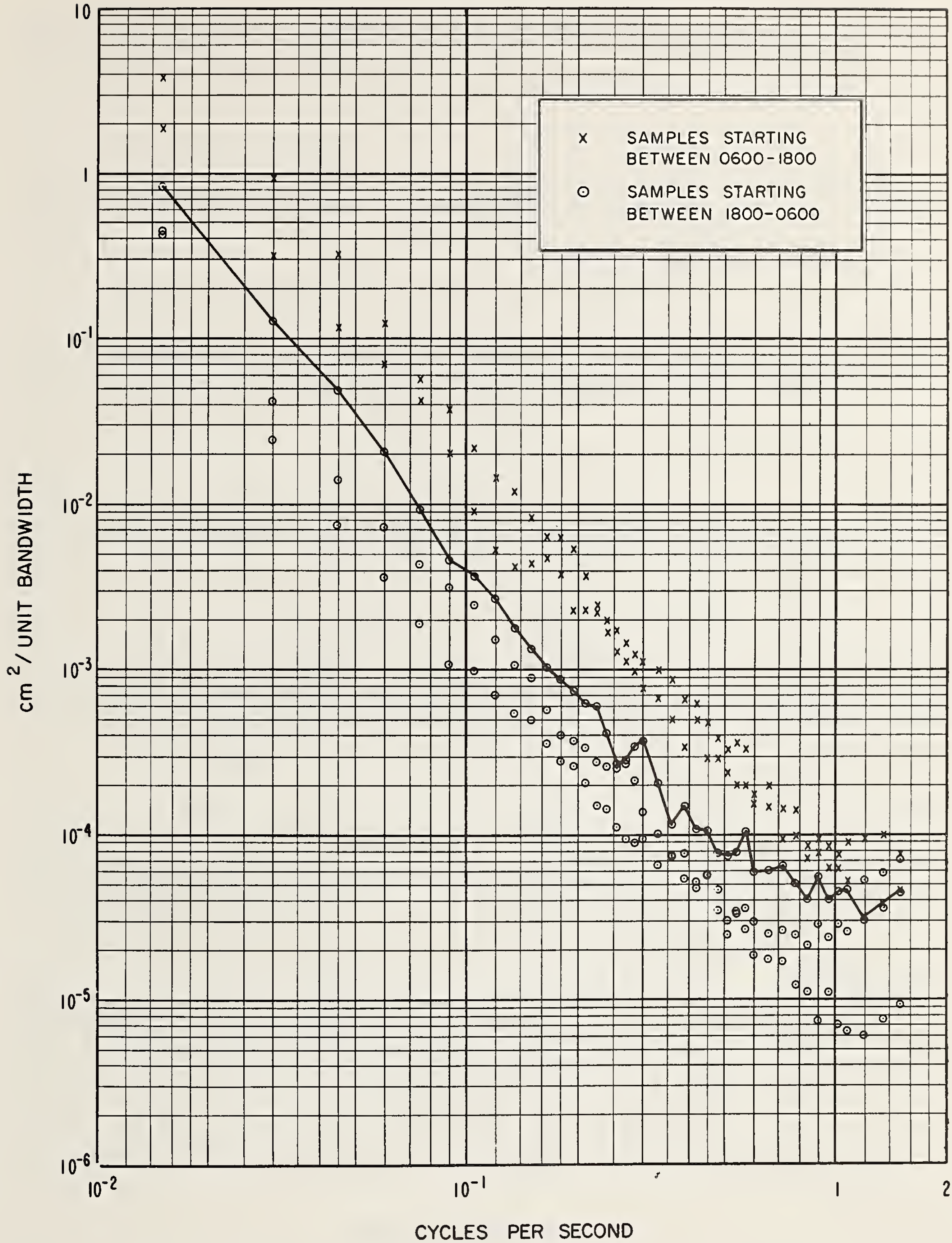

Figure 10

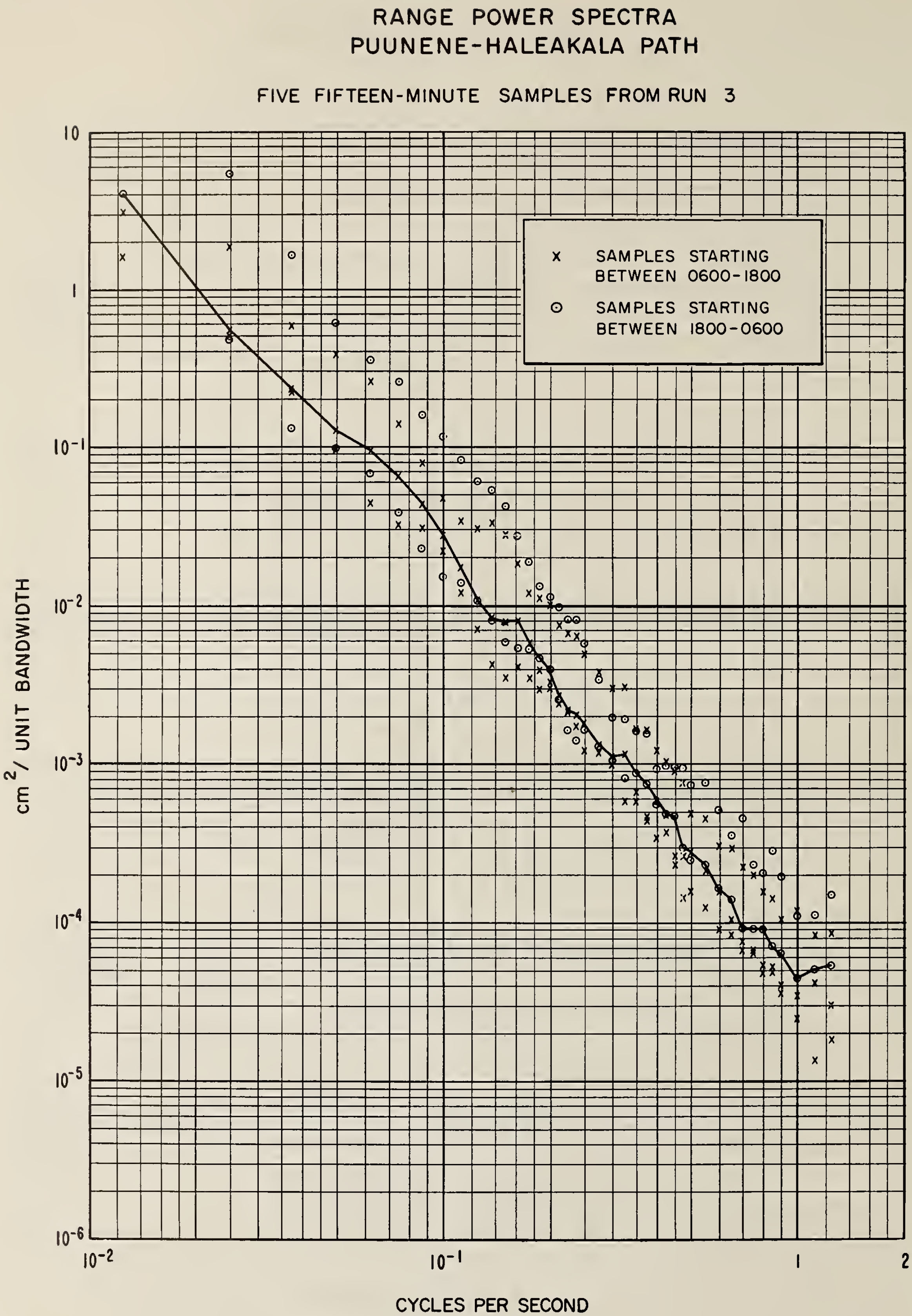
RANGE POWER SPECTRA
PUUNENE-HALEAKALA PATH
FIVE FIFTEEN-MINUTE SAMPLES FROM RUN 3
x SAMPLES STARTING BETWEEN 0600-1800
⊙ SAMPLES STARTING BETWEEN 1800-0600
cm²/ UNIT BANDWIDTH
CYCLES PER SECOND
10
1
10^{-1}
10^{-2}
10^{-3}
10^{-4}
10^{-5}
10^{-6}
10^{-2}
10^{-1}
1
2

Figure 11

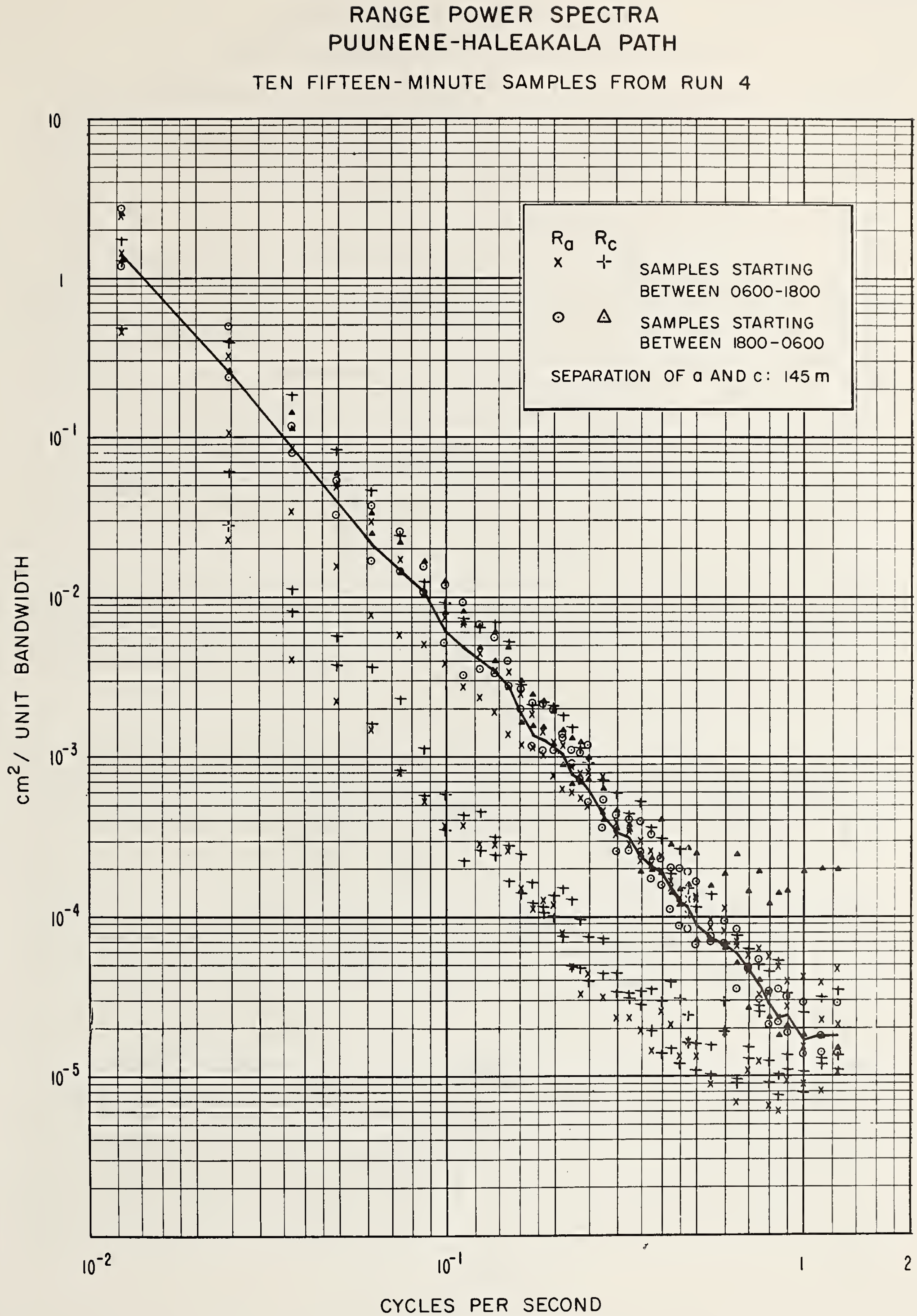
RANGE POWER SPECTRA
PUUNENE-HALEAKALA PATH
TEN FIFTEEN-MINUTE SAMPLES FROM RUN 4
R_a R_c
x +
SAMPLES STARTING BETWEEN 0600-1800
⊙ △
SAMPLES STARTING BETWEEN 1800-0600
SEPARATION OF a AND c: 145 m
10
1
10^{-1}
10^{-2}
10^{-3}
10^{-4}
10^{-5}
cm^2/ UNIT BANDWIDTH
10^{-2}
10^{-1}
1
2
CYCLES PER SECOND

Figure 12

RANGE POWER SPECTRA
PUUNENE-HALEAKALA PATH

TEN FIFTEEN-MINUTE SAMPLES FROM RUN 5

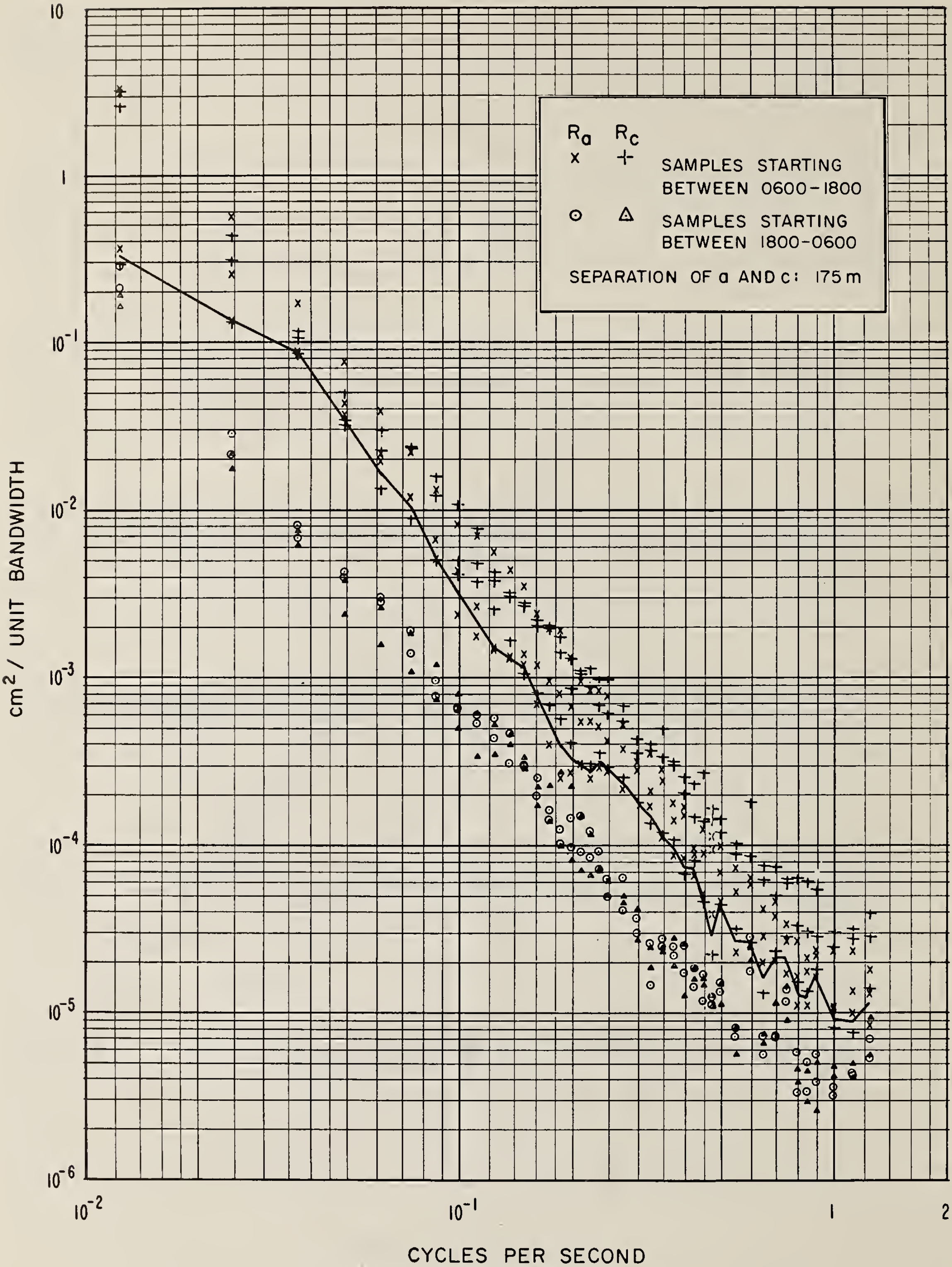

Figure 13

RANGE POWER SPECTRA
PUUNENE-HALEAKALA PATH

TEN FIFTEEN-MINUTE SAMPLES FROM RUN 6

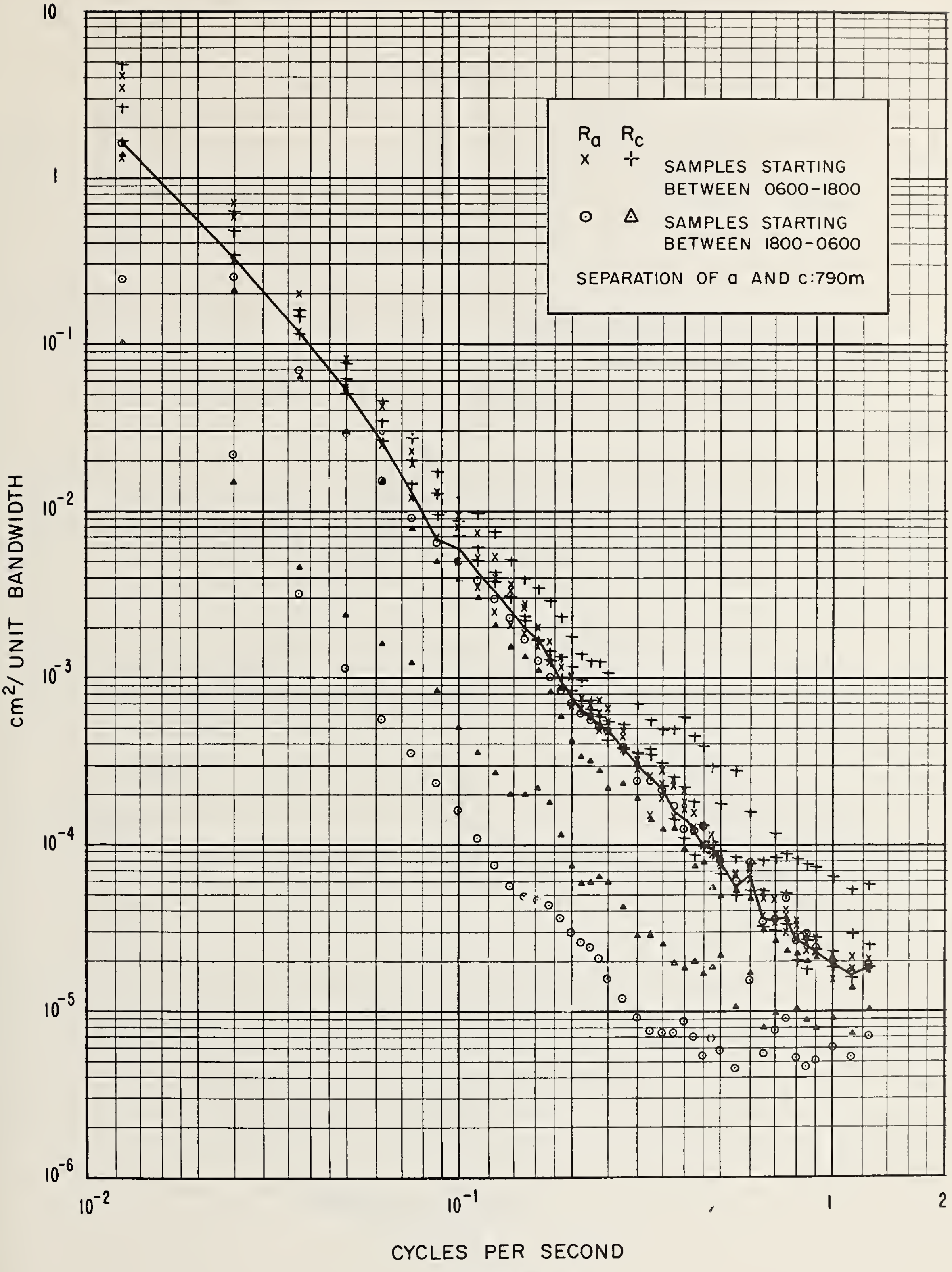

Figure 14

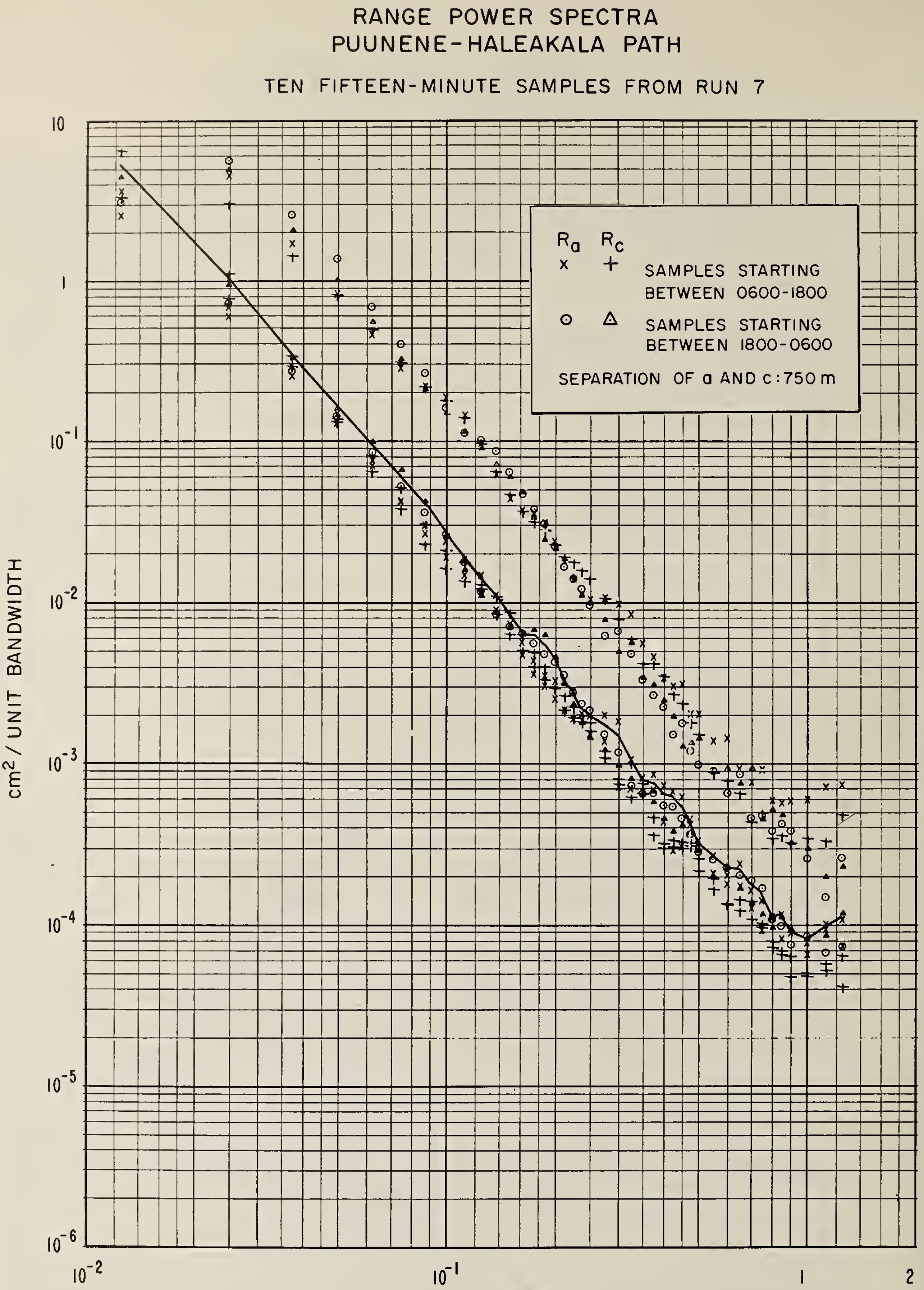
RANGE POWER SPECTRA
PUUNENE-HALEAKALA PATH
TEN FIFTEEN-MINUTE SAMPLES FROM RUN 7
R_a R_c
SAMPLES STARTING BETWEEN 0600-1800
SAMPLES STARTING BETWEEN 1800-0600
SEPARATION OF a AND c: 750 m
cm^2 / UNIT BANDWIDTH
10
1
10^{-1}
10^{-2}
10^{-3}
10^{-4}
10^{-5}
10^{-6}
10^{-2}
10^{-1}
1
2
CYCLES PER SECOND

Figure 15

RANGE POWER SPECTRA
PUUNENE-HALEAKALA PATH

TEN FIFTEEN-MINUTE SAMPLES FROM RUN 8

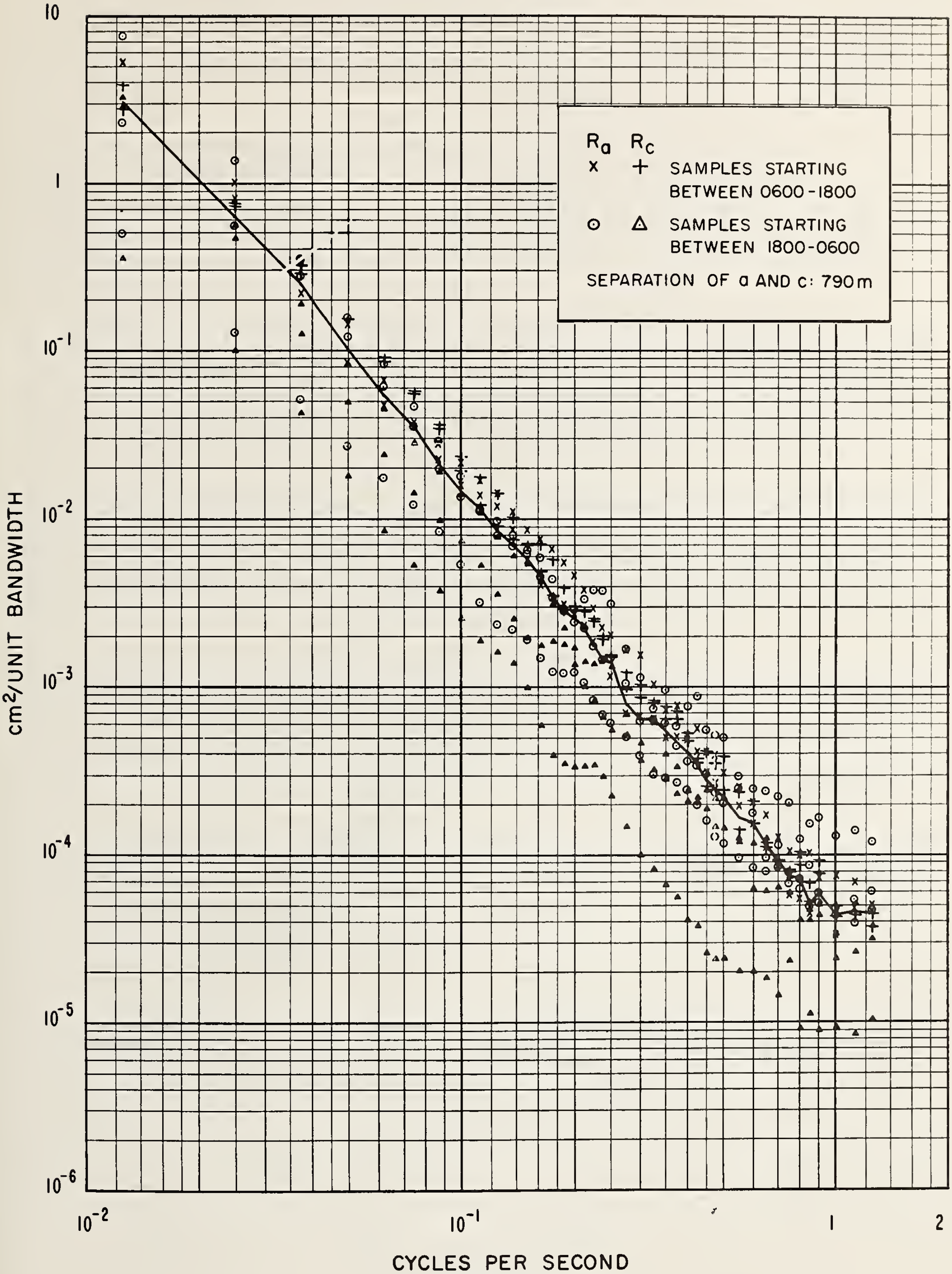

Figure 16

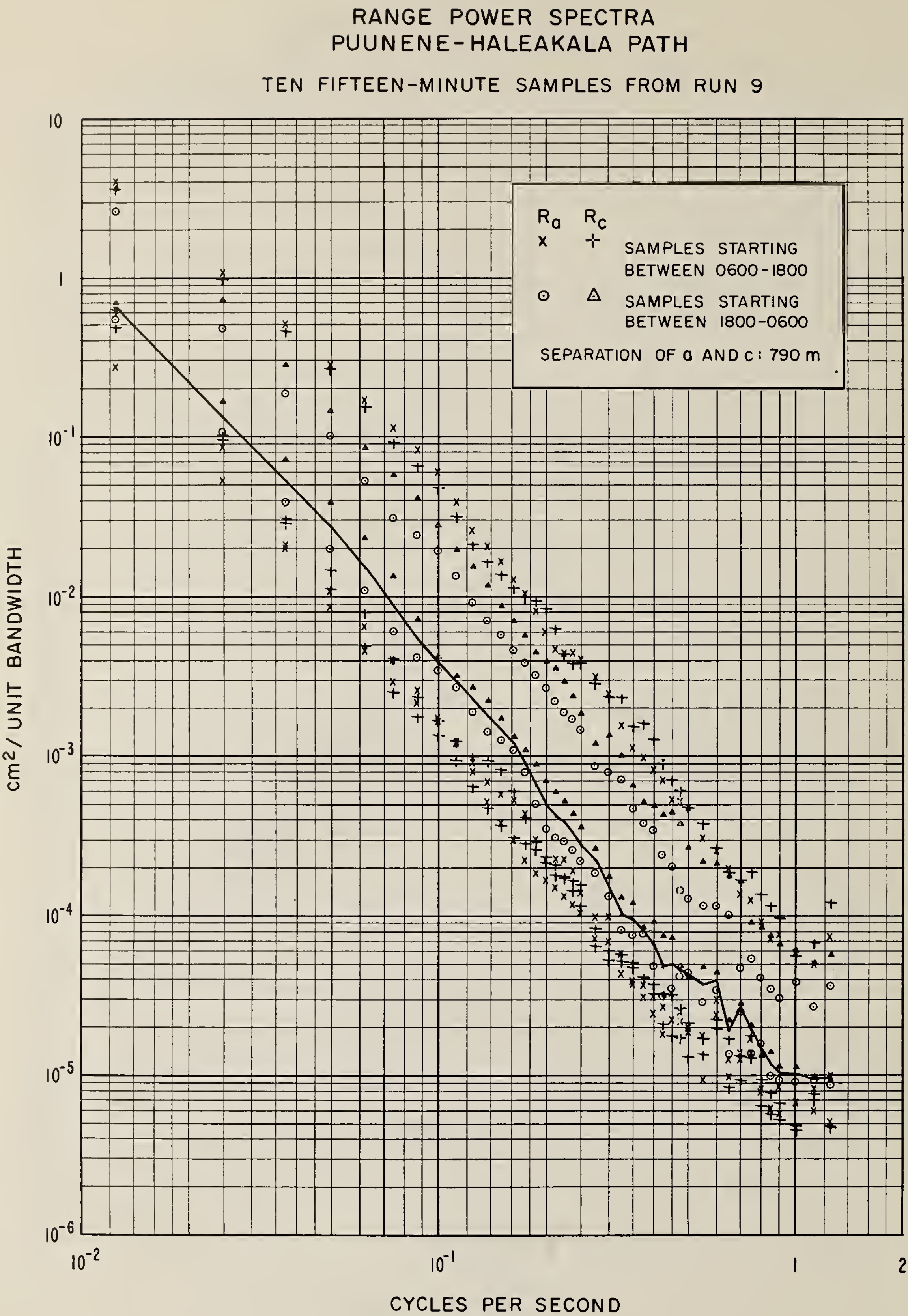
RANGE POWER SPECTRA
PUUNENE-HALEAKALA PATH
TEN FIFTEEN-MINUTE SAMPLES FROM RUN 9
R_a R_c
x +
SAMPLES STARTING BETWEEN 0600-1800
⊙ △
SAMPLES STARTING BETWEEN 1800-0600
SEPARATION OF a AND c: 790 m
10
1
10^{-1}
10^{-2}
10^{-3}
10^{-4}
10^{-5}
10^{-6}
10^{-2}
10^{-1}
1
2
cm^2/ UNIT BANDWIDTH
CYCLES PER SECOND

Figure 17

COMPARISON OF RANGE VARIANCES ON ADJACENT PATHS
(COMPUTED FROM 15-MINUTE SAMPLES)

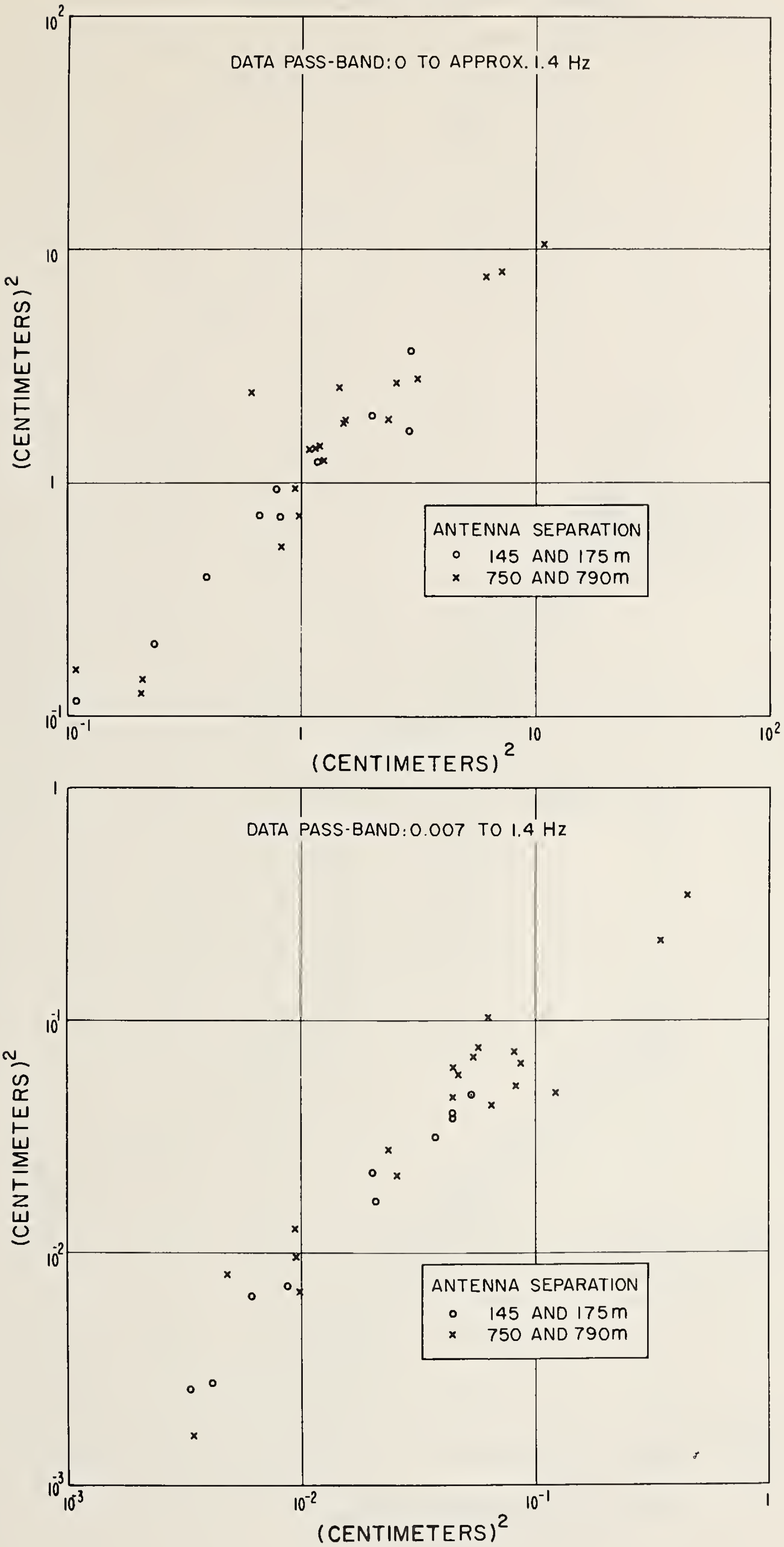

Figure 18

CORRELATION OF RANGE VARIATIONS vs ANTENNA SEPARATION AT UPPER TERMINAL

(COMPUTED FROM 15-MINUTE SAMPLES)

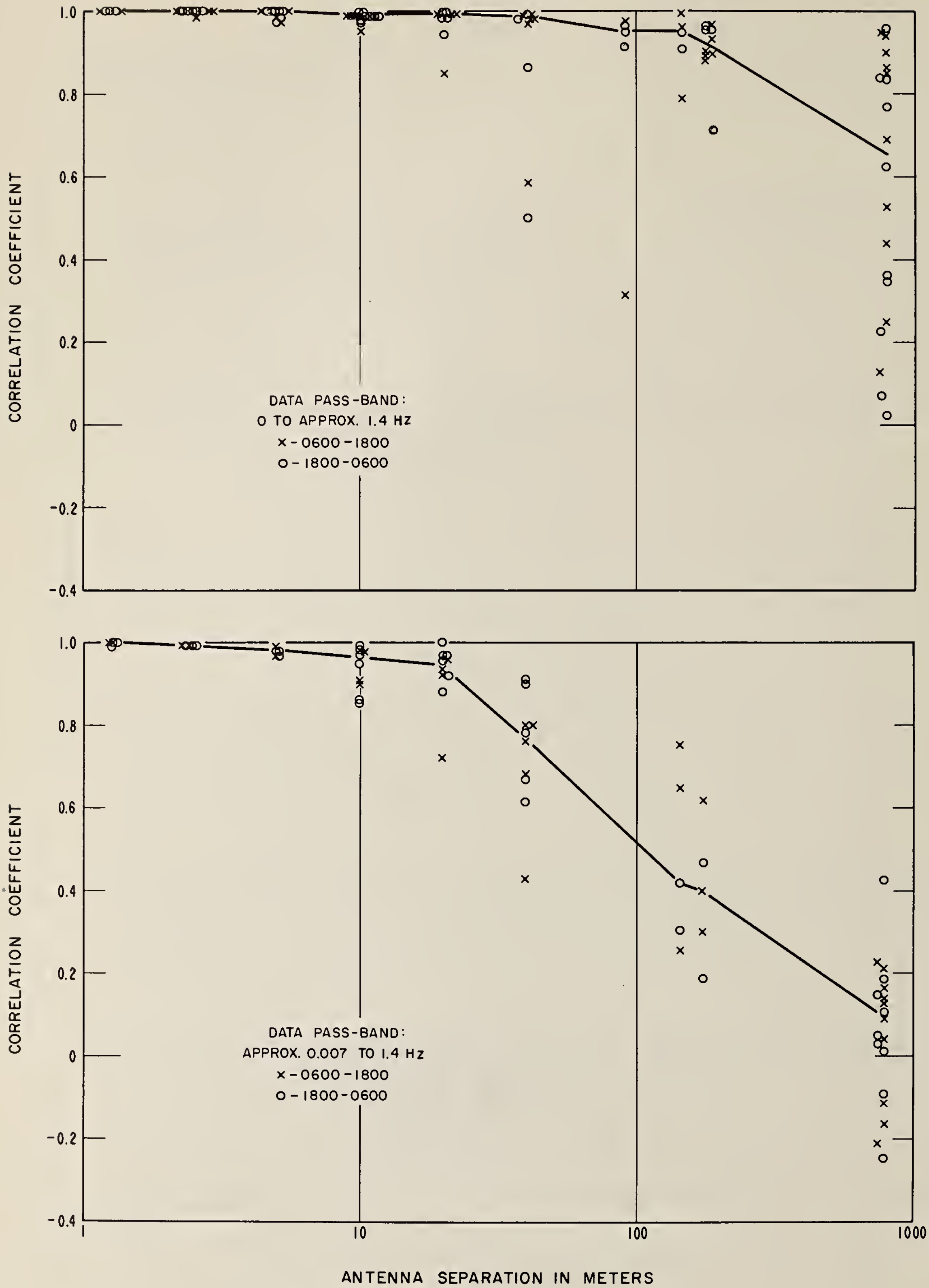

Figure 19

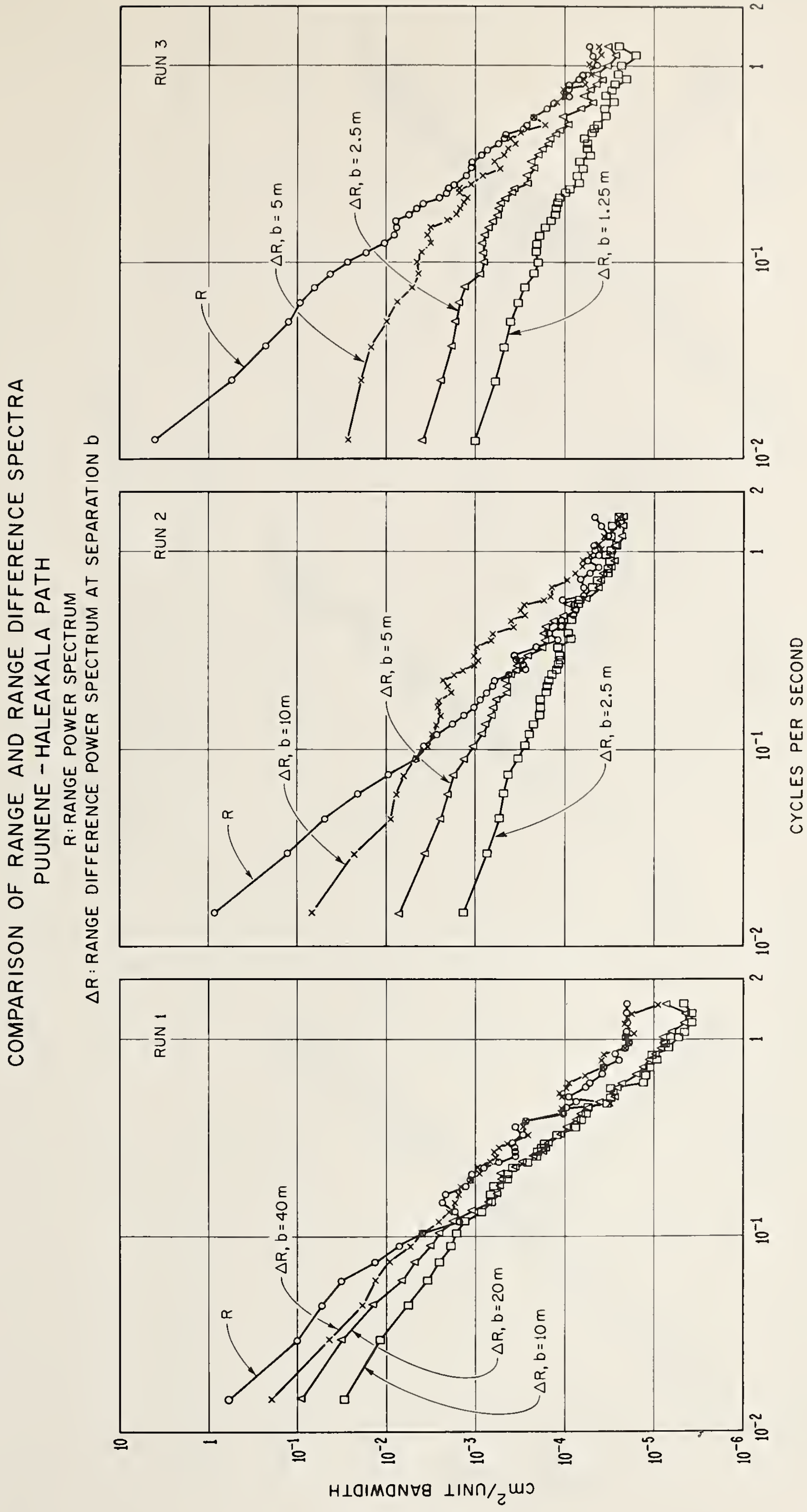
COMPARISON OF RANGE AND RANGE DIFFERENCE SPECTRA
PUUNENE - HALEAKALA PATH
R: RANGE POWER SPECTRUM
ΔR: RANGE DIFFERENCE POWER SPECTRUM AT SEPARATION b
RUN 1
RUN 2
RUN 3
R
ΔR, b=40m
ΔR, b=20m
ΔR, b=10m
ΔR, b=10m
ΔR, b=5m
ΔR, b=2.5m
ΔR, b=5m
ΔR, b=2.5m
ΔR, b=1.25m
cm²/UNIT BANDWIDTH
CYCLES PER SECOND

Figure 20

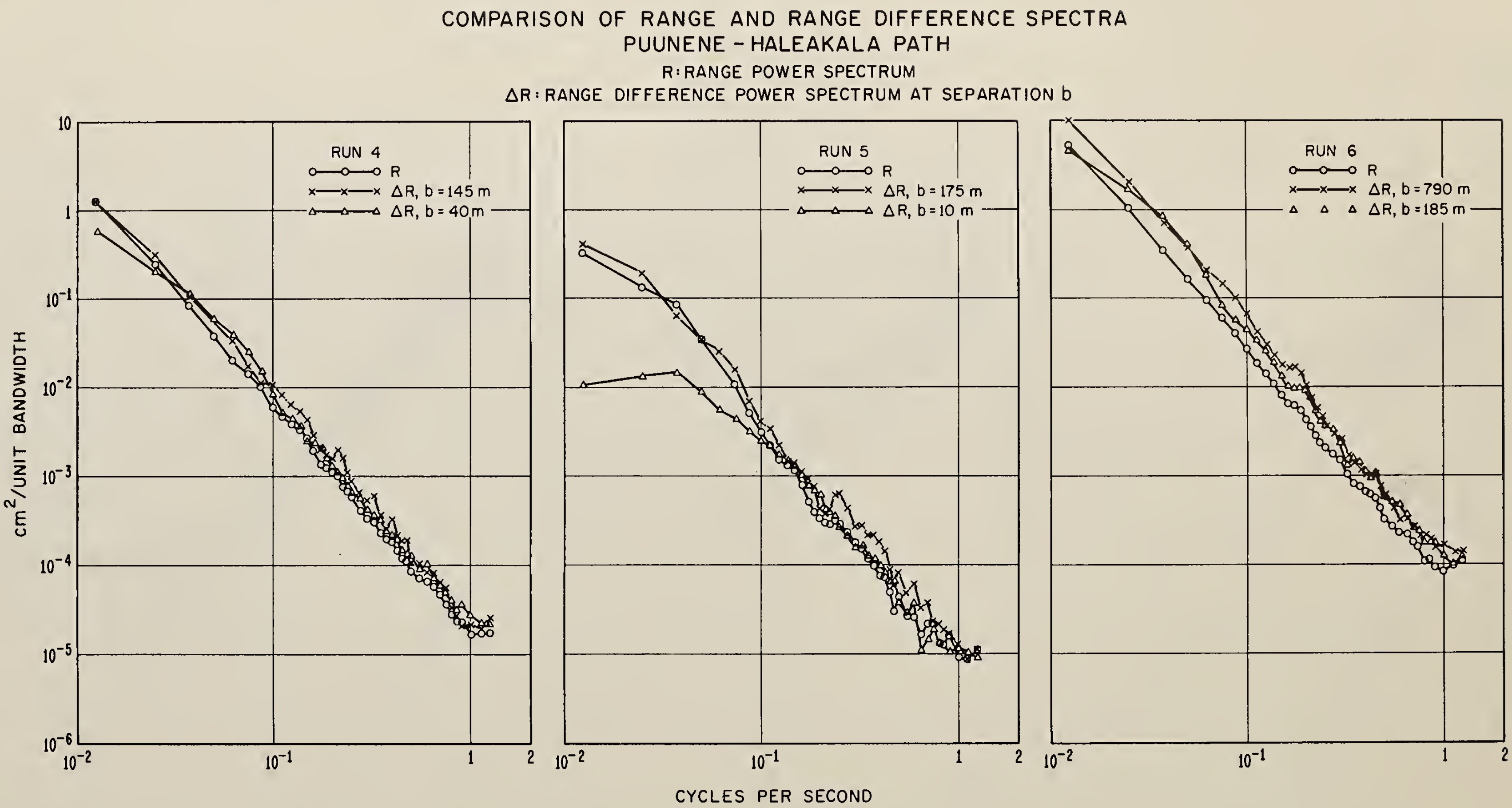
COMPARISON OF RANGE AND RANGE DIFFERENCE SPECTRA
PUUNENE - HALEAKALA PATH
R: RANGE POWER SPECTRUM
ΔR: RANGE DIFFERENCE POWER SPECTRUM AT SEPARATION b
RUN 4
R
ΔR, b = 145 m
ΔR, b = 40 m
RUN 5
R
ΔR, b = 175 m
ΔR, b = 10 m
RUN 6
R
ΔR, b = 790 m
ΔR, b = 185 m
cm²/UNIT BANDWIDTH
CYCLES PER SECOND

Figure 21

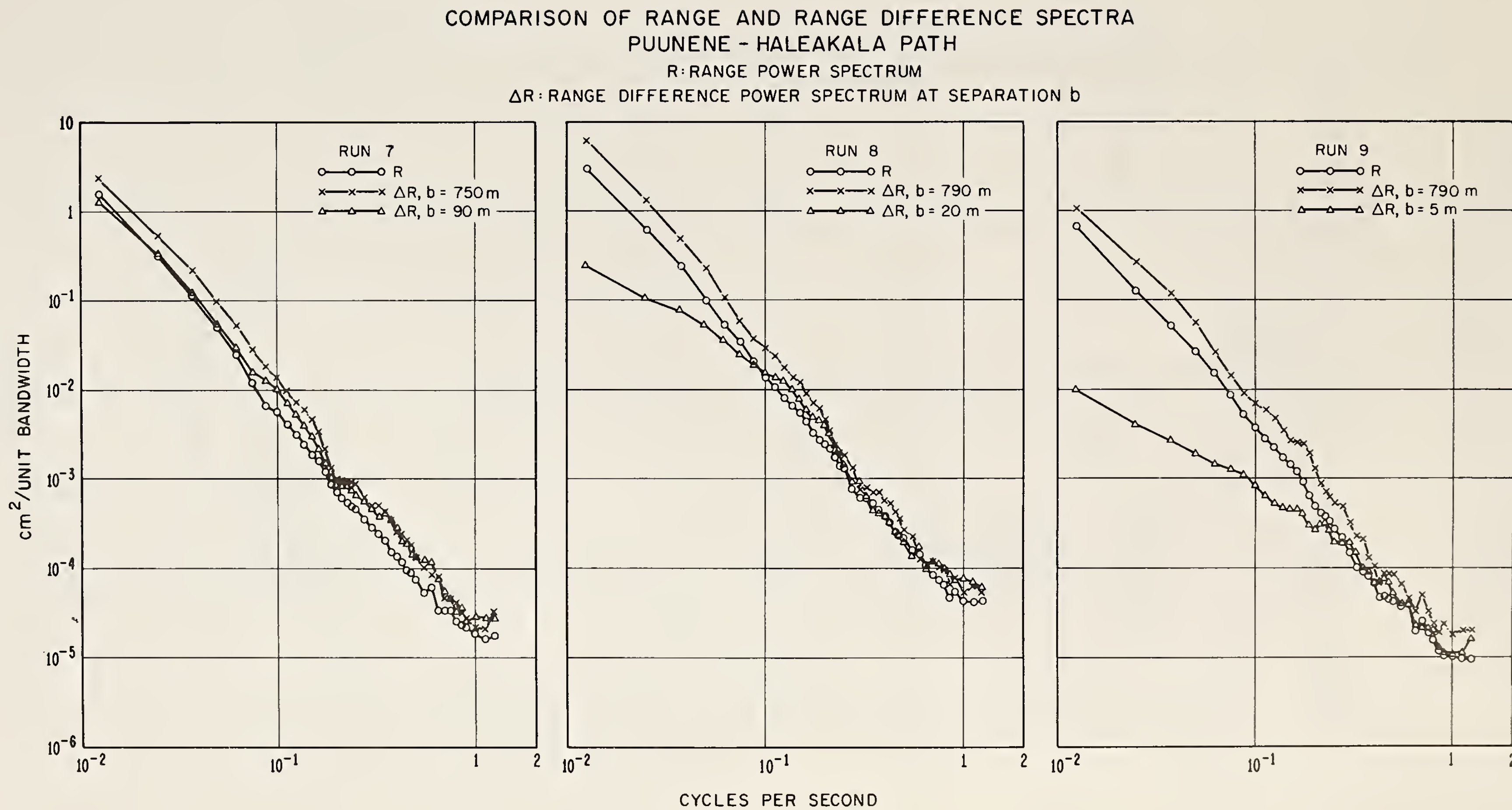
COMPARISON OF RANGE AND RANGE DIFFERENCE SPECTRA
PUUNENE - HALEAKALA PATH
R: RANGE POWER SPECTRUM
ΔR: RANGE DIFFERENCE POWER SPECTRUM AT SEPARATION b
RUN 7
R
ΔR, b = 750 m
ΔR, b = 90 m
RUN 8
R
ΔR, b = 790 m
ΔR, b = 20 m
RUN 9
R
ΔR, b = 790 m
ΔR, b = 5 m
cm²/UNIT BANDWIDTH
10
1
10⁻¹
10⁻²
10⁻³
10⁻⁴
10⁻⁵
10⁻⁶
10⁻²
10⁻¹
1
2
CYCLES PER SECOND

Figure 22

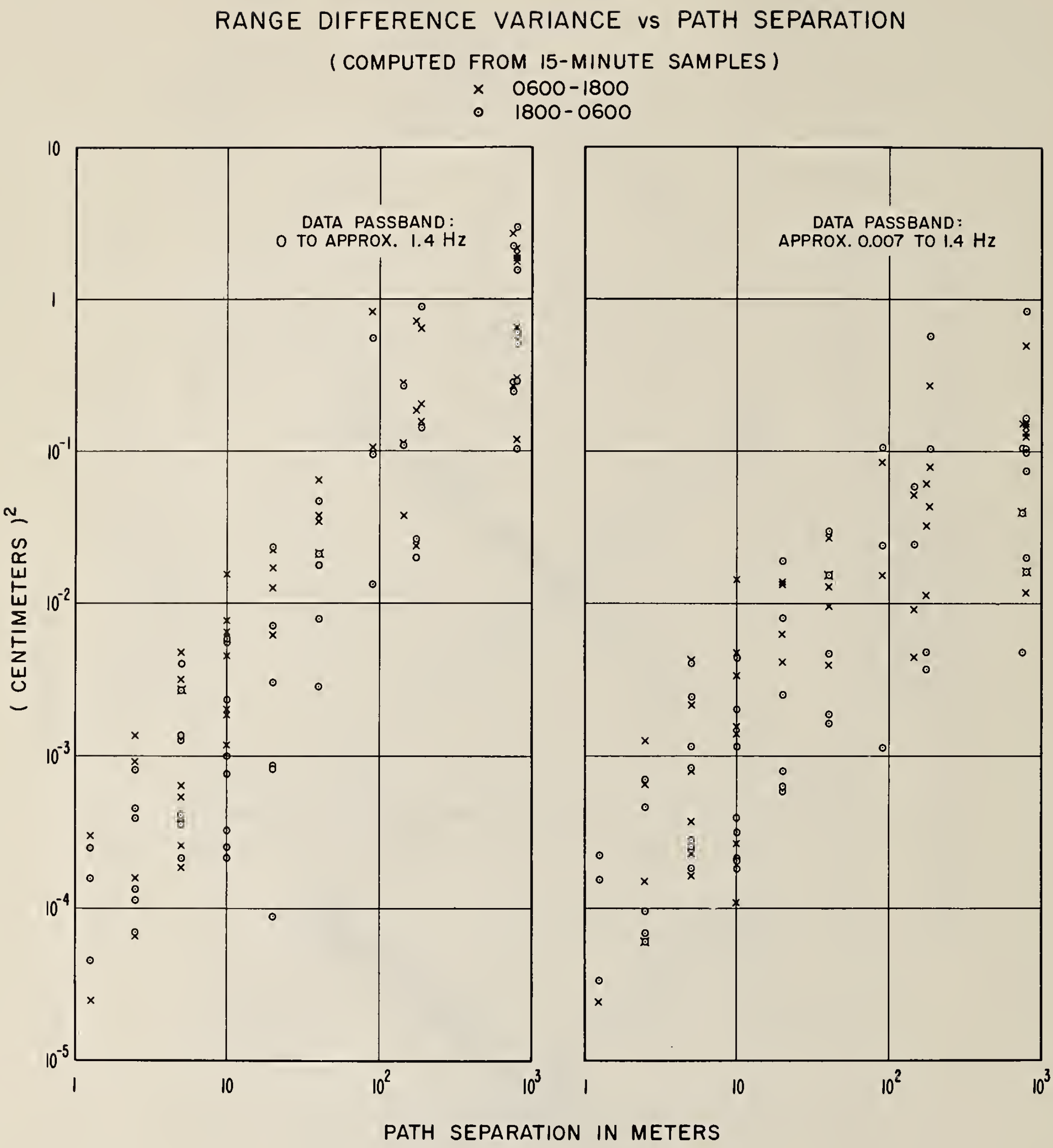
RANGE DIFFERENCE VARIANCE vs PATH SEPARATION
(COMPUTED FROM 15-MINUTE SAMPLES)
× 0600-1800
⊙ 1800-0600
DATA PASSBAND: 0 TO APPROX. 1.4 Hz
DATA PASSBAND: APPROX. 0.007 TO 1.4 Hz
(CENTIMETERS)^2
10
1
10^{-1}
10^{-2}
10^{-3}
10^{-4}
10^{-5}
1
10
10^2
10^3
PATH SEPARATION IN METERS

Figure 23

COMPARISON OF RANGE DIFFERENCE VARIANCES
ON ADJOINING PAIRS OF PATHS
(COMPUTED FROM FIFTEEN-MINUTE SAMPLES)

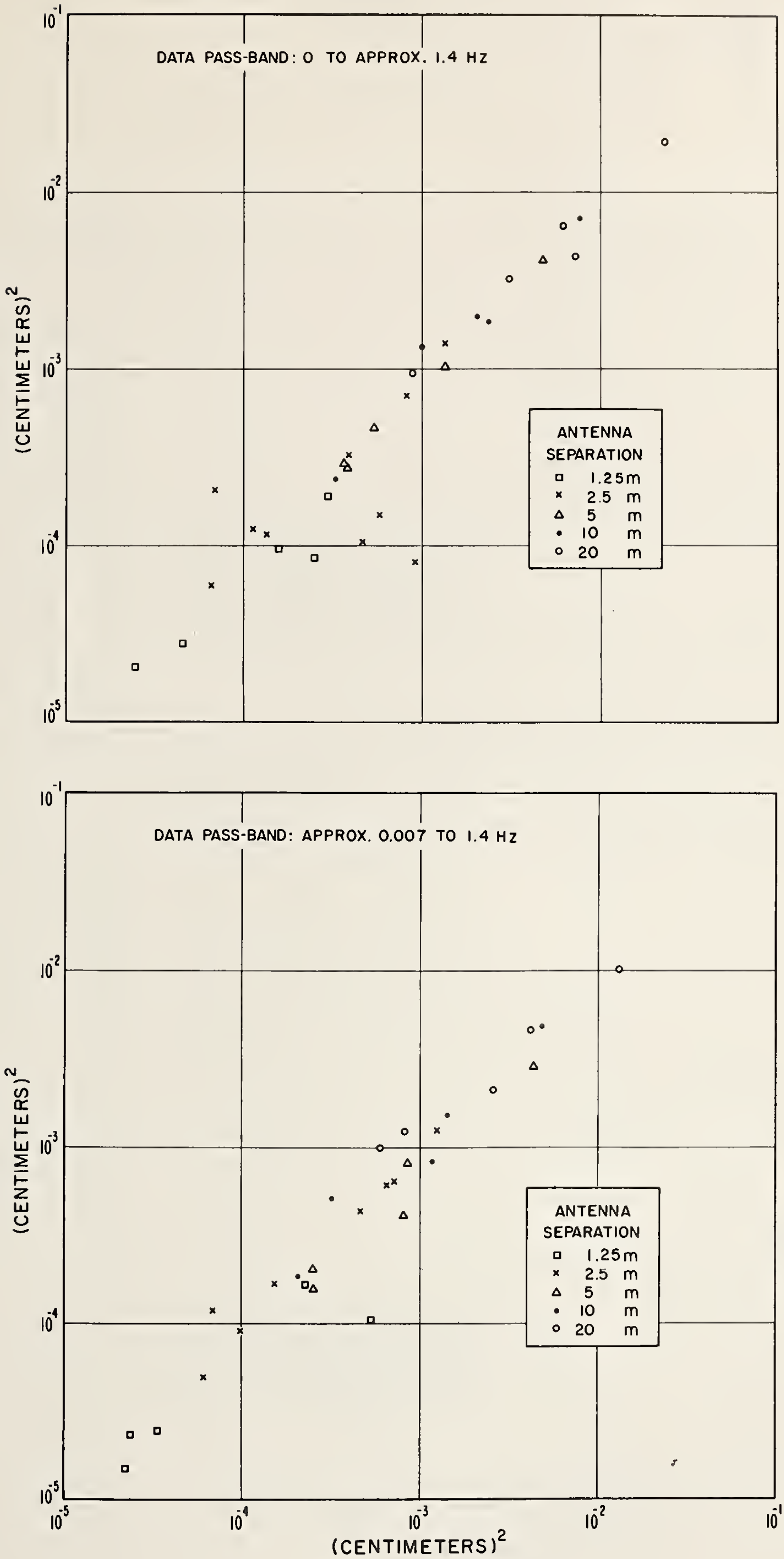

Figure 24

COMPARISON OF RANGE DIFFERENCE VARIANCES
ON SEPARATED PAIRS OF PATHS
(COMPUTED FROM 15-MINUTE SAMPLES)

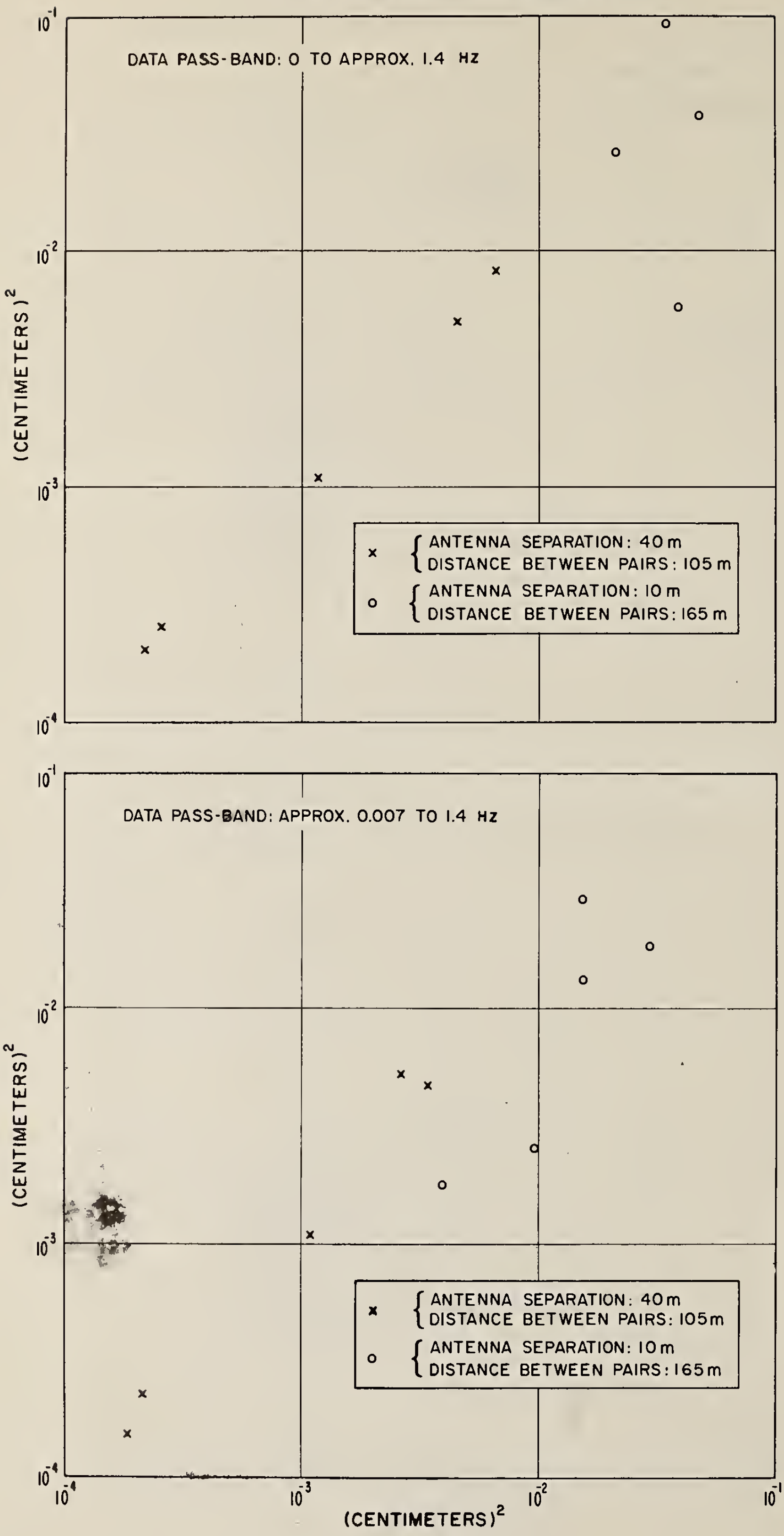

Figure 25

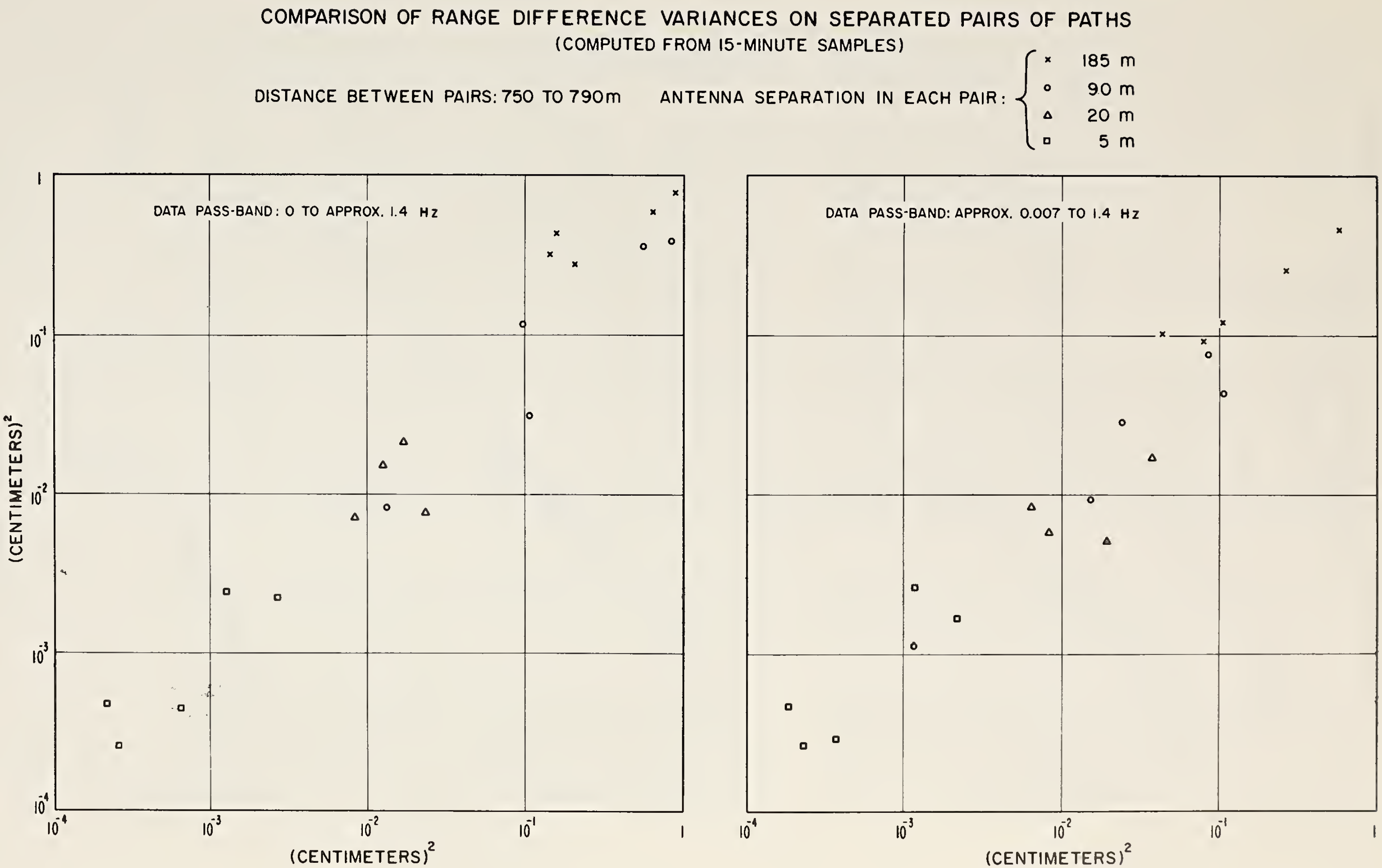
COMPARISON OF RANGE DIFFERENCE VARIANCES ON SEPARATED PAIRS OF PATHS
(COMPUTED FROM 15-MINUTE SAMPLES)
DISTANCE BETWEEN PAIRS: 750 TO 790m
ANTENNA SEPARATION IN EACH PAIR:
× 185 m
○ 90 m
△ 20 m
□ 5 m
DATA PASS-BAND: 0 TO APPROX. 1.4 Hz
DATA PASS-BAND: APPROX. 0.007 TO 1.4 Hz
(CENTIMETERS)^2
(CENTIMETERS)^2
(CENTIMETERS)^2
1
10^{-1}
10^{-2}
10^{-3}
10^{-4}

Figure 26

POWER SPECTRA OF FIRST AND SECOND RANGE DIFFERENCES ON ADJOINING PAIRS OF PATHS

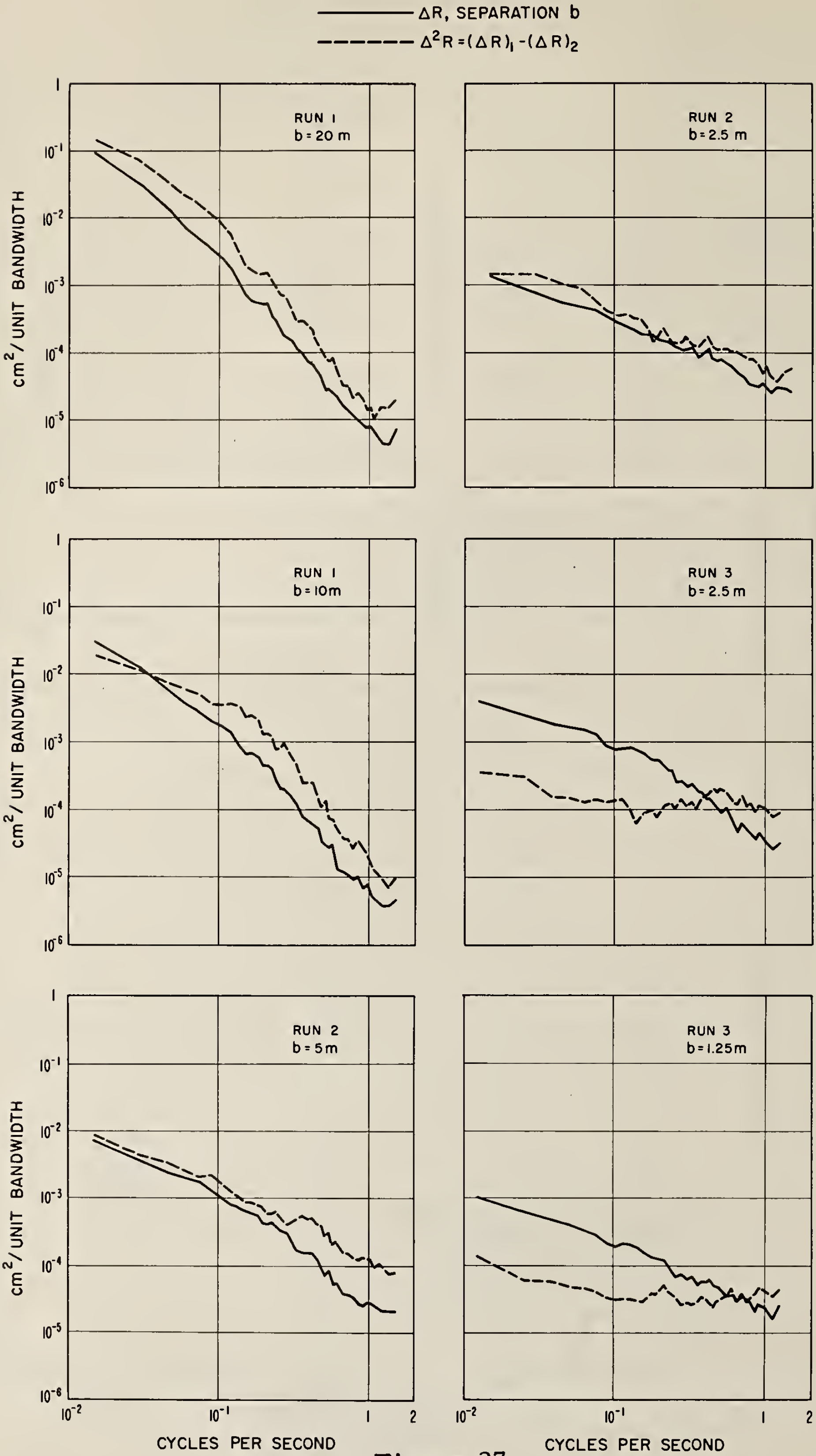

Figure 27

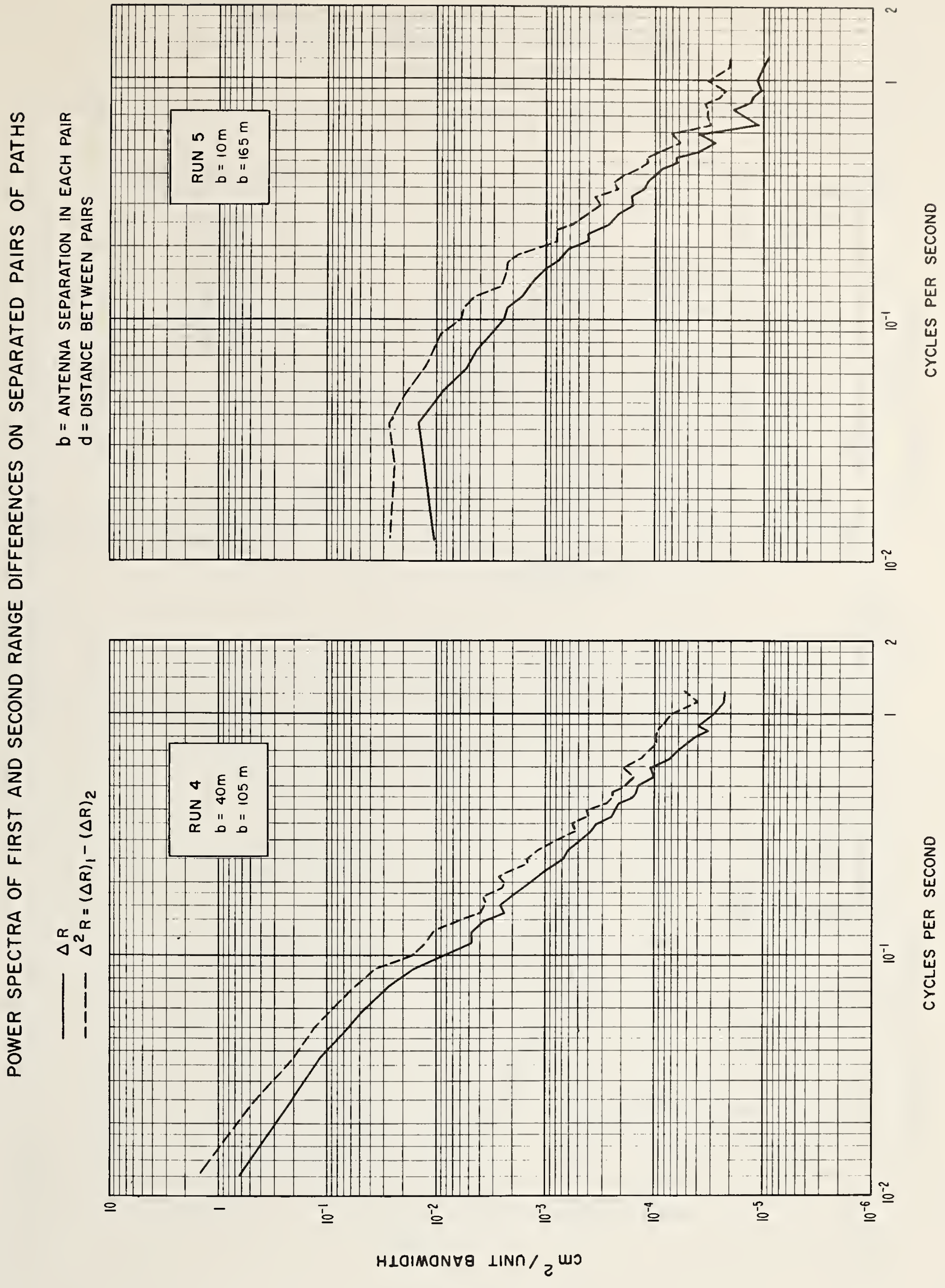

POWER SPECTRA OF FIRST AND SECOND RANGE DIFFERENCES ON SEPARATED PAIRS OF PATHS
ΔR
$\Delta^2 R = (\Delta R)_1 - (\Delta R)_2$
b = ANTENNA SEPARATION IN EACH PAIR
d = DISTANCE BETWEEN PAIRS
RUN 4
b = 40m
b = 105 m
RUN 5
b = 10m
b = 165 m
cm^2/UNIT BANDWIDTH
10
1
10^{-1}
10^{-2}
10^{-3}
10^{-4}
10^{-5}
10^{-6}
10^{-2}
10^{-1}
1
2
CYCLES PER SECOND
CYCLES PER SECOND

Figure 28

CORRELATION OF RANGE DIFFERENCE VARIATIONS VS. SEPARATION OF PATH PAIRS

(COMPUTED FROM 15-MINUTE SAMPLES)

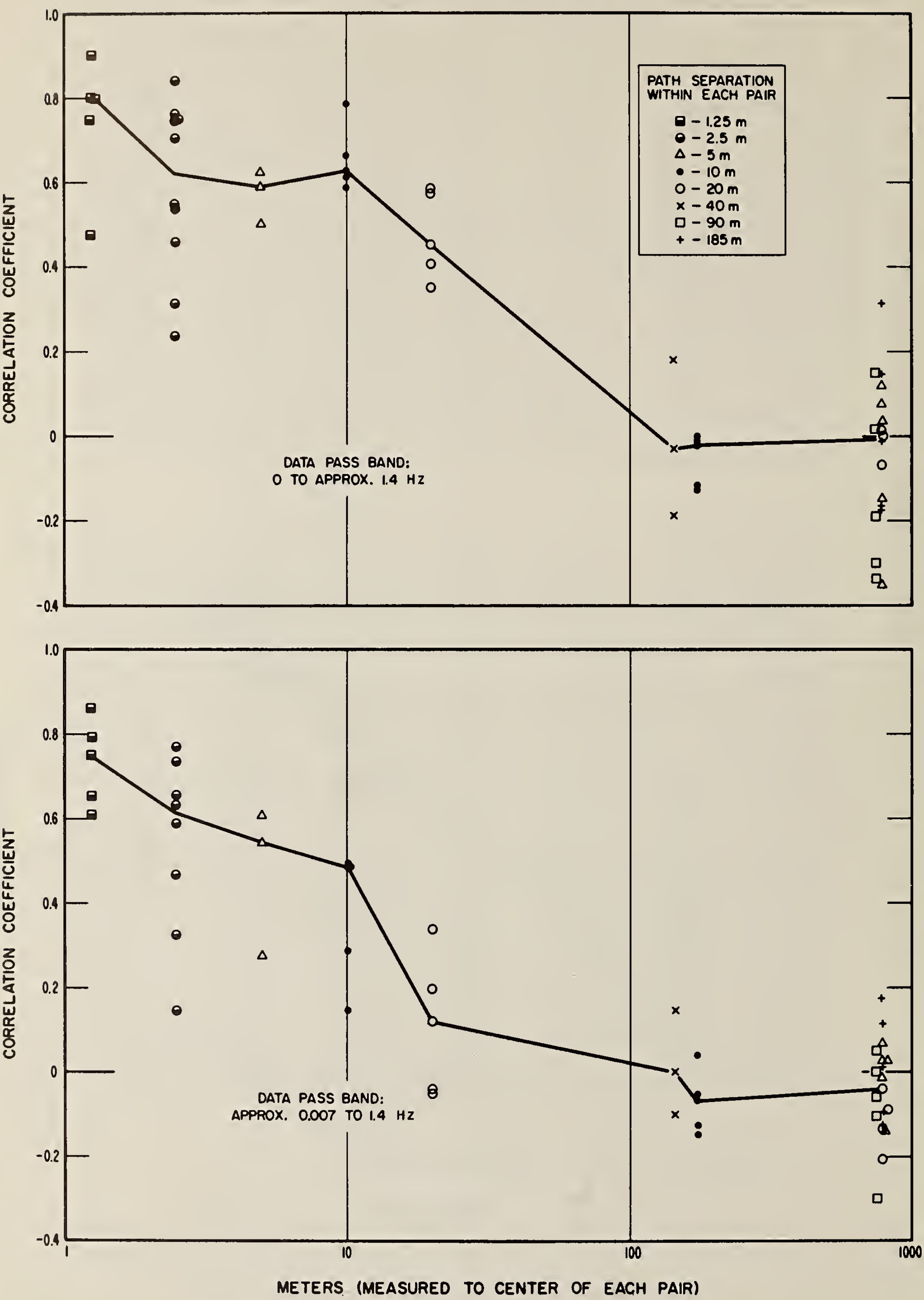

Figure 29

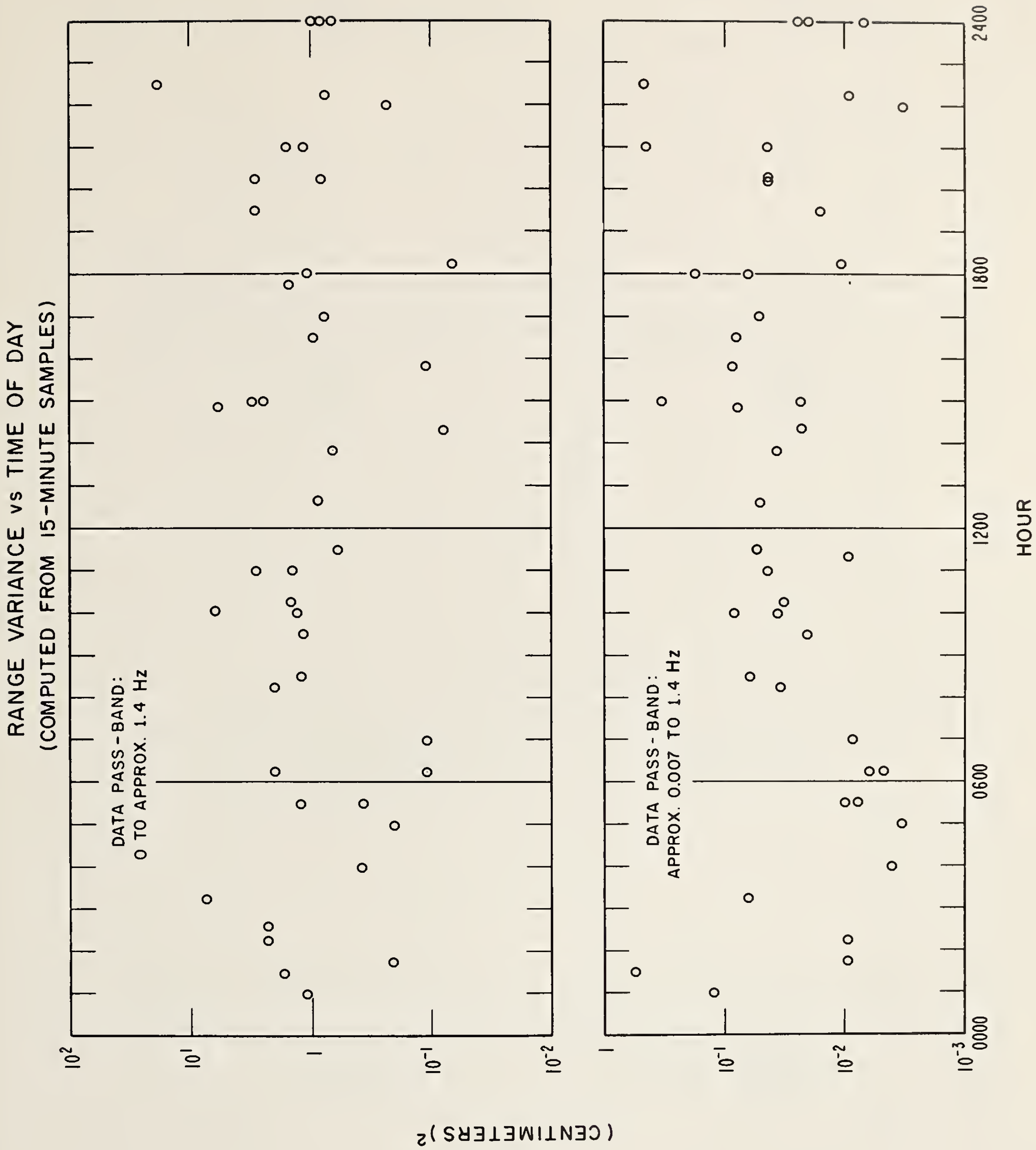
RANGE VARIANCE vs TIME OF DAY
(COMPUTED FROM 15-MINUTE SAMPLES)
DATA PASS-BAND:
0 TO APPROX. 1.4 Hz
DATA PASS-BAND:
APPROX. 0.007 TO 1.4 Hz
HOUR
0000
0600
1200
1800
2400
10^{2}
10^{1}
1
10^{-1}
10^{-2}
10^{-3}
(CENTIMETERS)²

Figure 30

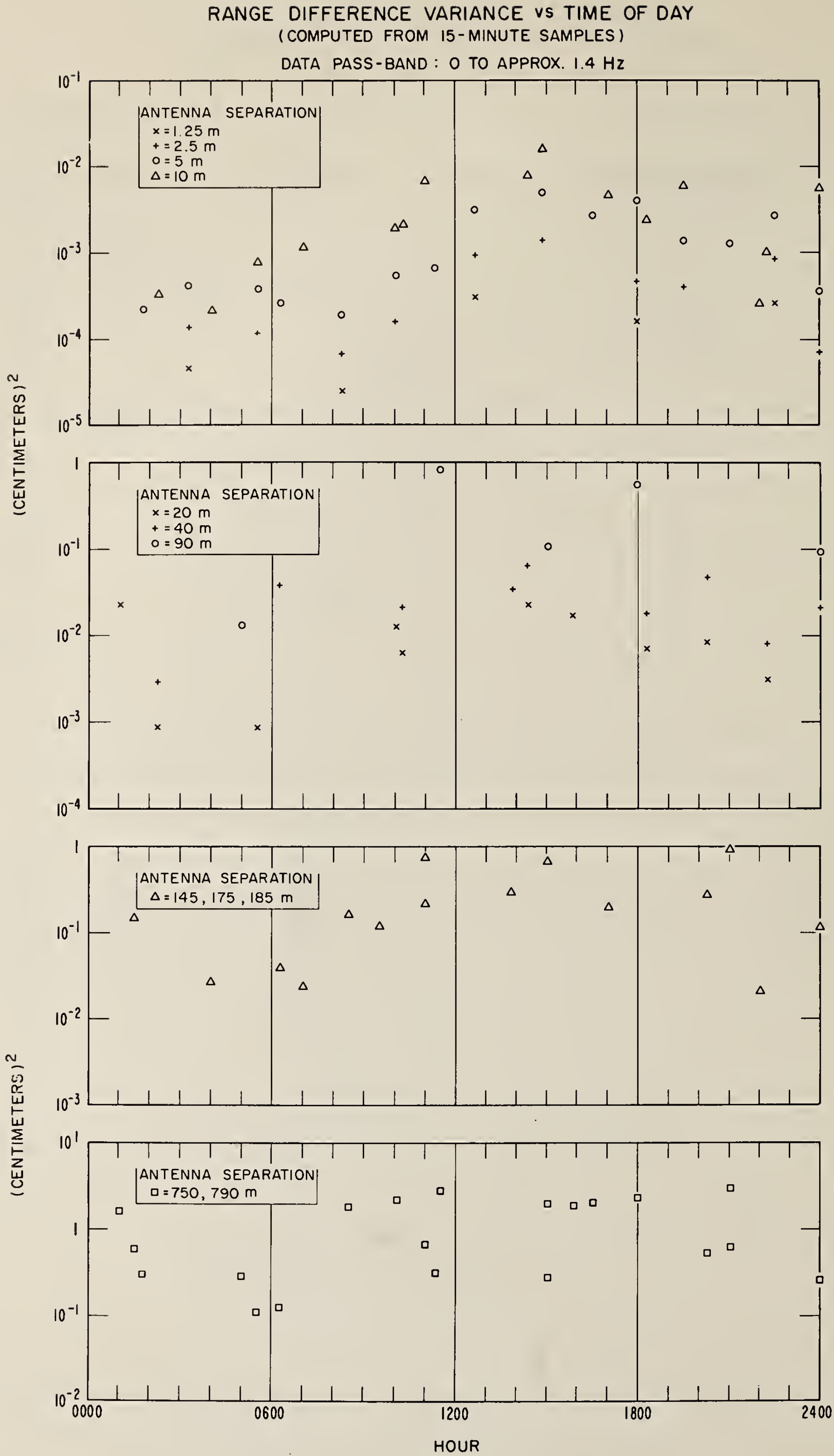

RANGE DIFFERENCE VARIANCE vs TIME OF DAY
(COMPUTED FROM 15-MINUTE SAMPLES)
DATA PASS-BAND : 0 TO APPROX. 1.4 Hz
ANTENNA SEPARATION
× = 1.25 m
+ = 2.5 m
o = 5 m
Δ = 10 m
ANTENNA SEPARATION
× = 20 m
+ = 40 m
o = 90 m
ANTENNA SEPARATION
Δ = 145, 175, 185 m
ANTENNA SEPARATION
□ = 750, 790 m
(CENTIMETERS)2
(CENTIMETERS)2
0000
0600
1200
1800
2400
HOUR

Figure 31

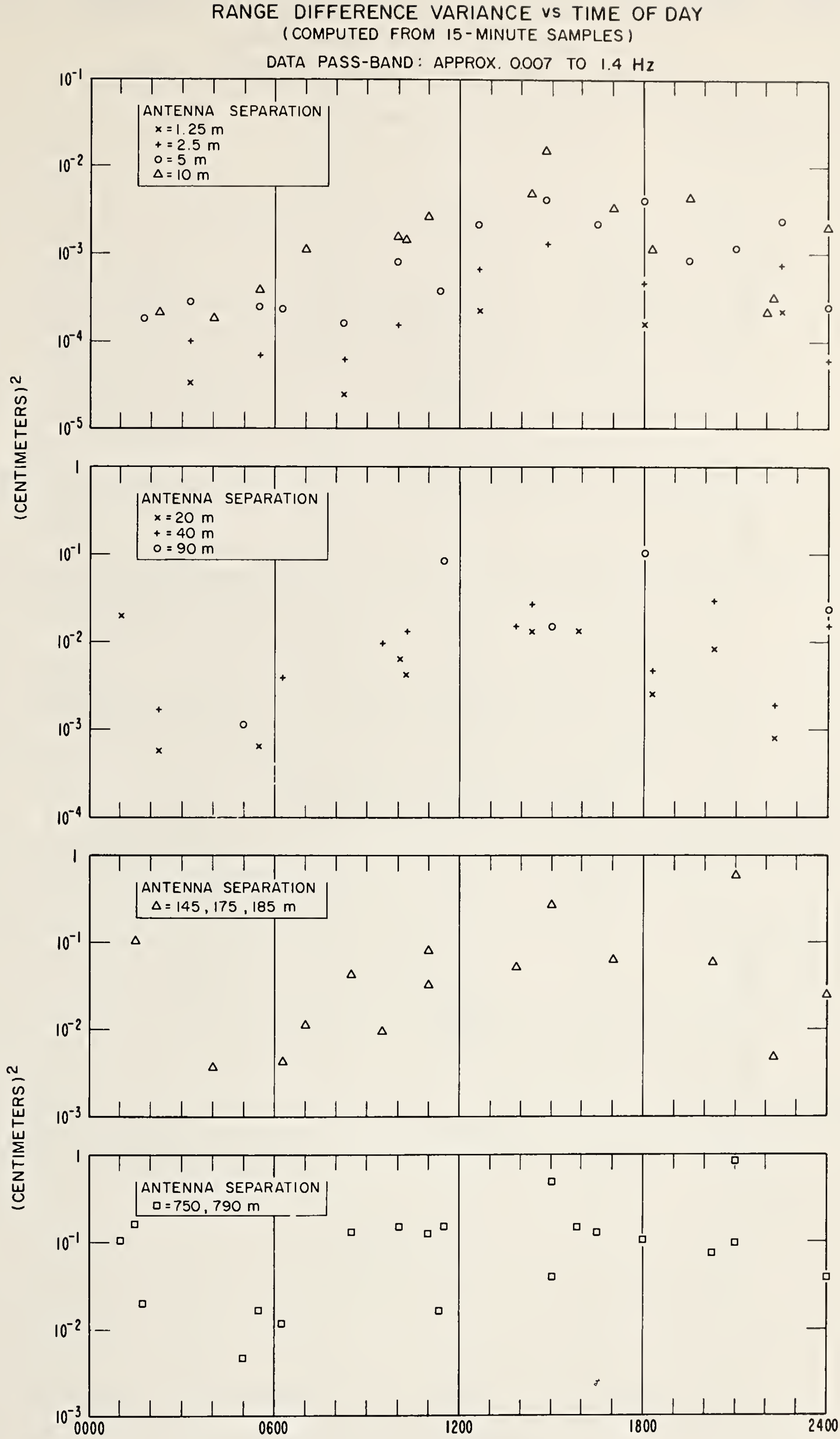

RANGE DIFFERENCE VARIANCE vs TIME OF DAY
(COMPUTED FROM 15-MINUTE SAMPLES)
DATA PASS-BAND: APPROX. 0.007 TO 1.4 Hz
ANTENNA SEPARATION
× = 1.25 m
+ = 2.5 m
○ = 5 m
△ = 10 m
ANTENNA SEPARATION
× = 20 m
+ = 40 m
○ = 90 m
ANTENNA SEPARATION
△ = 145, 175, 185 m
ANTENNA SEPARATION
□ = 750, 790 m
(CENTIMETERS)^2
(CENTIMETERS)^2
10^{-1}
10^{-2}
10^{-3}
10^{-4}
10^{-5}
1
0000
0600
1200
1800
2400
HOUR

Figure 32

RANGE VARIANCE vs SURFACE REFRACTIVITY* VARIANCE
(COMPUTED FROM 15-MINUTE SAMPLES)
*REFRACTIVITY MEASURED 1.5 m ABOVE GROUND AT PUUNENE

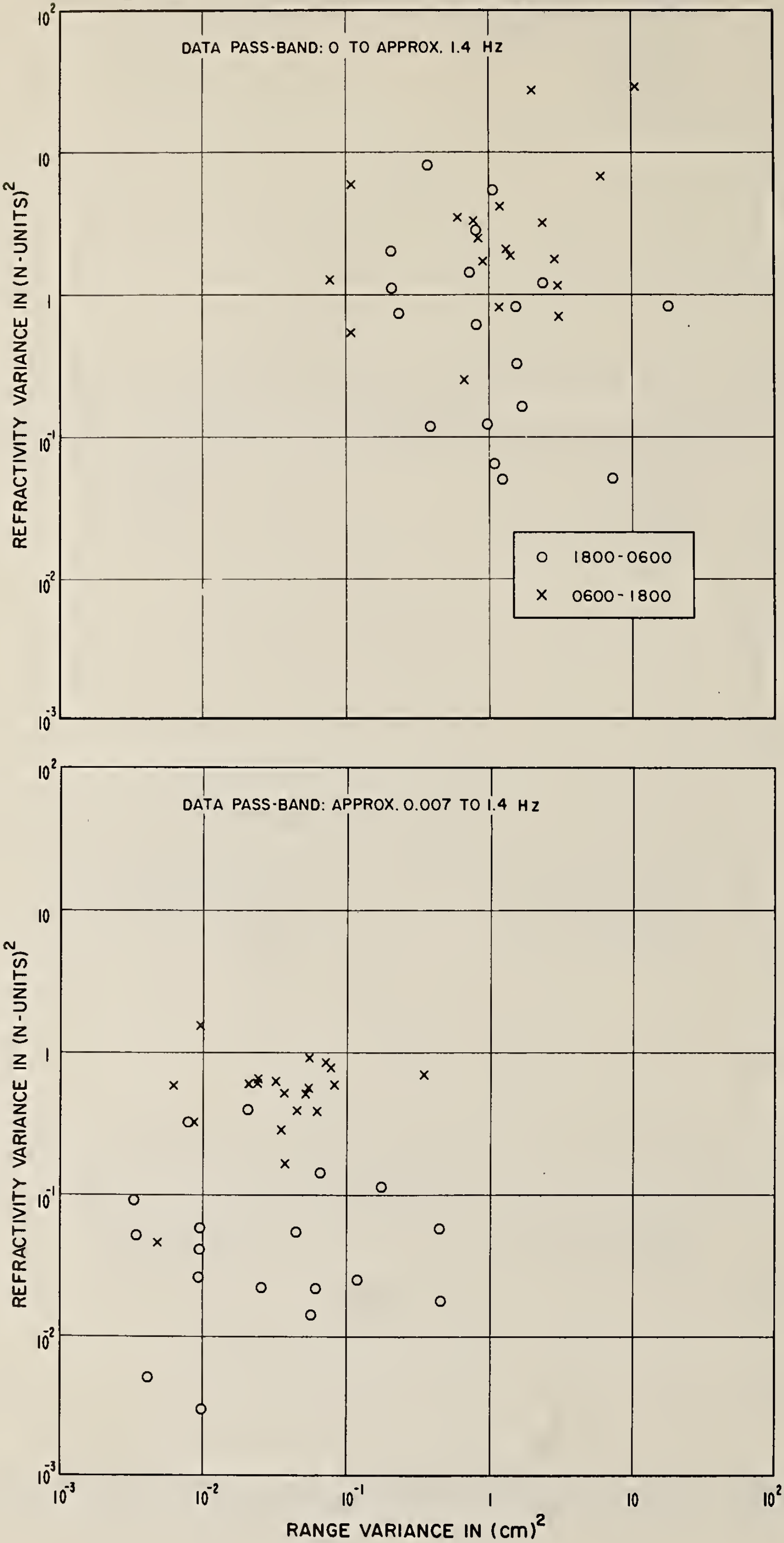

Figure 33

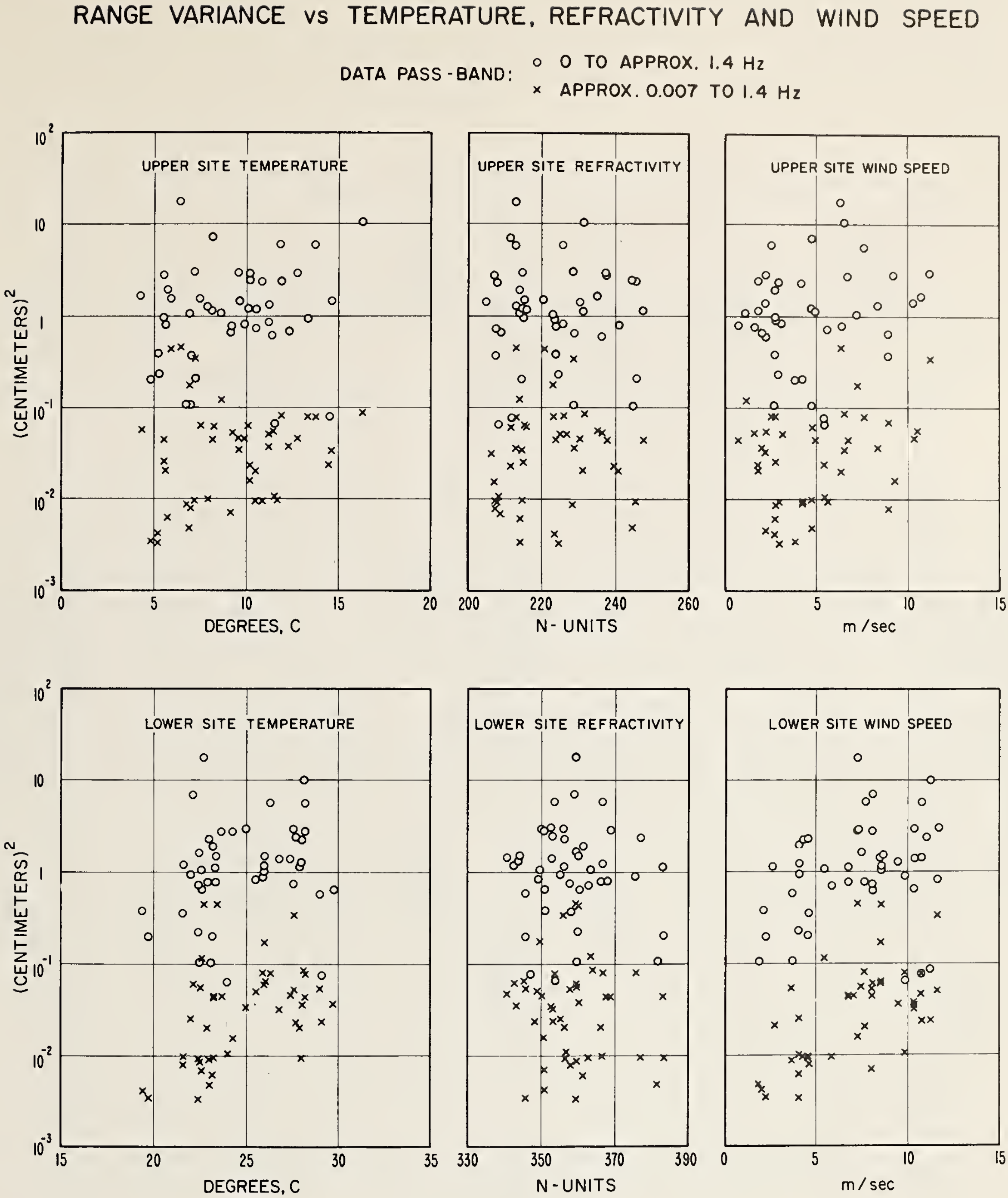
RANGE VARIANCE vs TEMPERATURE, REFRACTIVITY AND WIND SPEED
DATA PASS-BAND:
o 0 TO APPROX. 1.4 Hz
× APPROX. 0.007 TO 1.4 Hz
UPPER SITE TEMPERATURE
UPPER SITE REFRACTIVITY
UPPER SITE WIND SPEED
LOWER SITE TEMPERATURE
LOWER SITE REFRACTIVITY
LOWER SITE WIND SPEED
(CENTIMETERS)^2
DEGREES, C
N-UNITS
m/sec

Figure 34

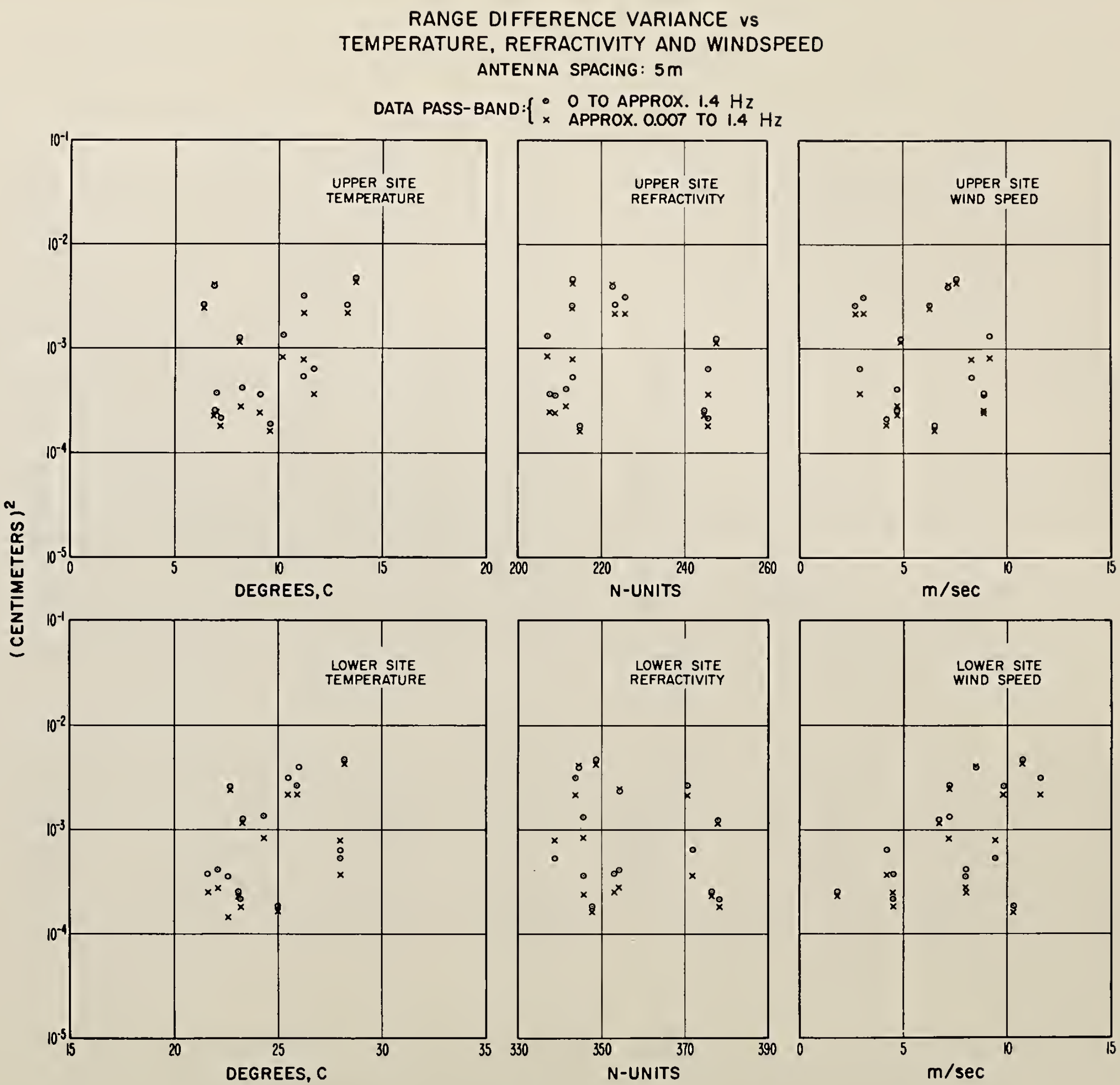

RANGE DIFFERENCE VARIANCE vs
TEMPERATURE, REFRACTIVITY AND WINDSPEED
ANTENNA SPACING: 5m
DATA PASS-BAND: o 0 TO APPROX. 1.4 Hz
x APPROX. 0.007 TO 1.4 Hz
UPPER SITE TEMPERATURE
UPPER SITE REFRACTIVITY
UPPER SITE WIND SPEED
LOWER SITE TEMPERATURE
LOWER SITE REFRACTIVITY
LOWER SITE WIND SPEED
(CENTIMETERS)²
DEGREES, C
N-UNITS
m/sec

Figure 35

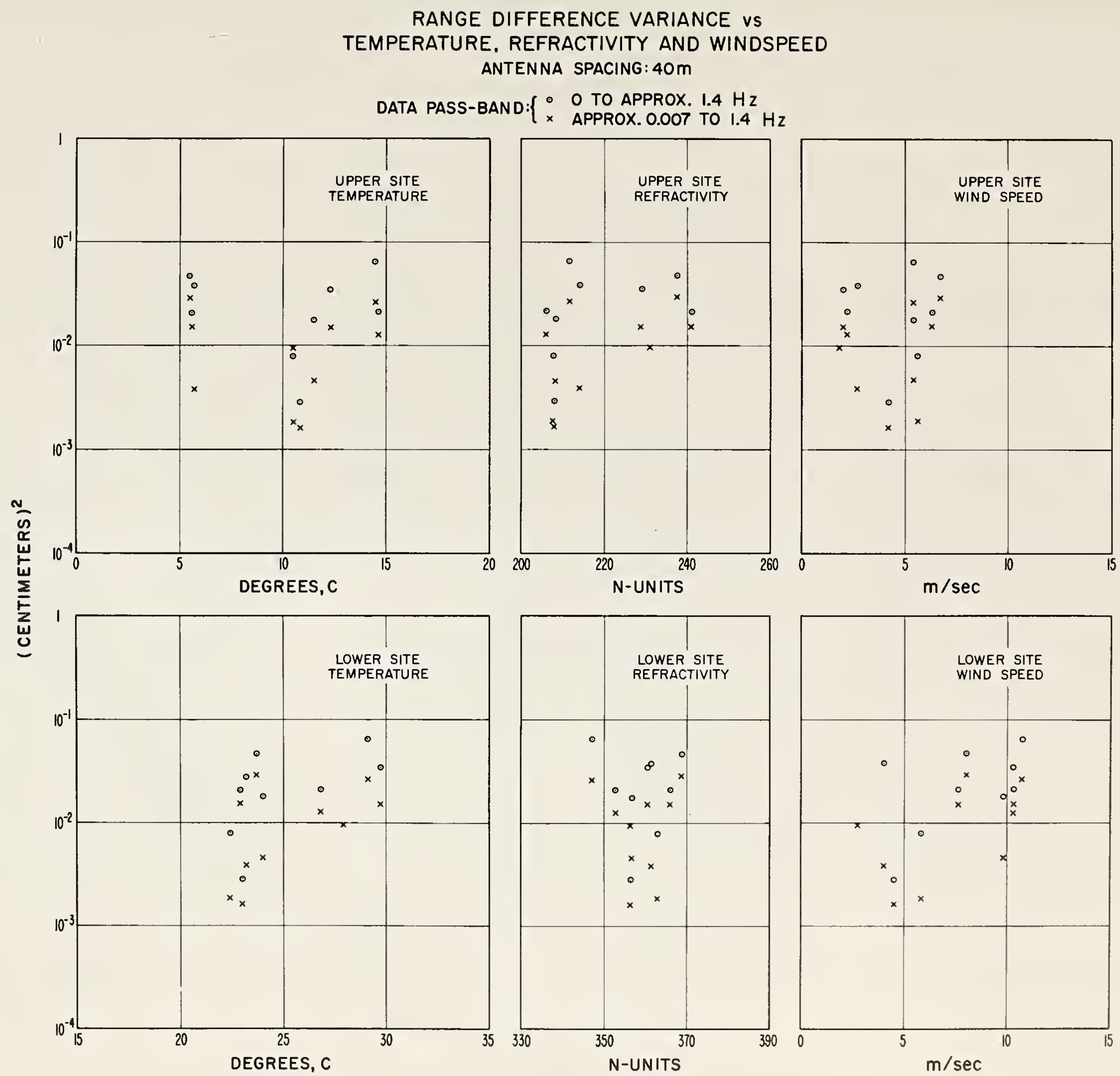

RANGE DIFFERENCE VARIANCE vs
TEMPERATURE, REFRACTIVITY AND WINDSPEED
ANTENNA SPACING: 40m
DATA PASS-BAND: ∘ 0 TO APPROX. 1.4 Hz
× APPROX. 0.007 TO 1.4 Hz
UPPER SITE TEMPERATURE
UPPER SITE REFRACTIVITY
UPPER SITE WIND SPEED
LOWER SITE TEMPERATURE
LOWER SITE REFRACTIVITY
LOWER SITE WIND SPEED
(CENTIMETERS)^2
DEGREES, C
N-UNITS
m/sec

Figure 36

RANGE DIFFERENCE VARIANCE vs
TEMPERATURE, REFRACTIVITY AND WINDSPEED
ANTENNA SPACING: 750-790 m

DATA PASS-BAND: { ○ 0 TO APPROX. 1.4 Hz; × APPROX. 0.007 TO 1.4 Hz }

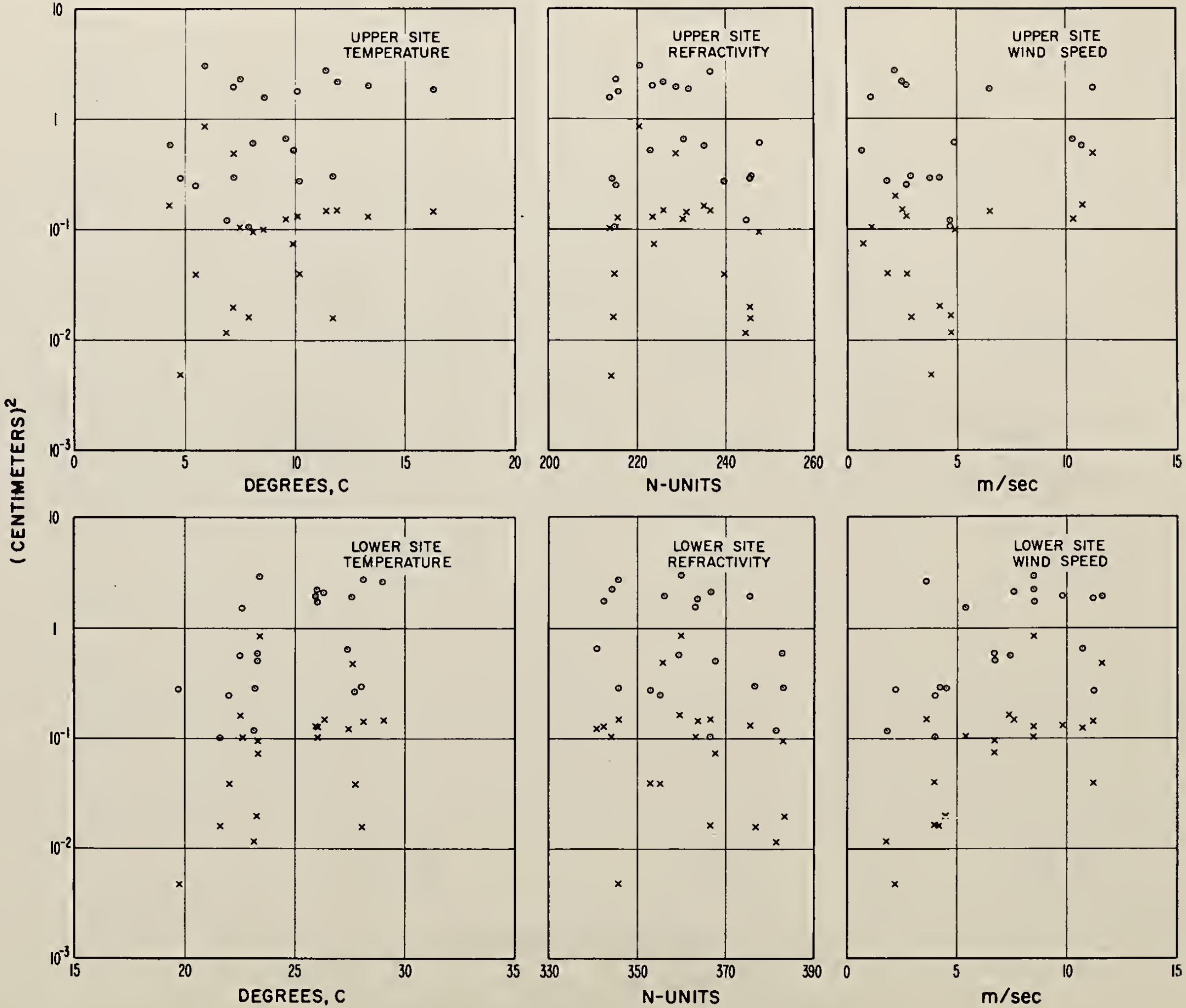

Figure 37

RANGE DIFFERENCE POWER SPECTRA
PUUNENE-HALEAKALA PATHS

FIFTEEN-MINUTE SAMPLES FROM RUN I

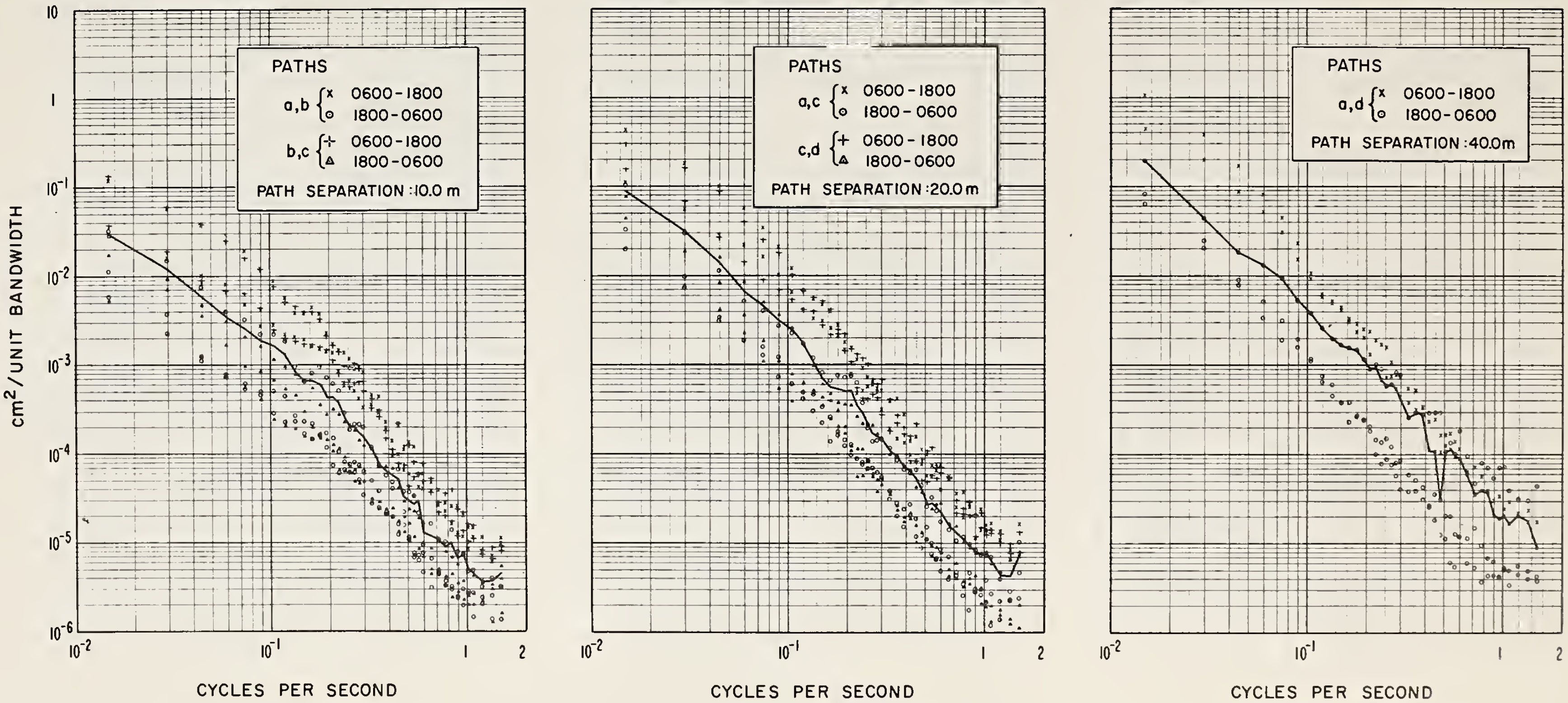

Figure 38

RANGE DIFFERENCE POWER SPECTRA
PUUNENE-HALEAKALA PATHS

FIFTEEN-MINUTE SAMPLES FROM RUN 2

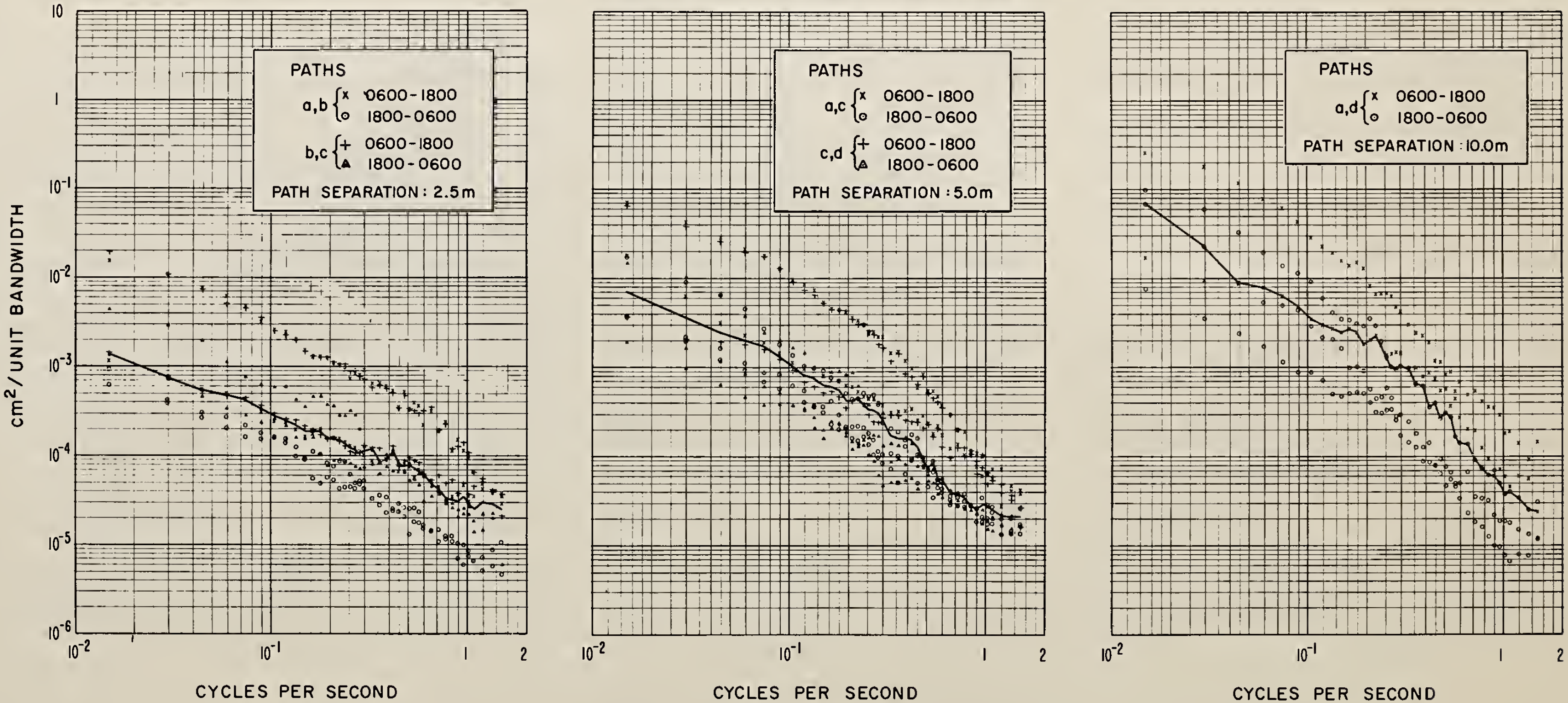

Figure 39

RANGE DIFFERENCE POWER SPECTRA
PUUNENE-HALEAKALA PATHS

FIFTEEN-MINUTE SAMPLES FROM RUN 3

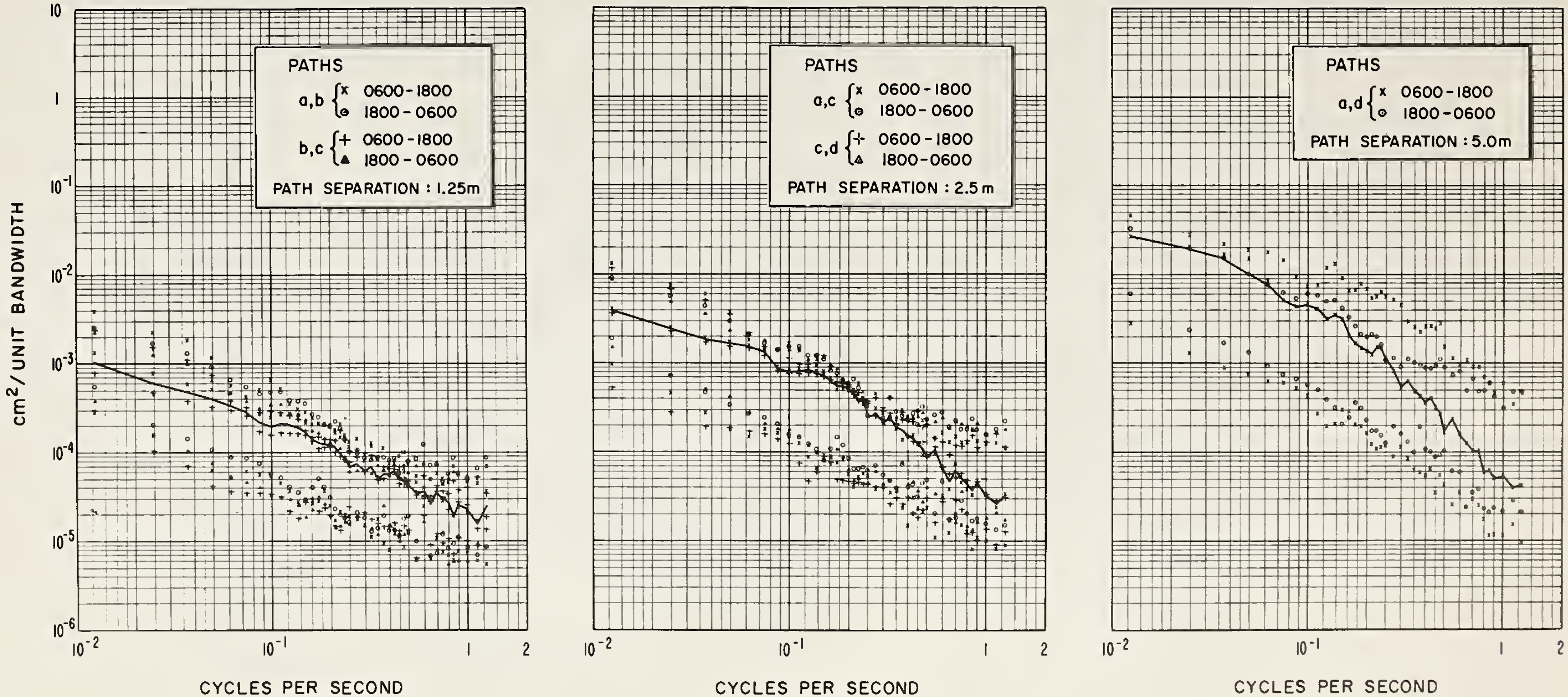

Figure 40

RANGE DIFFERENCE POWER SPECTRA
PUUNENE - HALEAKALA PATH

FIFTEEN-MINUTE SAMPLES FROM RUN 4

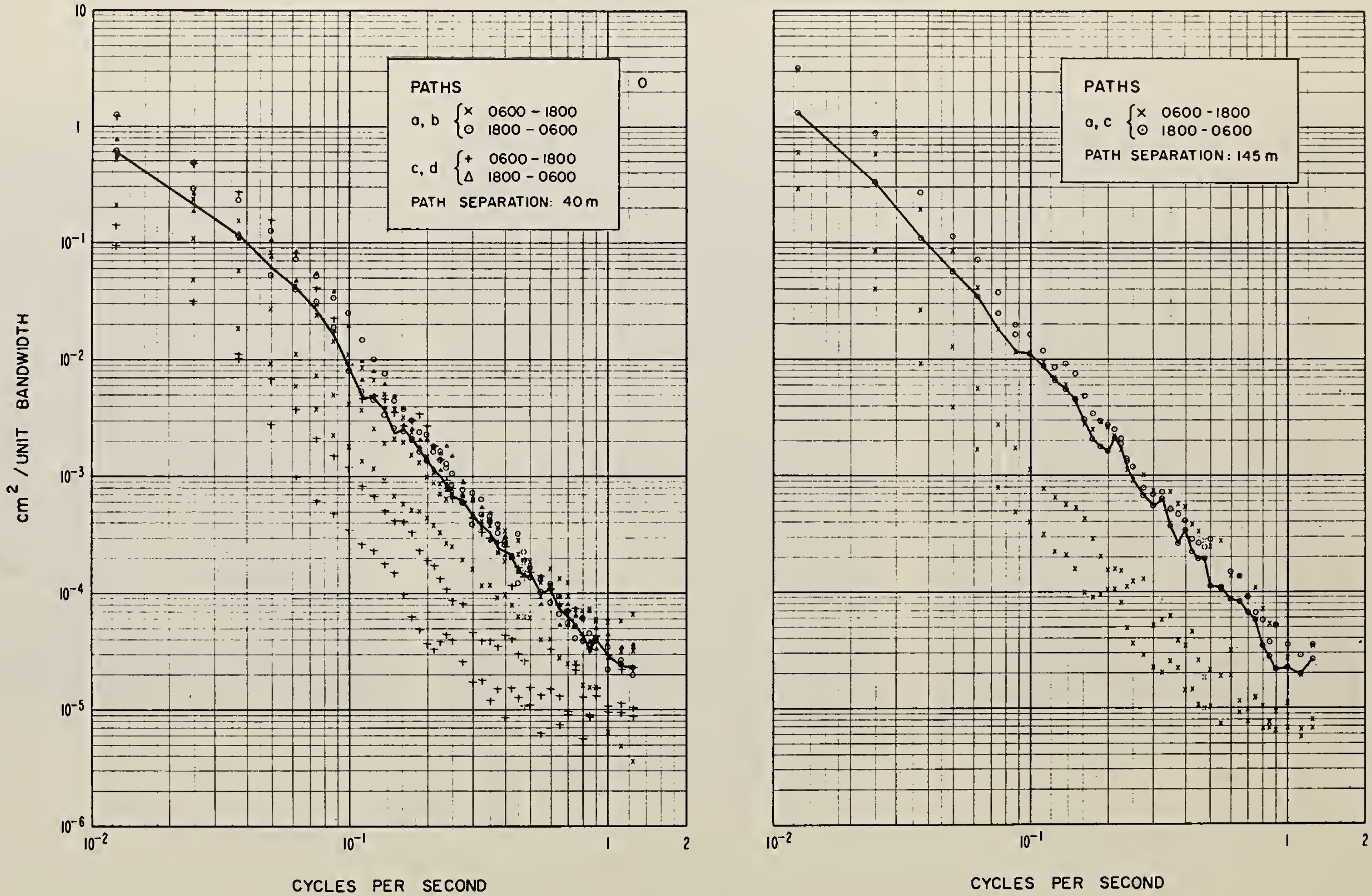

Figure 41

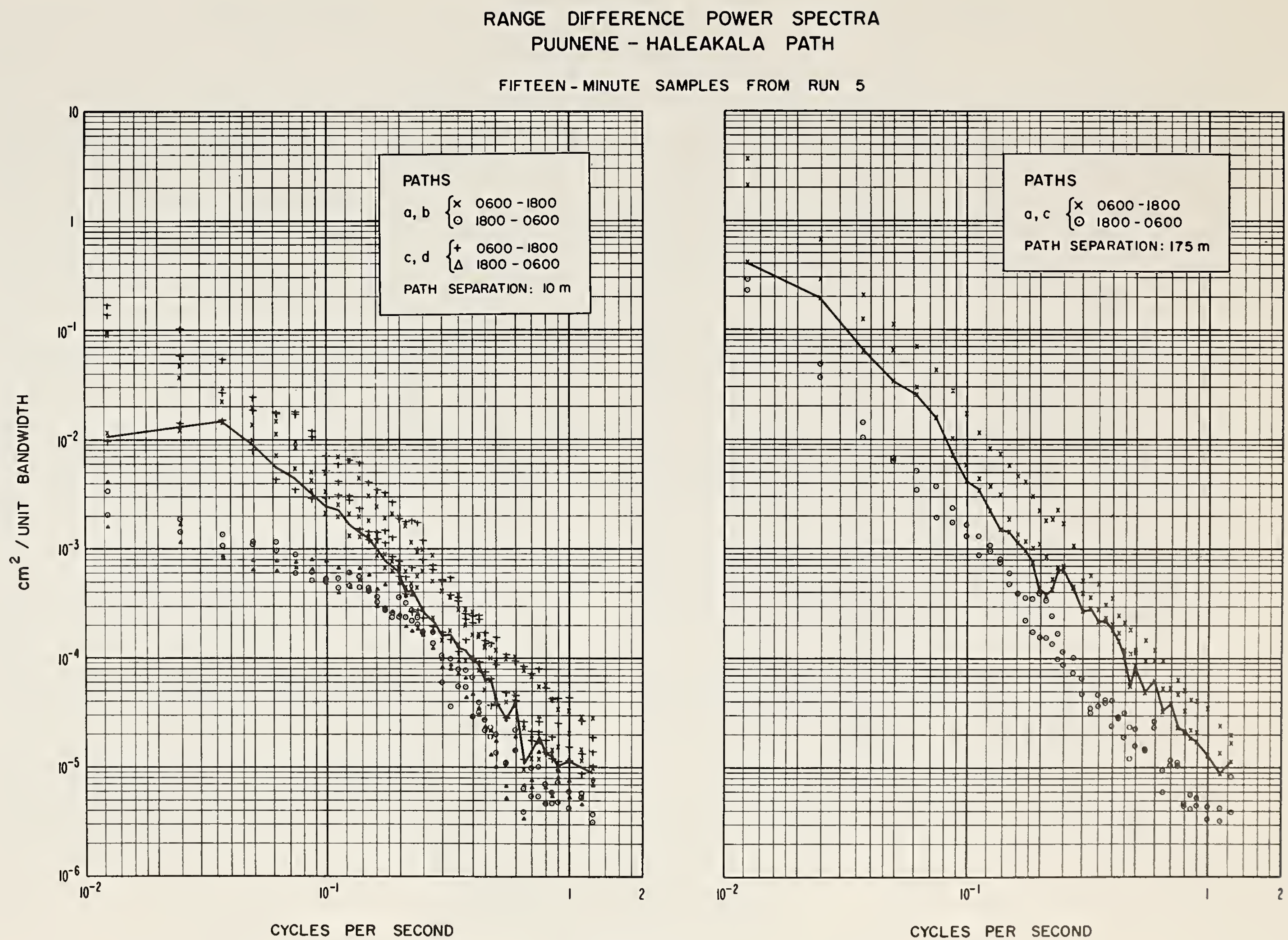
RANGE DIFFERENCE POWER SPECTRA
PUUNENE - HALEAKALA PATH
FIFTEEN - MINUTE SAMPLES FROM RUN 5
PATHS
a, b {× 0600 - 1800, ○ 1800 - 0600}
c, d {+ 0600 - 1800, Δ 1800 - 0600}
PATH SEPARATION: 10 m
PATHS
a, c {× 0600 - 1800, ⊙ 1800 - 0600}
PATH SEPARATION: 175 m
cm² / UNIT BANDWIDTH
10
1
10⁻¹
10⁻²
10⁻³
10⁻⁴
10⁻⁵
10⁻⁶
10⁻²
10⁻¹
1
2
CYCLES PER SECOND
CYCLES PER SECOND

Figure 42

RANGE DIFFERENCE POWER SPECTRA
PUUNENE - HALEAKALA PATH

FIFTEEN - MINUTE SAMPLES FROM RUN 6

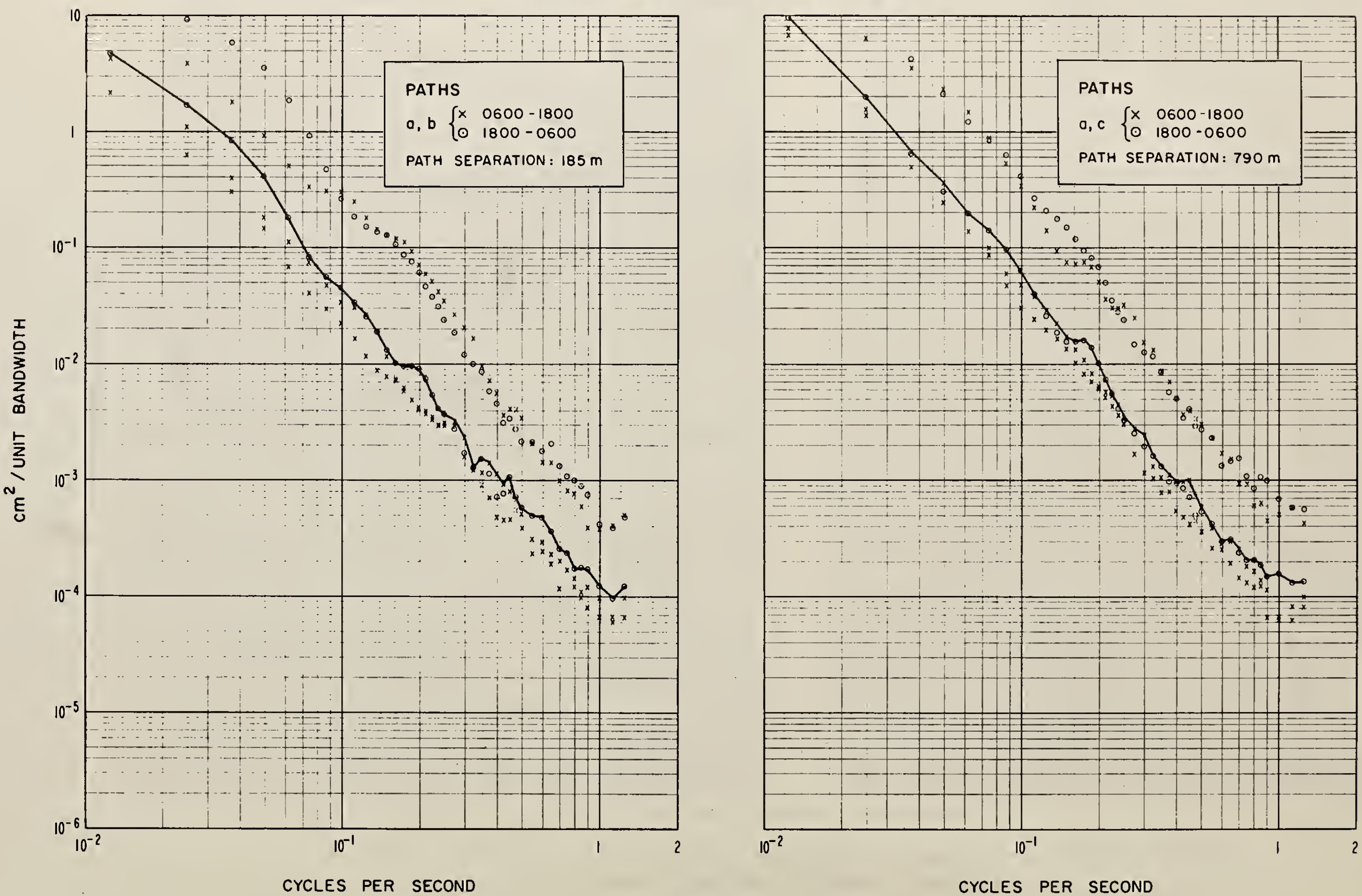

Figure 43

RANGE DIFFERENCE POWER SPECTRA
PUUNENE - HALEAKALA PATH

FIFTEEN - MINUTE SAMPLES FROM RUN 7

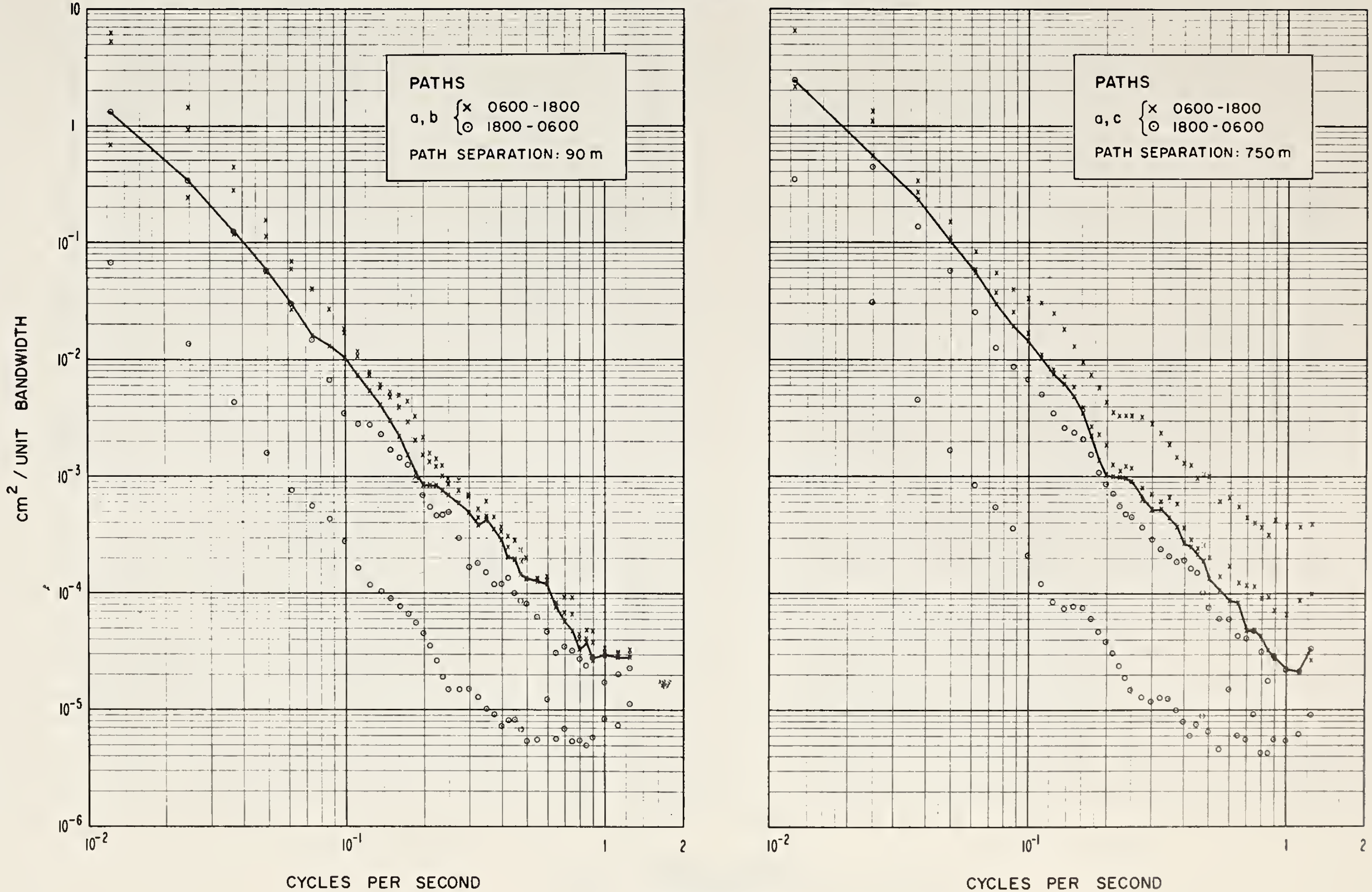

Figure 44

RANGE DIFFERENCE POWER SPECTRA
PUUNENE - HALEAKALA PATH

FIFTEEN-MINUTE SAMPLES FROM RUN 8

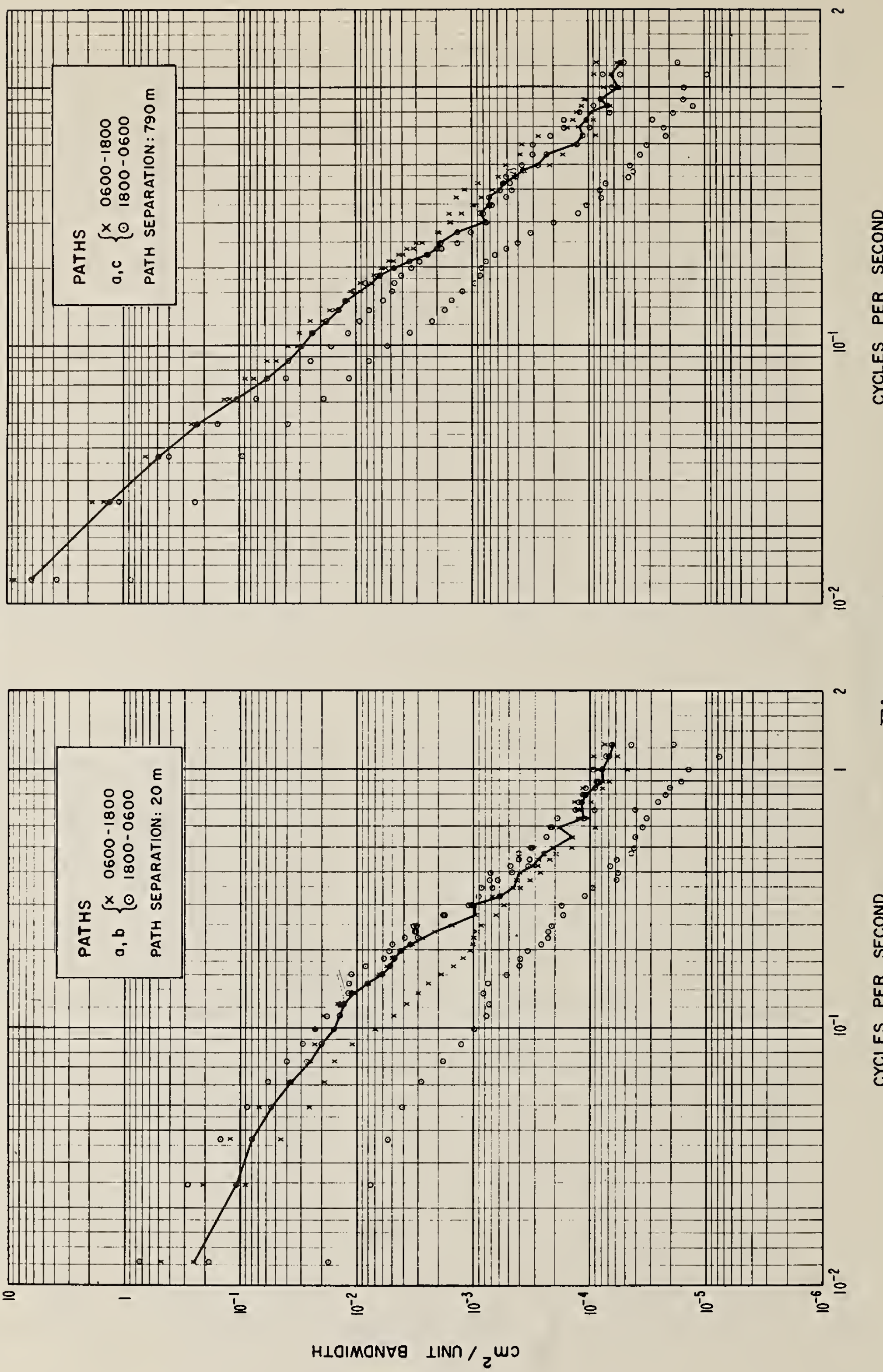

Figure 45

RANGE DIFFERENCE POWER SPECTRA
PUUNENE - HALEAKALA PATH

FIFTEEN - MINUTE SAMPLES FROM RUN 9

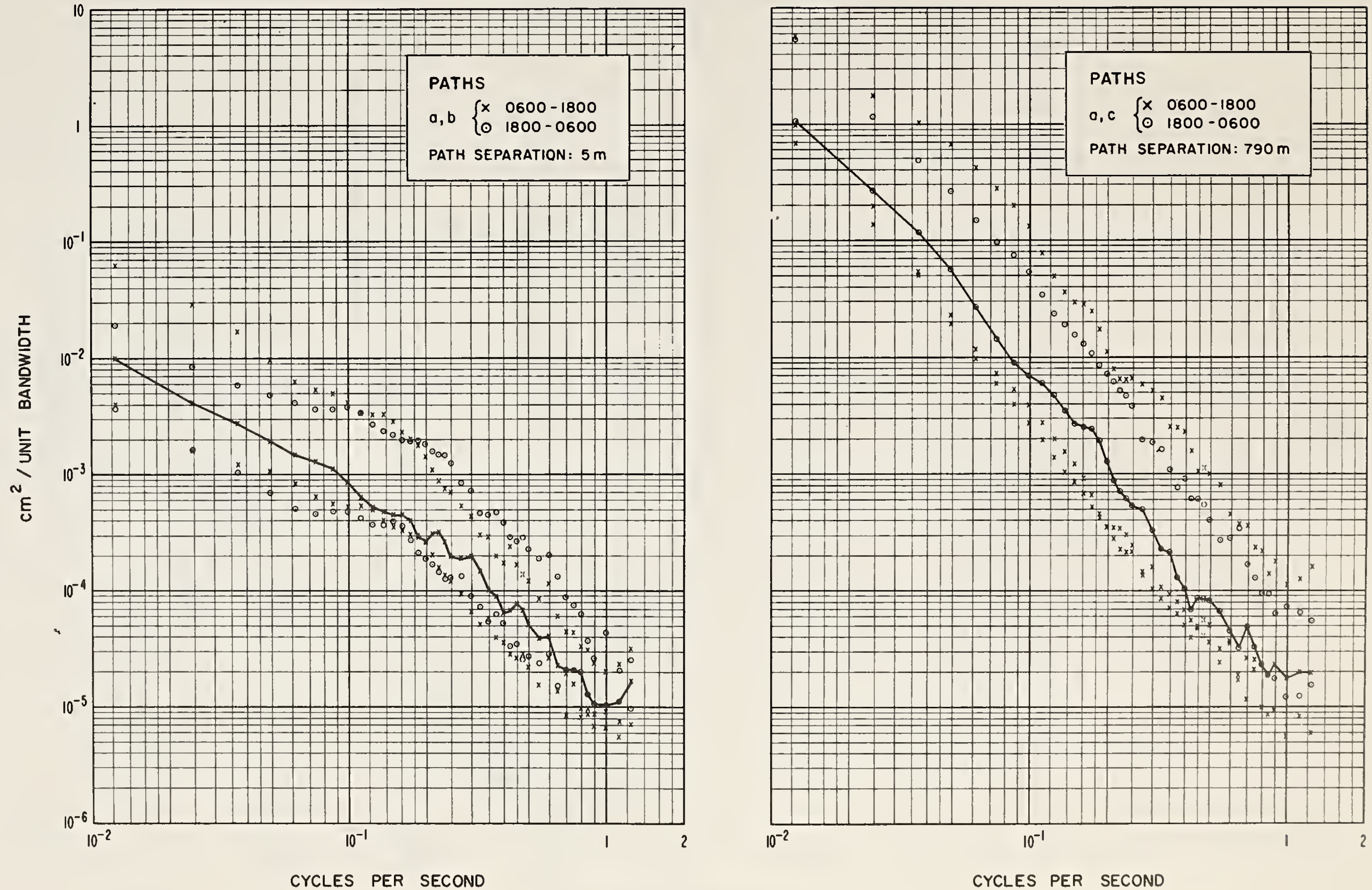

Figure 46

RANGE, REFRACTIVITY AND HUMIDITY DATA FROM RUN 1

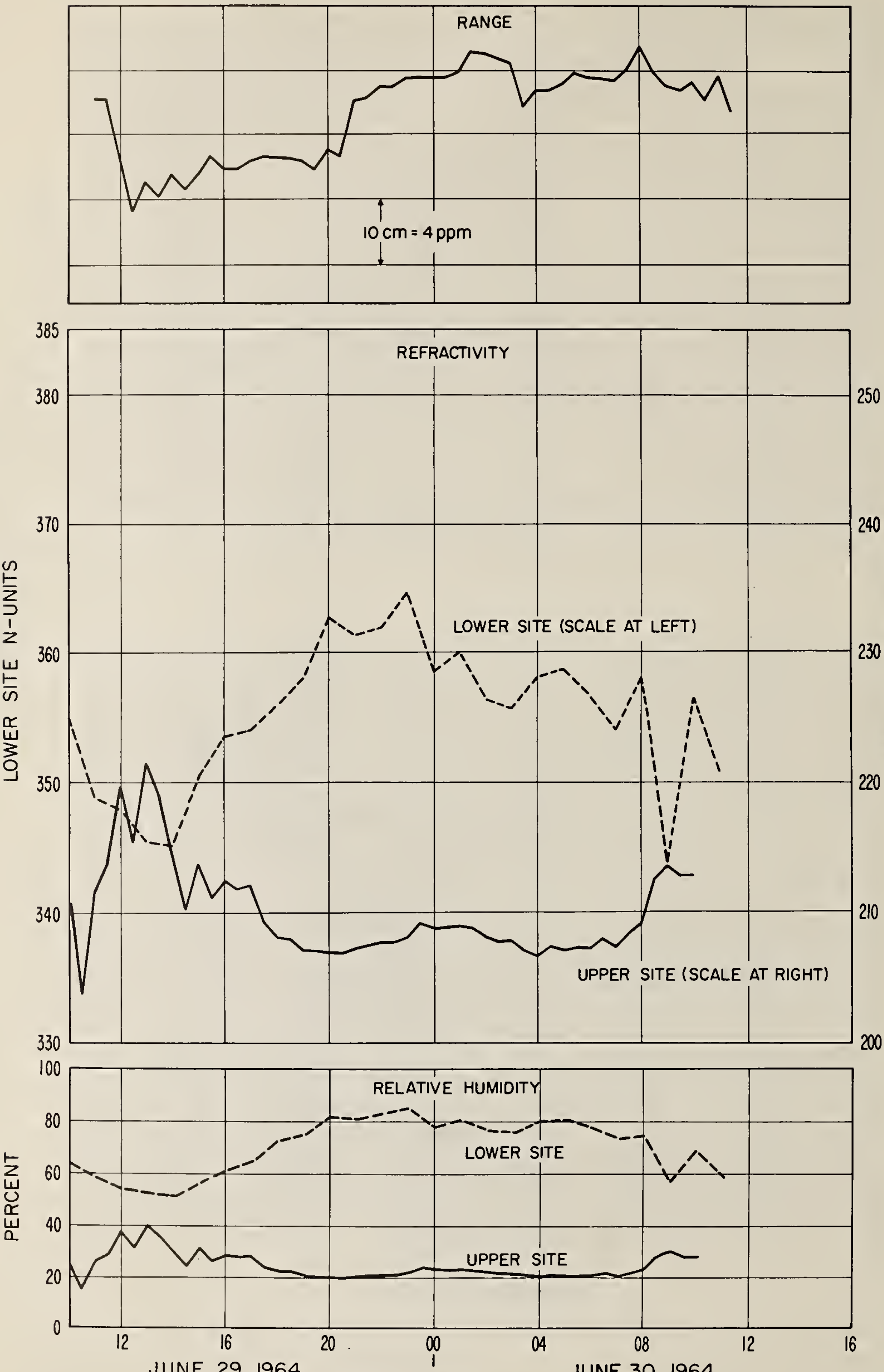

Figure 47

RANGE, REFRACTIVITY AND HUMIDITY DATA FROM RUN 2

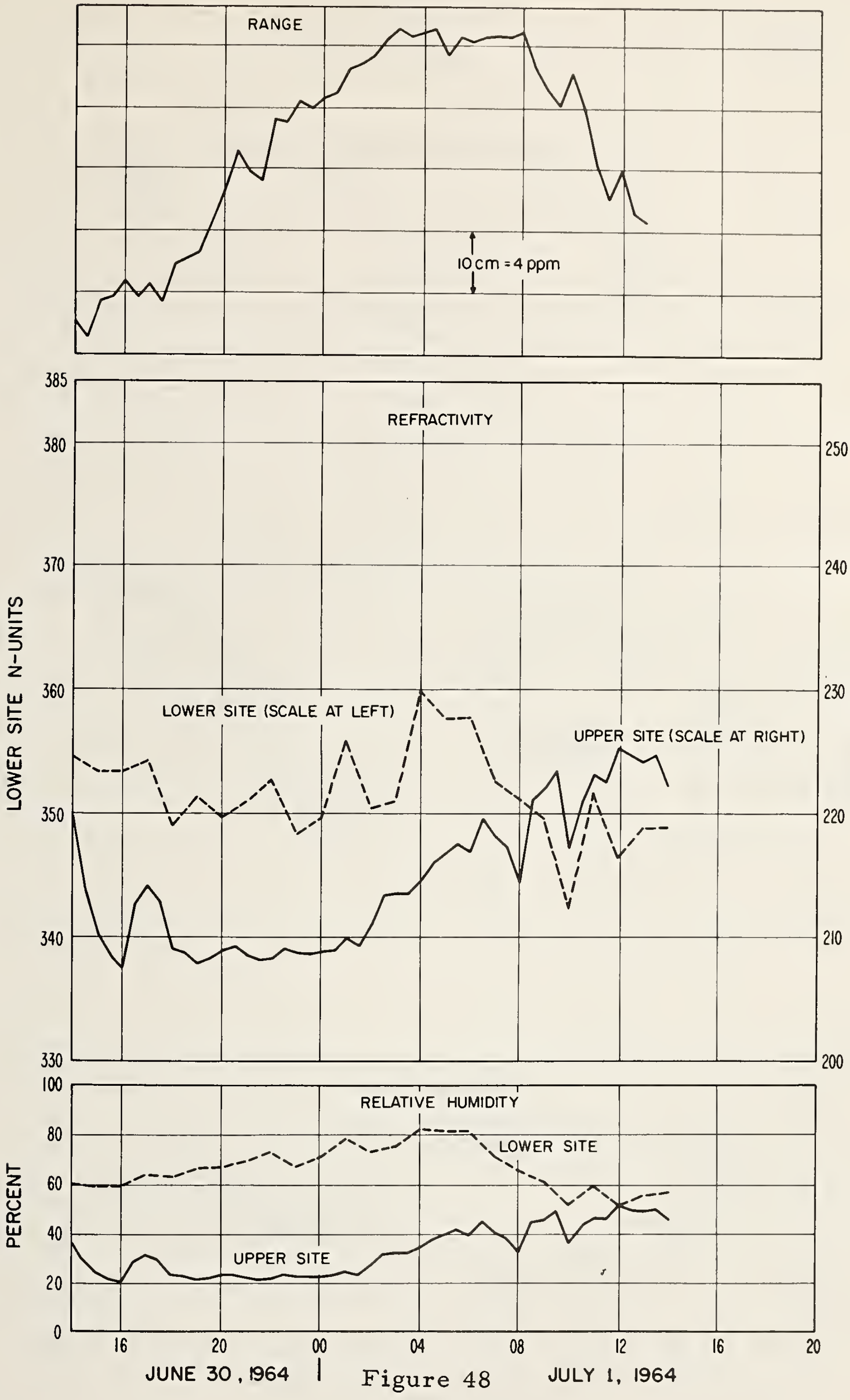

Figure 48

RANGE, REFRACTIVITY AND HUMIDITY DATA FROM RUN 3

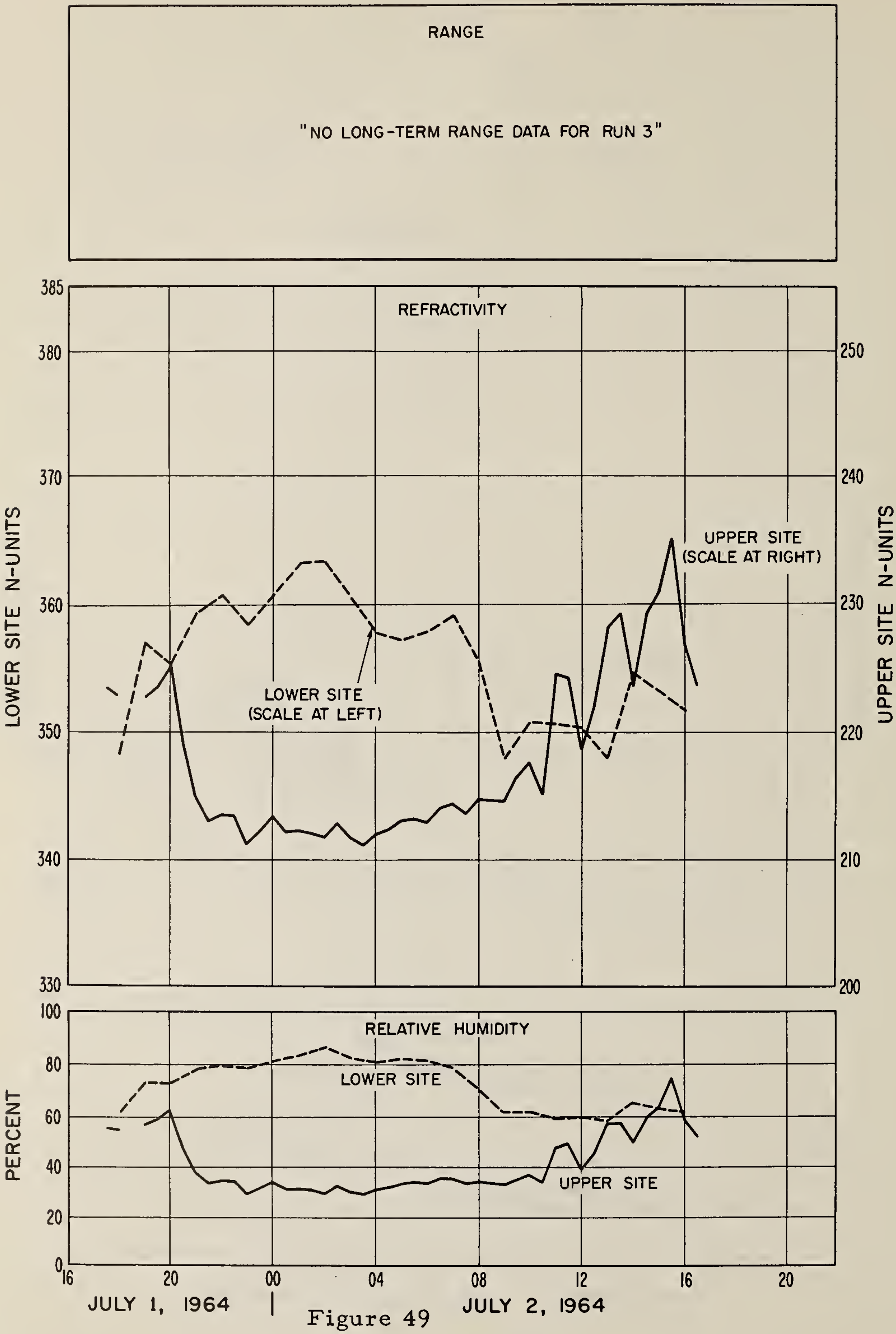

Figure 49

RANGE, REFRACTIVITY AND HUMIDITY DATA FROM RUN 4

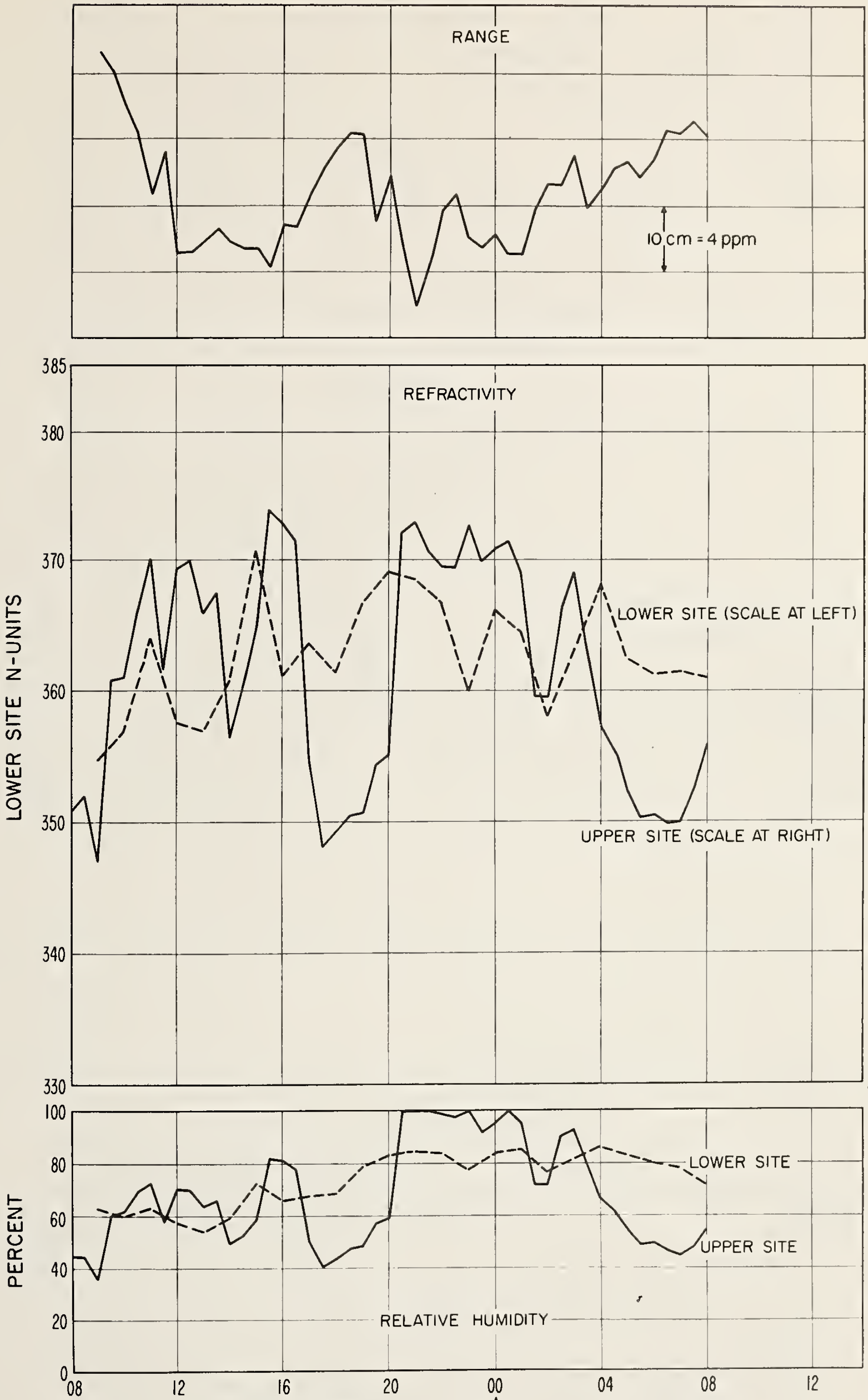

Figure 50

RANGE, REFRACTIVITY AND HUMIDITY DATA FROM RUN 5

Figure 51

RANGE, REFRACTIVITY AND HUMIDITY DATA FROM RUN 6

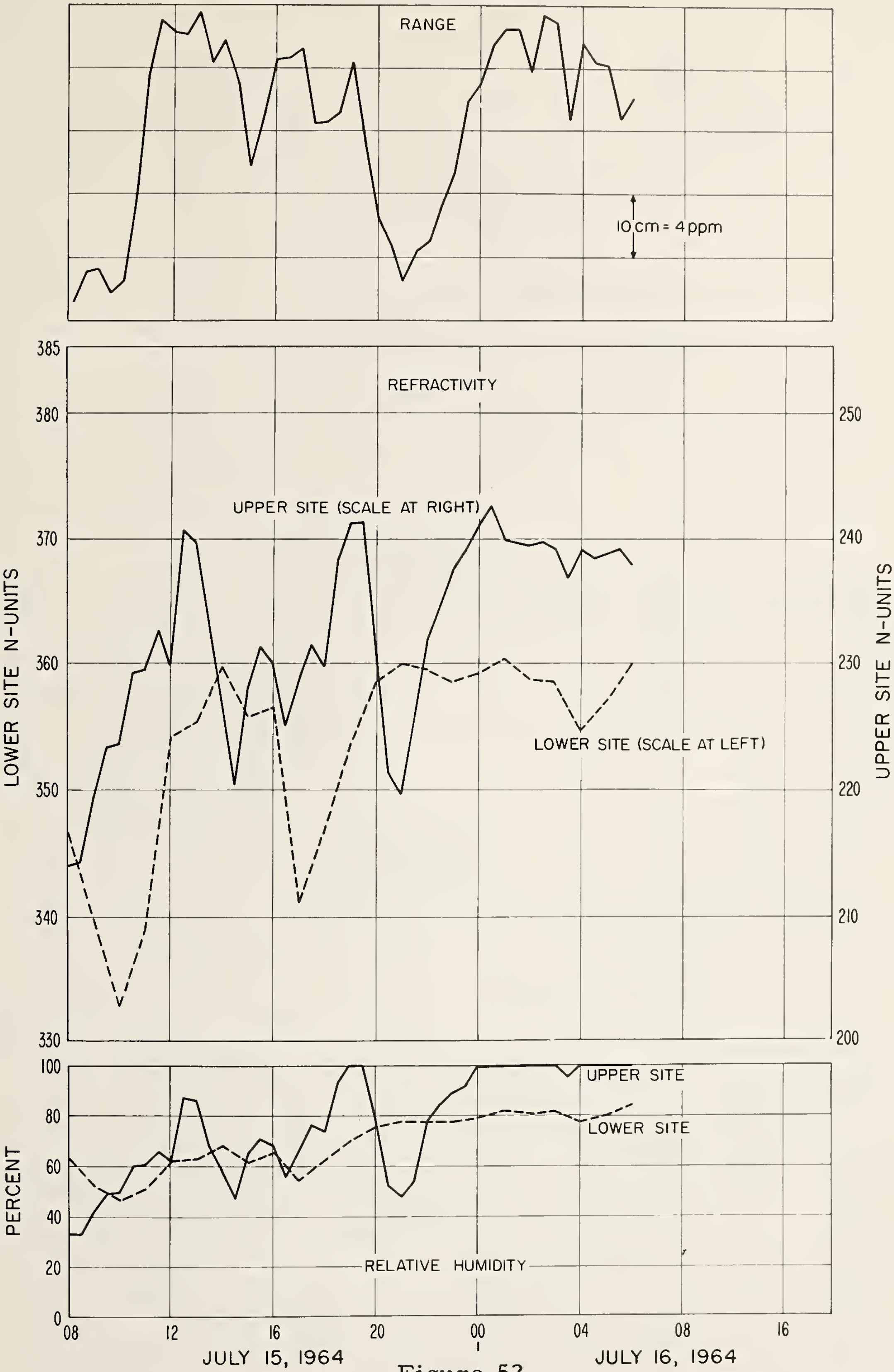

Figure 52

RANGE, REFRACTIVITY AND HUMIDITY DATA FROM RUN 7

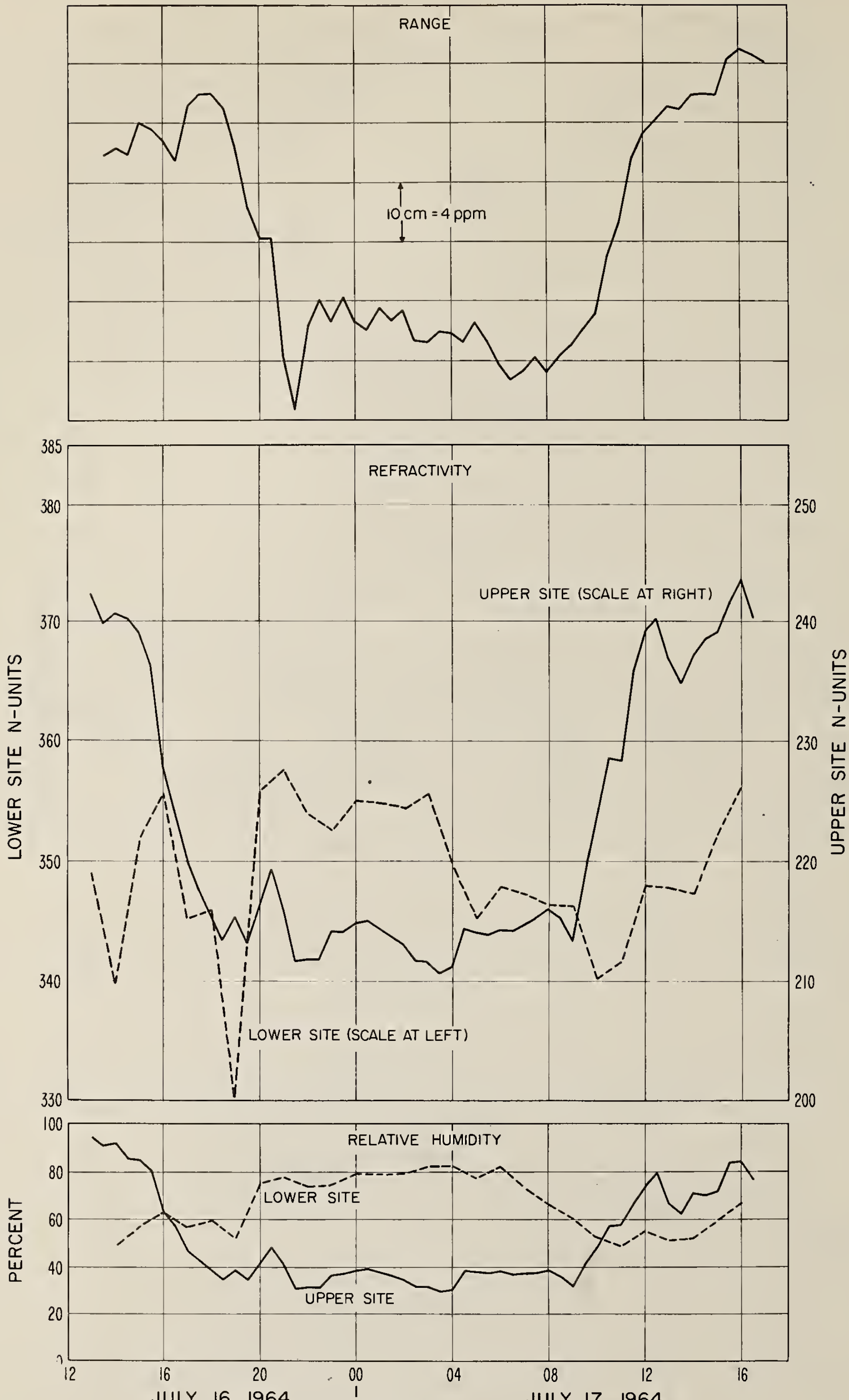

Figure 53

RANGE, REFRACTIVITY AND HUMIDITY DATA FROM RUN 8

Figure 54

RANGE, REFRACTIVITY AND HUMIDITY DATA FROM RUN 9

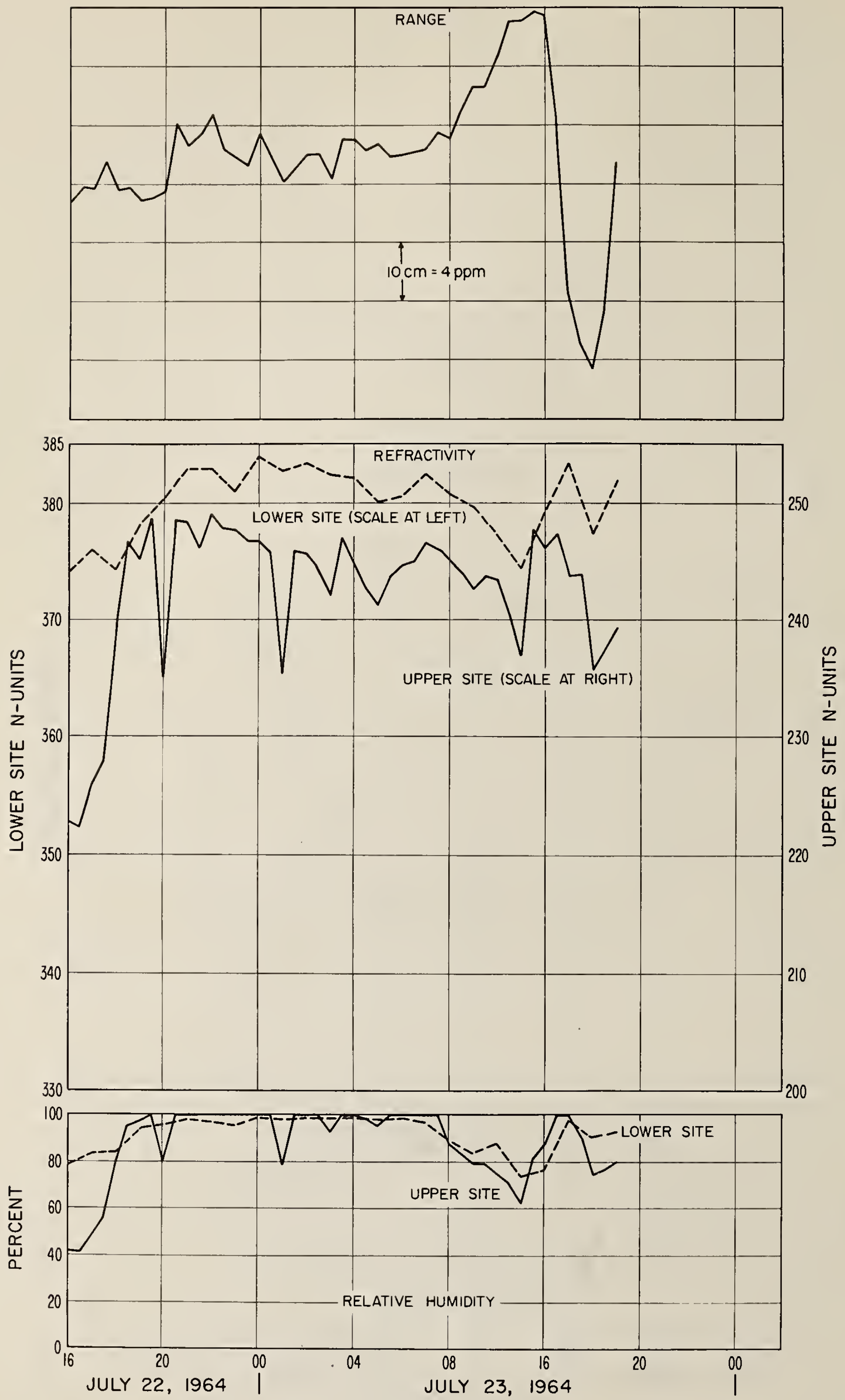

Figure 55

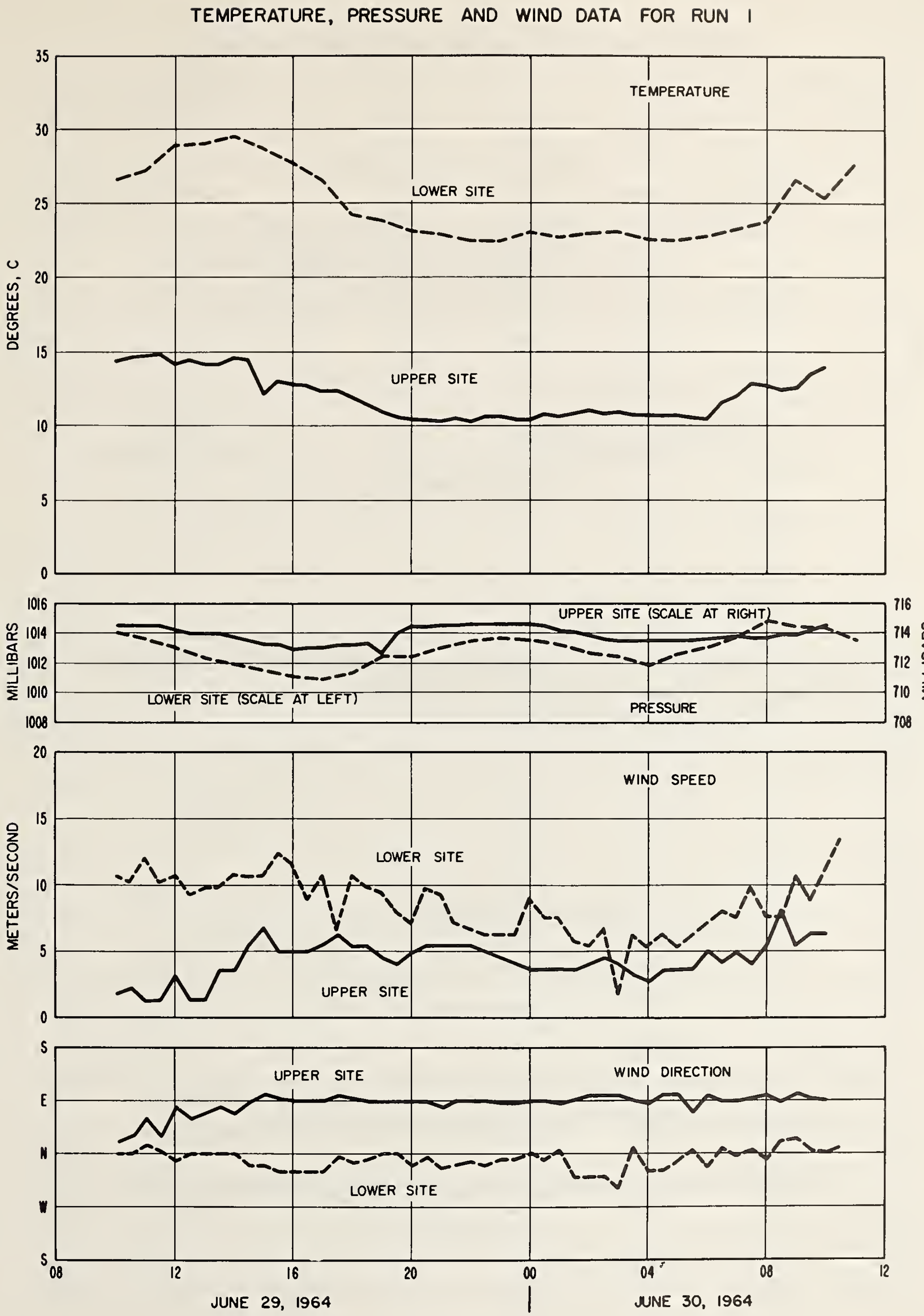
TEMPERATURE, PRESSURE AND WIND DATA FOR RUN I
TEMPERATURE
LOWER SITE
UPPER SITE
DEGREES, C
35
30
25
20
15
10
5
0
UPPER SITE (SCALE AT RIGHT)
LOWER SITE (SCALE AT LEFT)
PRESSURE
MILLIBARS
1016
1014
1012
1010
1008
716
714
712
710
708
WIND SPEED
LOWER SITE
UPPER SITE
METERS/SECOND
20
15
10
5
0
UPPER SITE
WIND DIRECTION
LOWER SITE
S
E
N
W
S
08
12
16
20
00
04
08
12
JUNE 29, 1964
JUNE 30, 1964

Figure 56

TEMPERATURE, PRESSURE AND WIND DATA FOR RUN 2

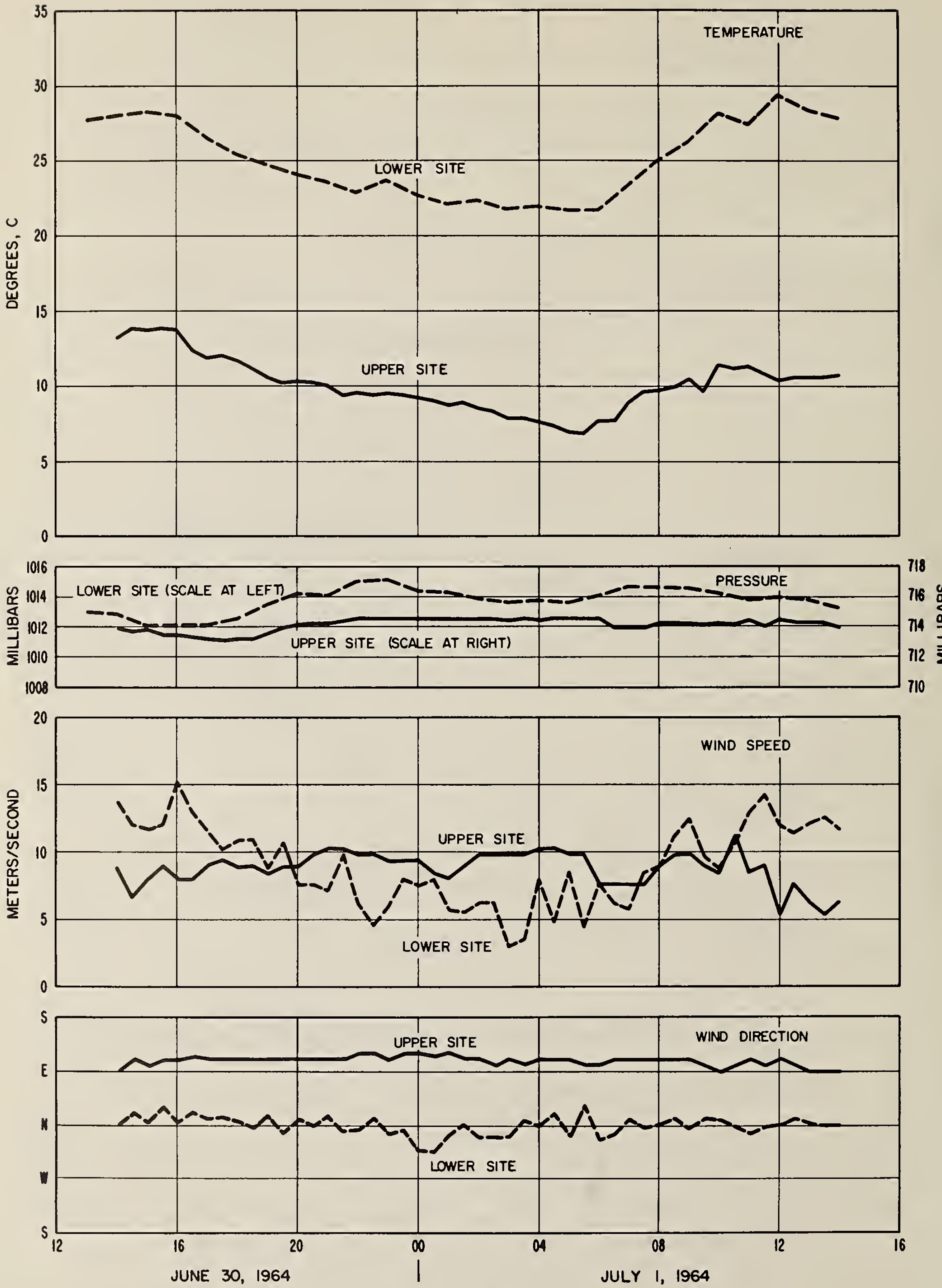

Figure 57

TEMPERATURE, PRESSURE AND WIND DATA FOR RUN 3

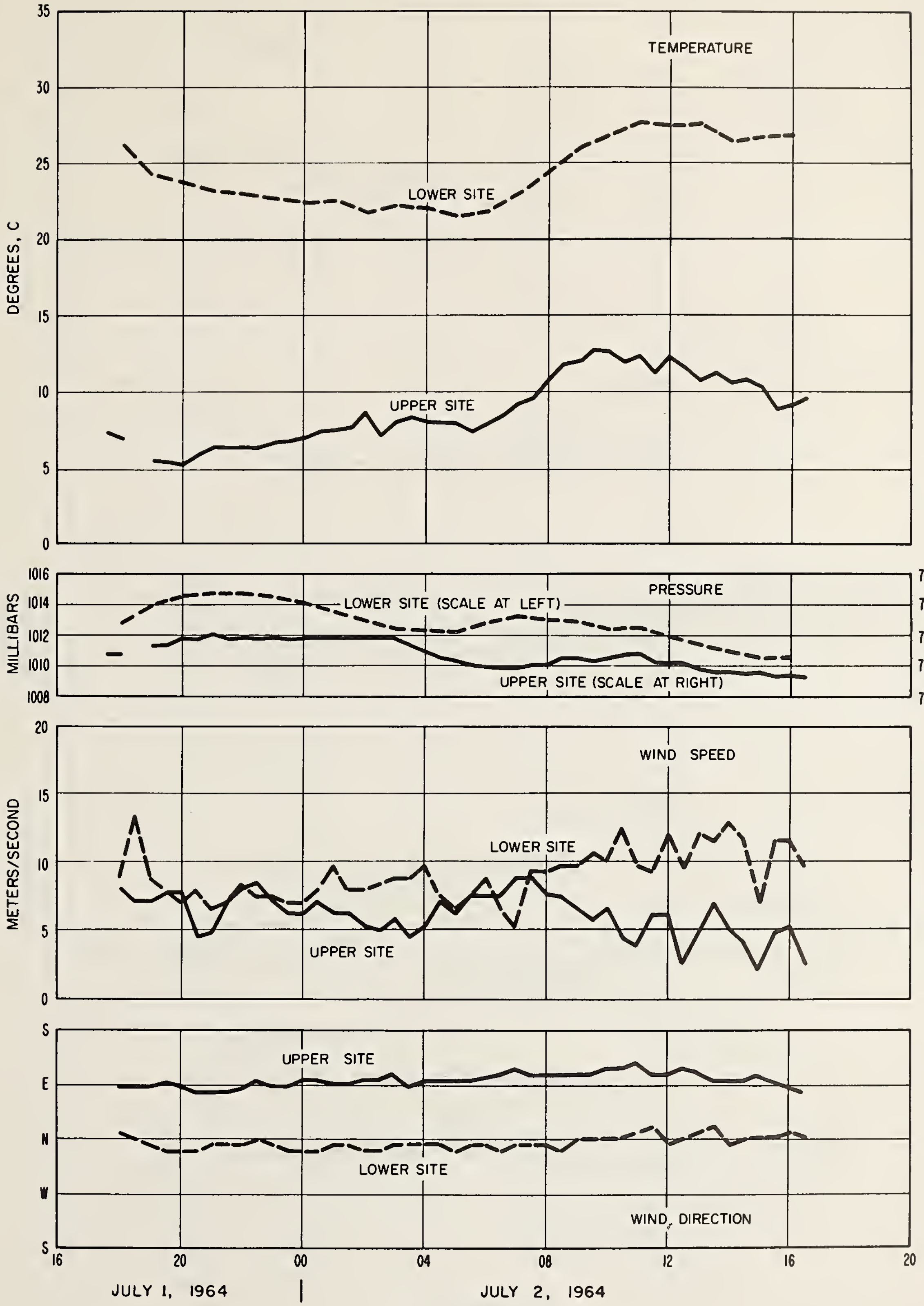

Figure 58

TEMPERATURE, PRESSURE AND WIND DATA FOR RUN 4

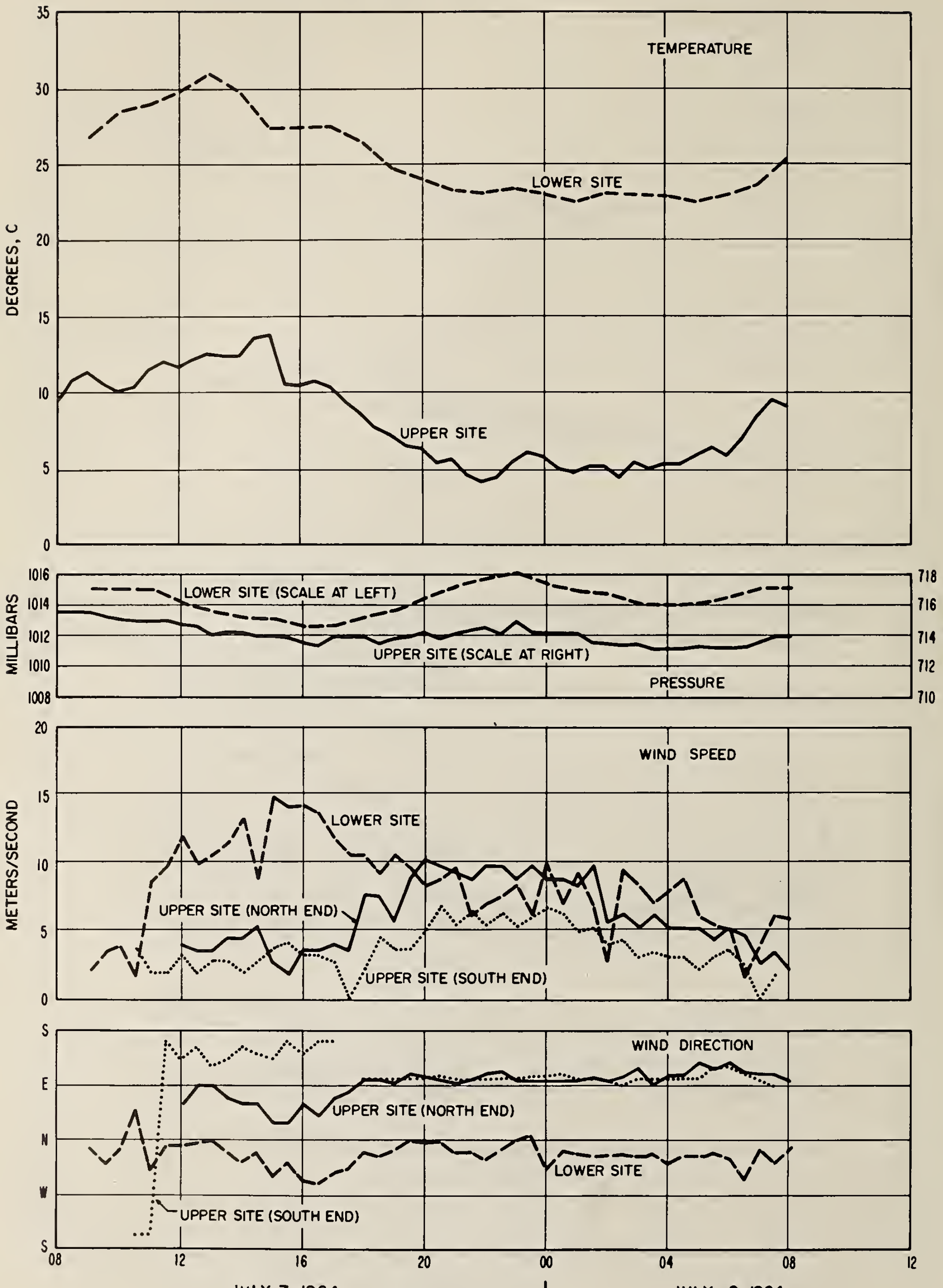

Figure 59

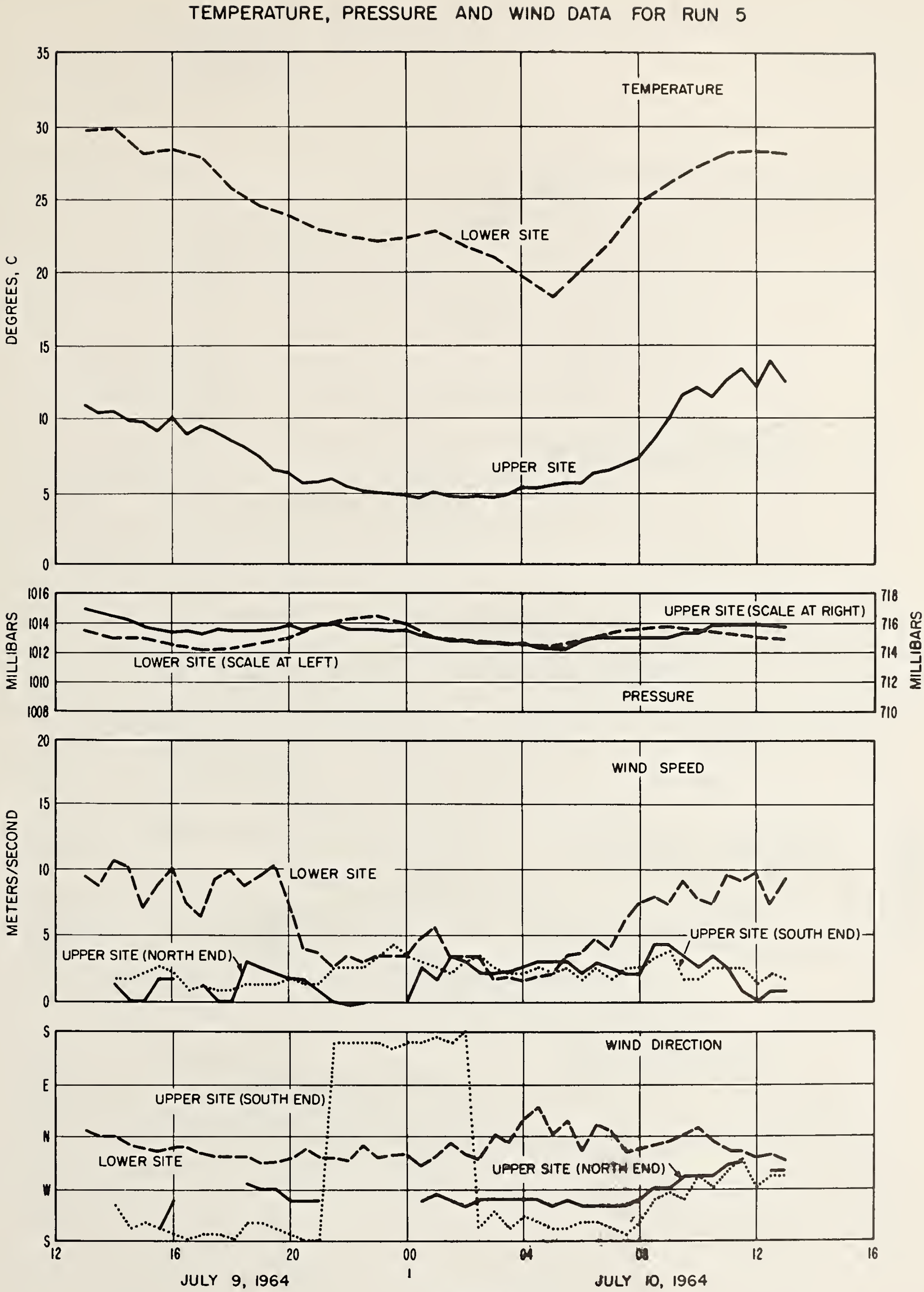
TEMPERATURE, PRESSURE AND WIND DATA FOR RUN 5
TEMPERATURE
LOWER SITE
UPPER SITE
DEGREES, C
35
30
25
20
15
10
5
0
MILLIBARS
1016
1014
1012
1010
1008
718
716
714
712
710
UPPER SITE (SCALE AT RIGHT)
LOWER SITE (SCALE AT LEFT)
PRESSURE
METERS/SECOND
WIND SPEED
LOWER SITE
UPPER SITE (SOUTH END)
UPPER SITE (NORTH END)
WIND DIRECTION
UPPER SITE (SOUTH END)
LOWER SITE
UPPER SITE (NORTH END)
S
E
N
W
12
16
20
00
04
08
16
JULY 9, 1964
JULY 10, 1964

Figure 60

TEMPERATURE, PRESSURE AND WIND DATA FOR RUN 6

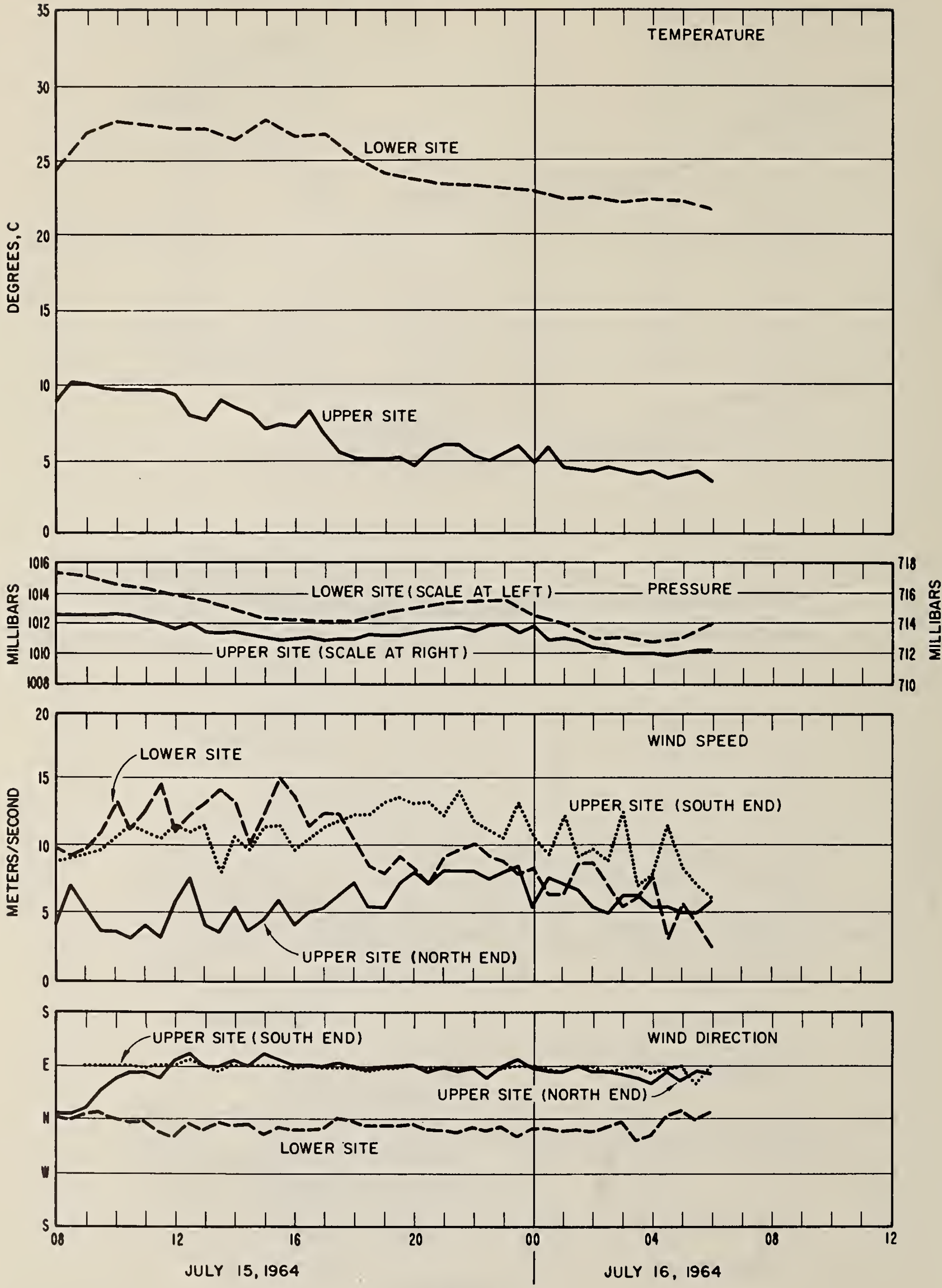

Figure 61

TEMPERATURE, PRESSURE AND WIND DATA FOR RUN 7

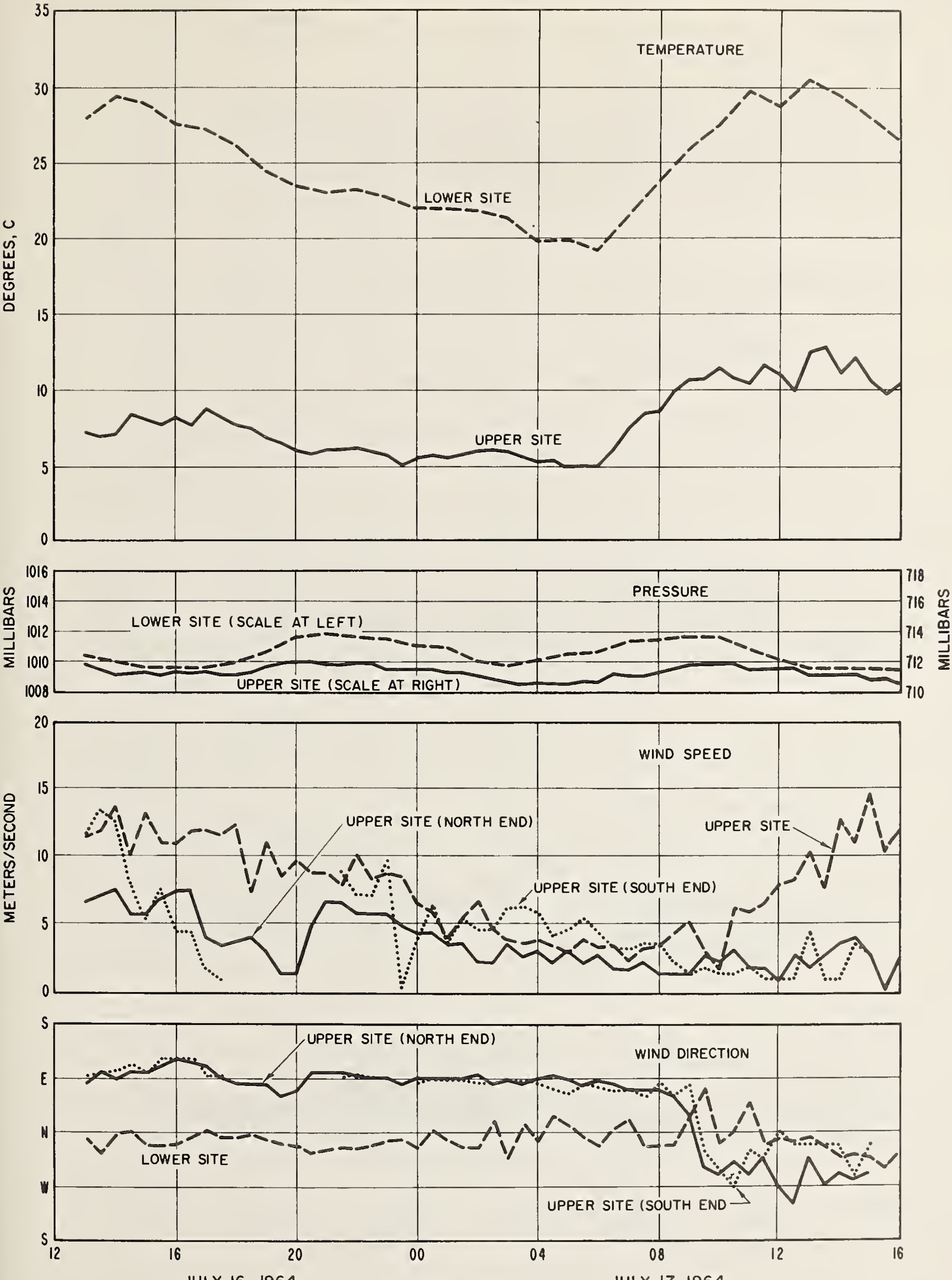

Figure 62

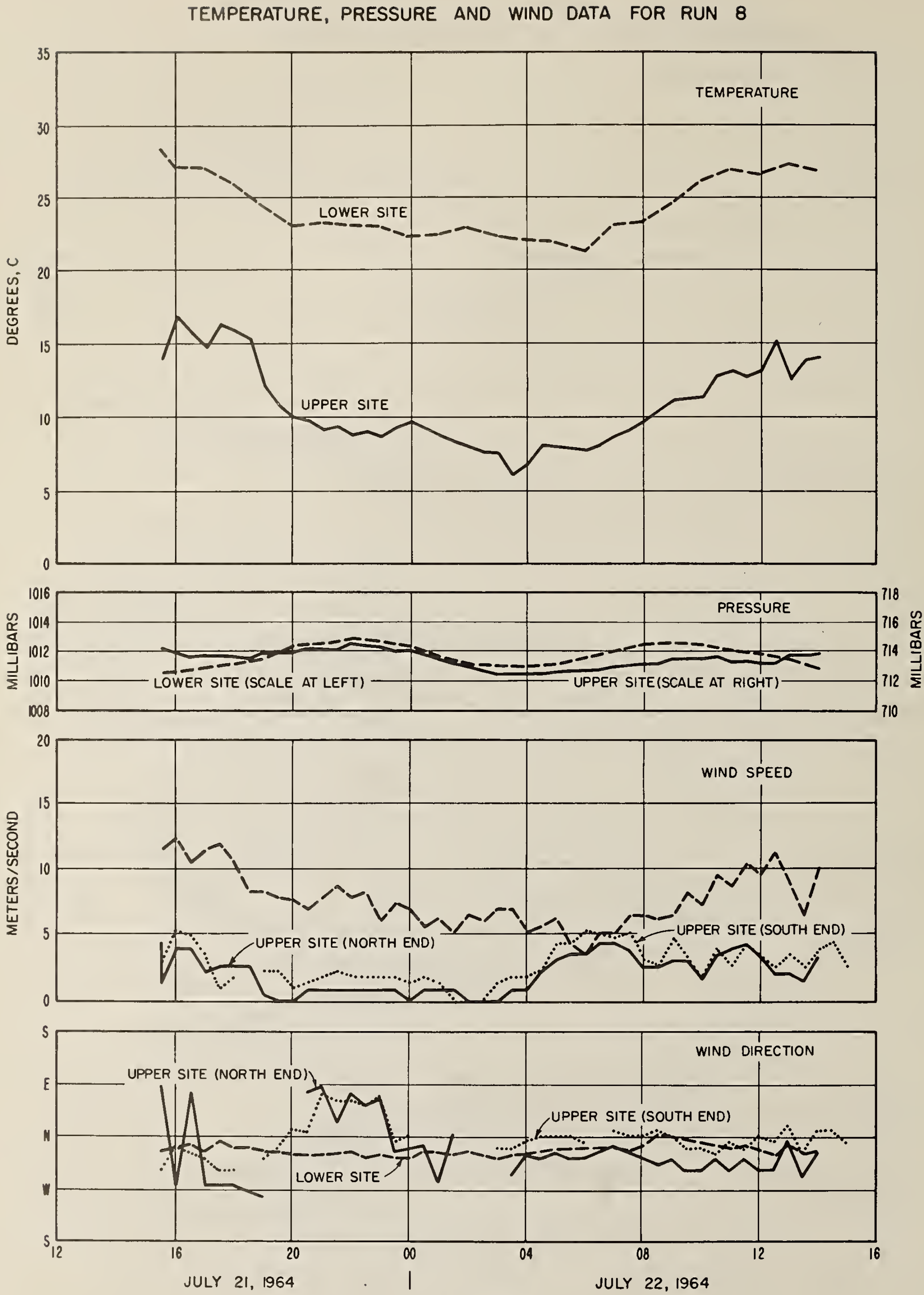

TEMPERATURE, PRESSURE AND WIND DATA FOR RUN 8
TEMPERATURE
LOWER SITE
UPPER SITE
DEGREES, C
PRESSURE
MILLIBARS
LOWER SITE (SCALE AT LEFT)
UPPER SITE (SCALE AT RIGHT)
WIND SPEED
METERS/SECOND
UPPER SITE (NORTH END)
UPPER SITE (SOUTH END)
WIND DIRECTION
UPPER SITE (NORTH END)
UPPER SITE (SOUTH END)
LOWER SITE
JULY 21, 1964
JULY 22, 1964

Figure 63

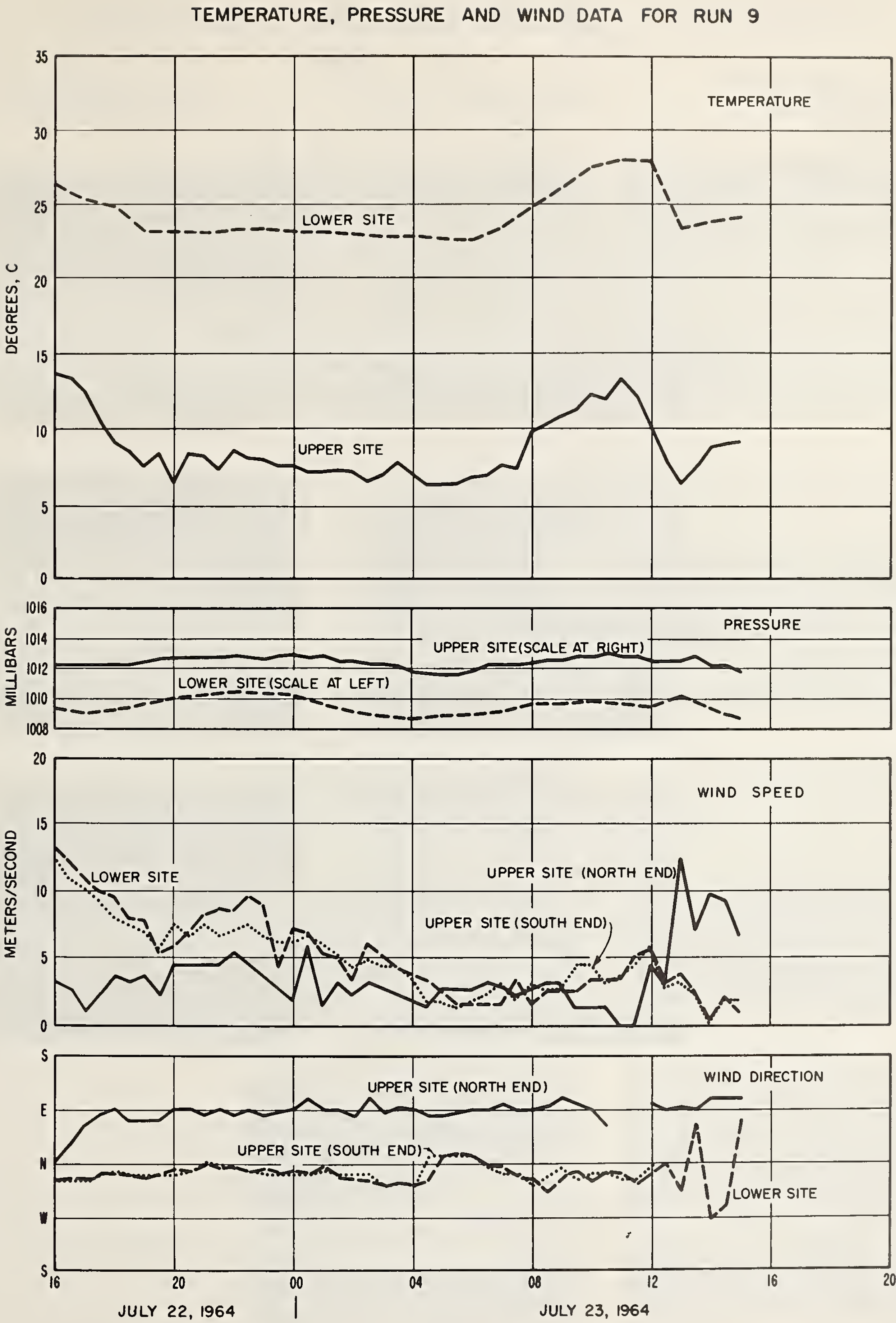
TEMPERATURE, PRESSURE AND WIND DATA FOR RUN 9
TEMPERATURE
DEGREES, C
LOWER SITE
UPPER SITE
PRESSURE
MILLIBARS
UPPER SITE (SCALE AT RIGHT)
LOWER SITE (SCALE AT LEFT)
WIND SPEED
METERS/SECOND
LOWER SITE
UPPER SITE (NORTH END)
UPPER SITE (SOUTH END)
WIND DIRECTION
UPPER SITE (NORTH END)
UPPER SITE (SOUTH END)
LOWER SITE
JULY 22, 1964
JULY 23, 1964

Figure 64

PATH PHOTOGRAPHS TAKEN AT TIMES INDICATED

RUN I

ASSOCIATED SAMPLE | FROM LOWER SITE | FROM UPPER SITE

I-1 (JUNE 29, 1016-1031)

I-2 (JUNE 29, 1418-1433)

I-3 (JUNE 29, 1815-1830)

Figure 65

PATH PHOTOGRAPHS TAKEN AT TIMES INDICATED

RUN 2

ASSOCIATED SAMPLE	FROM LOWER SITE	FROM UPPER SITE
2-1 (JUNE 30, 1452-1507)	1456	1500
2-2 (JUNE 30, 1930-1945)		1930
2-4 (JULY 1, 0531-0546)	0602	0600
2-5 (JULY 1, 1001-1016)	1001	0959

Figure 66

PATH PHOTOGRAPHS TAKEN AT TIMES INDICATED

RUN 3

FROM LOWER SITE | FROM UPPER SITE

3 - 1 (JULY 1, 1800 - 1815)

3 - 4 (JULY 2, 0815 - 0830)

3 - 5 (JULY 2, 1238 - 1253)

Figure 67

PATH PHOTOGRAPHS TAKEN AT TIMES INDICATED

RUN 4

ASSOCIATED SAMPLE	FROM LOWER SITE	FROM UPPER SITE
4-1 (JULY 7, 0930-0945)	1001	0929
4-2 (JULY 7, 1350-1405)	1358	1400
4-5 (JULY 8, 0615-0630)	0603	0629

Figure 68

PATH PHOTOGRAPHS TAKEN AT TIMES INDICATED

RUN 5

ASSOCIATED SAMPLE	FROM LOWER SITE	FROM UPPER SITE
5 -1 (JULY 9, 1700-1715)		
5-4 (JULY 10, 0700-0715)		
5-5 (JULY 10, 1100-1115)		

Figure 69

PATH PHOTOGRAPHS TAKEN AT TIMES INDICATED

RUN 6

ASSOCIATED SAMPLE	FROM LOWER SITE	FROM UPPER SITE
6-1 (JULY 15, 0830-0845)		
6-2 (JULY 15, 1100-1115)		
6-3 (JULY 15, 1500-1515)		

Figure 70

PATH PHOTOGRAPHS TAKEN AT TIMES INDICATED

RUN 7

ASSOCIATED SAMPLE	FROM LOWER SITE	FROM UPPER SITE
7-1 (JULY 16, 1800-1815)		
7-4 (JULY 17, 1130-1145)		
7-5 (JULY 17, 1500-1515)		

Figure 71

PATH PHOTOGRAPHS TAKEN AT TIMES INDICATED

RUN 8

ASSOCIATED SAMPLE	FROM LOWER SITE	FROM UPPER SITE
8-1 (JULY 21, 1550-1605)		
8-4 (JULY 22, 0530-0545)		
8-5 (JULY 22, 1003-1018)		

Figure 72

PATH PHOTOGRAPHS TAKEN AT TIMES INDICATED

RUN 9

ASSOCIATED SAMPLE | FROM LOWER SITE | FROM UPPER SITE

9 - 1 (JULY 22, 1629-1644)

9 - 4 (JULY 23, 0615-0630)

9 - 5 (JULY 23, 1120-1135)

Figure 73

TABLE II

Variances, in $(cm)^2$, of Range and First and Second Range Difference Data
(Computed from 15-minute samples; pass-band: 0 to approximately 1.4 Hz)

Sample No.	Date	Starting Time	R_a	ΔR_{ad}	ΔR_{ac}	ΔR_{cd}	ΔR_{ab}	ΔR_{bc}	$\Delta^2 R_{ac,cd}$	$\Delta^2 R_{ab,bc}$
1-1	6/29/64	1016	1.43	2.12(-2)	6.15(-3)	6.48(-3)	2.01(-3)	1.97(-3)	6.87(-3)	1.49(-3)
1-2	6/29/64	1418	7.85(-2)	6.50(-2)	2.29(-2)	1.92(-2)	7.64(-3)	7.04(-3)	2.51(-2)	6.10(-3)
1-3	6/29/64	1815	6.66(-2)	1.80(-2)	7.14(-3)	4.38(-3)	2.34(-3)	1.87(-3)	7.57(-3)	1.65(-3)
1-4	6/29/64	2215	7.38(-1)	7.98(-3)	3.03(-3)	3.22(-3)	1.01(-3)	1.29(-3)	2.59(-3)	5.10(-4)
1-5	6/30/64	0215	2.36	2.87(-3)	8.79(-4)	9.54(-4)	3.27(-4)	2.78(-4)	7.75(-4)	2.07(-4)
2-1	6/30/64	1452	5.97	1.54(-2)	4.73(-3)	4.16(-3)	1.35(-3)	1.39(-3)	3.35(-3)	6.92(-4)
2-2	6/30/64	1930	2.90	5.83(-3)	1.34(-3)	1.02(-3)	3.90(-4)	3.56(-4)	1.18(-3)	3.38(-4)
2-3	7/1/64	0000	6.63(-1)	5.58(-3)	3.61(-4)	2.91(-4)	6.99(-5)	2.18(-4)	--	2.29(-4)
2-4	7/1/64	0531	3.73(-1)	7.65(-4)	3.79(-4)	2.75(-4)	1.13(-4)	1.48(-4)	--	1.22(-4)
2-5	7/1/64	1001	1.32	1.87(-3)	5.38(-4)	4.61(-4)	1.57(-4)	1.98(-4)	4.11(-4)	1.94(-4)
3-1	7/1/64	1800	1.08	3.99(-3)	4.54(-4)	4.04(-4)	1.56(-4)	9.48(-5)	2.06(-4)	5.73(-5)
3-2	7/1/64	2230	1.81(+1)	2.66(-3)	8.15(-4)	7.11(-4)	2.49(-4)	1.85(-4)	2.44(-4)	4.64(-5)
3-3	7/2/64	0315	7.29	4.16(-4)	1.33(-4)	1.14(-4)	4.48(-5)	2.80(-5)	6.31(-5)	1.61(-5)
3-4	7/2/64	0815	3.05	1.87(-4)	6.52(-5)	5.98(-5)	2.45(-5)	2.09(-5)	8.52(-5)	2.38(-5)
3-5	7/2/64	1238	8.54(-1)	3.16(-3)	9.15(-4)	8.02(-4)	2.98(-4)	1.91(-4)	5.12(-4)	1.29(-4)

numbers in parentheses indicate powers of 10, i.e., $3.25(-2) = 3.25 \times 10^{-2}$

TABLE III

Variances, in $(cm)^2$, of Range and First and Second Range Difference Data

(Computed from 15-minute samples; pass-band: 0 to approximately 1.4 Hz)

Sample No.	Date	Starting Time	R_a	R_c	ΔR_{ac}	ΔR_{ab}	ΔR_{cd}	$\Delta^2 R_{ab,cd}$
4-1	7/7/64	0930	1.18	1.22	1.16(-1)	--	8.38(-3)	--
4-2	7/7/64	1350	6.63(-1)	7.29(-1)	2.86(-1)	3.49(-2)	9.30(-2)	1.07(-1)
4-3	7/7/64	2015	2.88	1.67	2.71(-1)	4.73(-2)	3.79(-2)	8.77(-2)
4-4	7/8/64	0000	8.01(-1)	7.13(-1)	1.10(-1)	2.11(-2)	2.63(-2)	5.62(-2)
4-5	7/8/64	0615	1.99	1.94	3.77(-2)	3.81(-2)	5.78(-3)	--
5-1	7/9/64	1700	7.79(-1)	9.41(-1)	1.87(-1)	4.56(-3)	5.01(-3)	1.07(-2)
5-2	7/9/64	2200	2.32(-1)	2.03(-1)	2.00(-2)	2.54(-4)	2.52(-4)	5.10(-4)
5-3	7/10/64	0400	3.89(-1)	3.90(-1)	2.68(-2)	2.18(-4)	2.04(-4)	4.23(-4)
5-4	7/10/64	0700	1.09(-1)	1.17(-1)	2.36(-2)	1.18(-3)	1.09(-3)	2.32(-3)
5-5	7/10/64	1100	2.91	3.66	7.09(-1)	6.55(-3)	8.41(-3)	1.31(-2)
6-1	7/15/64	0830	1.20	1.43	1.76	1.58(-1)	4.28(-1)	6.73(-1)
6-2	7/15/64	1100	1.47	2.55	6.55(-1)	2.04(-1)	2.74(-1)	5.61(-1)
6-3	7/15/64	1500	3.08	2.73	1.94	6.40(-1)	5.94(-1)	1.26
6-4	7/15/64	2100	1.54	1.83	2.99	8.88(-1)	7.96(-1)	1.44
6-5	7/16/64	0130	1.71	1.81	5.75(-1)	1.44(-1)	3.23(-1)	3.30(-1)
7-1	7/16/64	1800	1.52	1.81	2.26	5.58(-1)	3.64(-1)	1.16
7-2	7/17/64	0000	9.67(-1)	7.19(-1)	2.49(-1)	9.60(-2)	1.18(-1)	2.78(-1)
7-3	7/17/64	0500	2.04(-1)	1.22(-1)	2.85(-1)	1.33(-2)	8.26(-3)	1.84(-2)
7-4	7/17/64	1130	6.02(-1)	2.42	2.72	8.23(-1)	3.91(-1)	1.61
7-5	7/17/64	1500	2.50	2.63	2.73(-1)	1.07(-1)	3.18(-2)	1.37(-1)
8-1	7/21/64	1550	1.07(+1)	1.05(+1)	1.86	1.70(-2)	2.17(-2)	1.68(-1)
8-2	7/21/64	2015	8.03(-1)	5.25(-1)	5.15(-1)	8.26(-3)	7.12(-3)	1.64(-2)
8-3	7/22/64	0100	1.09	1.39	1.57	2.32(-2)	7.84(-3)	3.07(-2)
8-4	7/22/64	0530	1.23	1.25	1.04(-1)	8.83(-4)	--	2.10(-3)
8-5	7/22/64	1003	6.09	7.63	2.14	1.26(-2)	1.55(-2)	2.80(-2)
9-1	7/22/64	1629	9.25(-1)	9.49(-1)	1.98	2.64(-3)	2.26(-3)	5.63(-3)
9-2	7/22/64	2100	1.16	1.41	6.02(-1)	1.26(-3)	2.47(-3)	3.45(-3)
9-3	7/23/64	0145	2.09(-1)	1.42(-1)	2.90(-1)	2.16(-4)	4.79(-4)	6.16(-4)
9-4	7/23/64	0615	1.08(-1)	1.56(-1)	1.20(-1)	2.57(-4)	2.63(-4)	5.02(-4)
9-5	7/23/64	1120	2.36	2.87	3.00(-1)	6.43(-4)	4.53(-4)	1.47(-3)

numbers in parentheses indicate powers of 10, i.e., 3.25(-2) = 3.25×10^{-2}.

TABLE IV

Variances, in $(cm)^2$, of Range and First and Second Range Difference Data
(Computed from 15-minute samples; pass-band: approximately 0.007 to 1.4 Hz)

Sample No.	Date	Starting Time	R_a	ΔR_{ad}	ΔR_{ac}	ΔR_{cd}	ΔR_{ab}	ΔR_{bc}	$\Delta^2 R_{ac,cd}$	$\Delta^2 R_{ab,bc}$
1-1	6/29/64	1016	3.25(-2)	1.29(-2)	4.10(-3)	4.67(-3)	1.40(-3)	1.54(-3)	7.72(-3)	1.52(-3)
1-2	6/29/64	1418	2.36(-2)	2.68(-2)	1.31(-2)	1.02(-2)	4.77(-3)	4.84(-3)	2.44(-2)	6.82(-3)
1-3	6/29/64	1815	1.06(-2)	4.66(-3)	2.54(-3)	2.27(-3)	1.15(-3)	8.38(-4)	5.02(-3)	1.70(-3)
1-4	6/29/64	2215	9.55(-3)	1.89(-3)	8.02(-4)	1.23(-3)	3.16(-4)	5.19(-4)	1.64(-3)	4.36(-4)
1-5	6/30/64	0215	9.33(-3)	1.64(-3)	5.88(-4)	5.97(-4)	2.06(-4)	1.88(-4)	7.80(-4)	2.02(-4)
2-1	6/30/64	1452	7.87(-2)	1.44(-2)	4.24(-3)	3.89(-3)	1.25(-3)	1.27(-3)	3.69(-3)	8.68(-4)
2-2	6/30/64	1930	1.58(-2)	4.44(-3)	8.39(-4)	8.14(-4)	--	3.00(-4)	1.19(-3)	3.86(-4)
2-3	7/1/64	0000	6.95(-3)	2.02(-3)	2.47(-4)	2.02(-4)	6.05(-5)	--	--	2.09(-4)
2-4	7/1/64	0531	7.89(-3)	3.94(-4)	2.50(-4)	1.58(-4)	6.87(-5)	1.19(-4)	--	1.29(-4)
2-5	7/1/64	1001	3.66(-2)	1.56(-3)	7.92(-4)	4.10(-4)	1.51(-4)	1.69(-4)	5.08(-4)	1.70(-4)
3-1	7/1/64	1800	1.74(-1)	4.08(-3)	4.63(-4)	4.32(-4)	1.53(-4)	1.05(-4)	2.37(-4)	5.63(-5)
3-2	7/1/64	2230	4.56(-1)	2.43(-3)	7.09(-4)	6.44(-4)	2.26(-4)	1.69(-4)	3.12(-4)	5.84(-5)
3-3	7/2/64	0315	6.14(-2)	2.81(-4)	9.74(-5)	9.06(-5)	3.38(-5)	2.47(-5)	6.87(-5)	1.48(-5)
3-4	7/2/64	0815	3.45(-2)	1.62(-4)	6.03(-5)	4.96(-5)	2.43(-5)	2.34(-5)	9.37(-5)	1.85(-5)
3-5	7/2/64	1238	5.10(-2)	2.19(-3)	6.45(-4)	6.15(-4)	2.21(-4)	1.50(-4)	5.16(-4)	1.32(-4)

numbers in parentheses indicate powers of 10, i.e., 3.25(-2) = 3.25×10^{-2}.

TABLE V

Variances, in $(cm)^2$, of Range and First and Second Range Difference Data

(Computed from 15-minute samples; pass-band: approximately 0.007 to 1.4 Hz)

Sample No.	Date	Starting Time	R_a	R_c	ΔR_{ac}	ΔR_{ab}	ΔR_{cd}	$\Delta^2 R_{ab,cd}$
4-1	7/7/64	0930	2.04(-2)	1.69(-2)	9.26(-3)	9.60(-3)	2.58(-3)	--
4-2	7/7/64	1350	3.72(-2)	3.15(-2)	5.09(-2)	1.52(-2)	2.90(-2)	3.78(-2)
4-3	7/7/64	2015	4.41(-2)	4.02(-2)	5.87(-2)	2.96(-2)	1.87(-2)	4.83(-2)
4-4	7/8/64	0000	2.02(-2)	2.22(-2)	2.46(-2)	1.53(-2)	1.33(-2)	3.14(-2)
4-5	7/8/64	0615	6.17(-3)	6.57(-3)	4.43(-3)	3.91(-3)	1.80(-3)	--
5-1	7/9/64	1700	5.29(-2)	4.83(-2)	6.07(-2)	3.38(-3)	4.38(-3)	7.45(-3)
5-2	7/9/64	2200	3.32(-3)	2.60(-3)	4.80(-3)	2.12(-4)	2.28(-4)	4.63(-4)
5-3	7/10/64	0400	4.15(-3)	2.79(-3)	3.76(-3)	1.83(-4)	1.52(-4)	3.56(-4)
5-4	7/10/64	0700	8.64(-3)	7.38(-3)	1.12(-2)	1.10(-3)	1.09(-3)	2.51(-3)
5-5	7/10/64	1100	4.46(-2)	3.90(-2)	3.20(-2)	2.62(-3)	5.30(-3)	8.86(-3)
6-1	7/15/64	0830	6.23(-2)	1.02(-1)	1.30(-1)	4.38(-2)	1.05(-1)	1.62(-1)
6-2	7/15/64	1100	4.69(-2)	5.90(-2)	1.23(-1)	7.87(-2)	9.49(-2)	1.95(-1)
6-3	7/15/64	1500	3.44(-1)	2.22(-1)	4.90(-1)	2.67(-1)	2.63(-1)	4.36(-1)
6-4	7/15/64	2100	4.43(-1)	3.44(-1)	8.58(-1)	5.62(-1)	4.65(-1)	9.12(-1)
6-5	7/16/64	0130	5.65(-2)	7.64(-2)	1.65(-1)	1.03(-1)	1.21(-1)	2.26(-1)
7-1	7/16/64	1800	6.47(-2)	4.36(-2)	1.05(-1)	1.05(-1)	4.38(-2)	1.63(-1)
7-2	7/17/64	0000	2.54(-2)	2.13(-2)	3.98(-2)	2.40(-2)	2.94(-2)	5.61(-2)
7-3	7/17/64	0500	3.45(-3)	1.64(-3)	4.84(-3)	1.15(-3)	1.15(-3)	2.19(-3)
7-4	7/17/64	1130	5.41(-2)	7.02(-2)	1.50(-1)	8.40(-2)	7.92(-2)	2.12(-1)
7-5	7/17/64	1500	2.34(-2)	2.81(-2)	4.00(-2)	1.52(-2)	9.50(-3)	2.47(-2)
8-1	7/21/64	1550	8.73(-2)	6.57(-2)	1.47(-1)	1.37(-2)	9.31(-3)	2.61(-2)
8-2	7/21/64	2015	4.44(-2)	4.74(-2)	7.46(-2)	8.13(-3)	5.97(-3)	1.54(-2)
8-3	7/22/64	0100	1.20(-1)	4.91(-2)	1.04(-1)	1.90(-2)	5.21(-3)	2.34(-2)
8-4	7/22/64	0530	9.86(-3)	6.83(-3)	1.65(-2)	6.38(-4)	--	1.37(-3)
8-5	7/22/64	1003	8.17(-2)	5.31(-2)	1.50(-1)	6.30(-3)	8.59(-3)	1.79(-2)
9-1	7/22/64	1629	8.06(-2)	7.20(-2)	1.31(-1)	2.17(-3)	1.70(-3)	3.89(-3)
9-2	7/22/64	2100	4.45(-2)	6.32(-2)	9.74(-2)	1.17(-3)	2.65(-3)	3.58(-3)
9-3	7/23/64	0145	9.43(-3)	1.29(-2)	2.00(-2)	1.84(-4)	4.75(-4)	6.35(-4)
9-4	7/23/64	0615	4.80(-3)	8.10(-3)	1.18(-2)	2.30(-4)	2.69(-4)	4.85(-4)
9-5	7/23/64	1120	9.52(-3)	9.75(-3)	1.61(-2)	3.70(-4)	2.98(-4)	7.60(-4)

numbers in parentheses indicate powers of 10, i.e., 3.25(-2) = 3.25×10^{-2}.

GPO 858-469

U.S. DEPARTMENT OF COMMERCE
WASHINGTON, D.C. 20230

OFFICIAL BUSINESS

POSTAGE AND FEES PAID
U.S. DEPARTMENT OF COMMERCE